Natural organic matter (NOM) electron shuttling stimulates microbial Fe(III)-mineral reduction at centimeter-scales

Dissertation

der Mathematisch-Naturwissenschaftlichen Fakultät

der Eberhard Karls Universität Tübingen

zur Erlangung des Grades eines

Doktors der Naturwissenschaften

(Dr. rer. nat.)

vorgelegt von

M. Sc. Yuge Bai

aus Inner Mongolia, VR China

Tübingen 2020

Gedruckt mit Genehmigung der Mathematisch-Naturwissenschaftlichen Fakultät der Eberhard

Karls Universität Tübingen

Tag der mündlichen Qualifikation: 07.07.2020

Dekan: Prof. Dr. Wolfgang Rosenstiel

1. Berichterstatter: Prof. Dr. Andreas Kappler

2. Berichterstatter: Prof. Dr. Stefan B. Haderlein

Contents

1. Summary

1.1 Abstract

Iron (Fe)(III) minerals are an important terminal electron acceptor for microbial respiration under anoxic conditions. However, under neutral pH conditions, Fe(III) minerals have very low solubility and are mostly present as solid (oxyhydr)oxide. This imposes a limitation on the rate and extent of electron transfer between microbes and Fe(III) minerals. Therefore, microbes have developed several strategies to enable extracellular electron transfer. One of the most important strategies is to use the natural organic matter (NOM) as electron shuttles.

NOM represents the complex of organic compounds that are derived from the decay of plant and animal matters in natural systems. Due to the presence of functional groups such as quinone and hydroquinone, NOM can undergo redox cycles and act as electron shuttles between spatially separated microbes and Fe(III) minerals. Although many previous studies have shown the stimulatory effects of NOM on the microbial Fe(III)-mineral reduction as electron shuttles, it remains unknown whether such a NOM electron shuttling process can happen over long (centimeter (cm)) distance. Moreover, the mechanism of NOM electron shuttling is still unclear, i.e., if the electron shuttling process is driven by the diffusion of the NOM or the "hop" of electrons between NOM molecules. Finally, previous studies used chemically extracted humic substances (HS) as a proxy for NOM. It is, however, unknown to which extent this chemical extraction method alters the redox properties of the HS.

In Chapter 3 of this thesis, we extracted NOM from a forest soil (thus referred to as soil organic matter (SOM)) at neutral pH using water, and subsequently isolated HS chemically from the water-extracted SOM using sodium hydroxide (NaOH) at pH 12. Our results showed that, under anoxic extraction conditions, the HS extracted chemically from the water-extractable SOM had a 3-times higher electron exchange capacity (EEC) than the water-

extracted SOM itself. With higher EEC, the HS also showed more stimulation effects (i.e., higher reduction rate and extent) on the microbial Fe(III)-mineral reduction as electron shuttles than the water-extracted SOM. Therefore, we suggest future studies to carefully consider the influence of the chemical extraction on the redox properties of HS when using HS to represent NOM in laboratory studies.

In studies presented in Chapter 4 and Chapter 5, we developed a novel agar-solidified setup that separates the Fe(III)-reducing bacteria (*Shewanella oneidensis* MR-1 or *Geobacter sulfurreducens*) and Fe(III) minerals (ferrihydrite or goethite) over 2 cm distance, with either anthraquinone-2,6-disulfonate (AQDS) or NOM as electron shuttles. Fe concentration measurements coupled to a diffusion-reaction model clearly indicated Fe(III)-mineral reduction in the presence of AQDS or NOM as electron shuttles over 2 cm distance, independent of the type of the Fe(III)-reducing bacteria. Moreover, a linear correlation between the heterogeneous electron transfer rate constant and the diffusion coefficient of AQDS was obtained from the cyclic voltammogram of AQDS. This linear correlation is in good agreement with the "diffusion-electron hopping" model proposed in previous studies, indicating that the electron transfer via AQDS was accomplished by a combination of diffusion and electron hopping between AQDS molecules. Since AQDS is commonly used as the analogue for quinone and hydroquinone functional groups in NOM, we postulate that electron hopping also plays a crucial role to facilitate the electron transfer via NOM molecules over cm distance.

Overall, studies in this thesis showed that, microbial Fe(III)-mineral reduction can happen at cm-scales with NOM as electron shuttles, and the long-distance electron shuttling is achieved by a combination of NOM diffusion and electron hopping between NOM molecules. These findings improved our understanding of the feasibility and mechanism of microbial Fe(III)-mineral reduction at cm-scales with NOM as electron shuttles in the environment.

1.2 Zusammenfassung

Eisen (Fe)(III)-Minerale sind wichtige terminale Elektronakzeptoren für mikrobielle Respiration unter anoxischen Bedingungen. Jedoch haben Fe(III)-Minerale unter neutralen pH-Bedingungen eine sehr geringe Löslichkeit und kommen hauptsächlich als festes (Oxyhydr)Oxid vor. Dies stellt eine Einschränkung für die Rate und das Ausmaß des Elektronentransfers zwischen Mikroben und Fe(III)-Mineralen dar. Deswegen haben Mikroben mehrere Strategien entwickelt, um extrazellulären Elektronentransfer zu ermöglichen. Eine der wichtigsten Strategien ist die Nutzung natürlicher organischer Substanz (NOS) als Elektronenshuttle.

NOS repräsentiert den Komplex organischer Verbindungen, die durch den Zerfall pflanzlicher und tierischer Materie in natürlichen Systemen entstehen. Aufgrund der Präsenz von funktionellen Gruppen, wie z.B. Chinon- und Hydrochinongruppen, kann NOS Redoxzyklen durchlaufen und somit als Elektronenshuttle zwischen räumlich getrennten Mikroben und Fe(III)-Mineralen fungieren. Obwohl viele frühere Studien die stimulierenden Effekte von NOS auf mikrobielle Fe(III)-Reduktion, wenn NOS als Elektronenshuttle fungiert, gezeigt haben, bleibt es ungeklärt, ob ein solcher NOS-Elektronenshuttleprozess über lange (Zentimeter (cm)) Distanzen stattfinden kann. Außerdem ist der Mechanismus hinter NOS-Elektronenshuttling immer noch unklar, d.h. ob der Elektronenshuttleprozess durch Diffusion der NOS angetrieben wird oder durch das „Springen" von Elektronen zwischen NOS-Molekülen. Schließlich verwendeten frühere Studien chemisch extrahierte Huminstoffe (HS) um NOS als Elektronenshuttle darzustellen. Es ist jedoch unbekannt, in welchem Ausmaß diese chemische Extraktionsmethode die Redoxeigenschaften der HS verändert.

In Kapitel 3 dieser Arbeit extrahierten wir NOS bei neutralem pH mit Wasser aus einem Waldboden (daher als organische Bodensubstanz, OBS, bezeichnet) und isolierten anschließend, unter Verwendung einer Natriumhydroxydextraktion (NaOH) bei pH 12, HS chemisch aus der wasserextrahierten OBS. Unsere Ergebnisse zeigten, dass unter anoxischen

Extraktionsbedingungen die chemisch aus der wasserextrahierten OBS isolierten HS eine dreifach höhere Elektronenaustauschkapazität (EAK) hatten als die wasserextrahierte OBS selbst, was auf die Bildung von redoxaktiven funktionellen Gruppen während der NaOH Extraktion hindeutet. Mit höherer EAK zeigten die HS auch einen ausgeprägteren stimulierenden Effekt (d.h. höhere Reduktionsrate und größeres Reduktionsausmaß) auf die mikrobielle Fe(III)-Reduktion als die wasserextrahierte OBS wenn sie als Elektronenshuttle fungierten. Deswegen schlagen wir vor, in zukünftigen Studien den Einfluss der chemischen Extraktionsmethode auf die Redoxeigenschaften von HS sorgsam in Betracht zu ziehen, wenn HS benutzt werden, um OBS in Laborstudien darzustellen.

In den in Kapitel 4 und Kapitel 5 vorgestellten Studien entwickelten wir ein neuartiges mit Agar stabilisiertes Set-up, welches Fe(III)-reduzierende Bakterien (*Shewanella oneidensis* MR-1 oder *Geobacter sulfurreducens*) und Fe(III)-Minerale (Ferrihydrit oder Goethit) über einen Abstand von 2 cm trennt, mit entweder Anthrachinon-2,6-disulfonat (AQDS) oder NOS als Elektronenshuttles. AQDS ist das häufig genutzte Analogon für die funktionellen Chinongruppen, die in NOS Redoxzyklen durchlaufen, um Elektronen über Distanz zu transportieren. Eisenkonzentrationsmessungen gekoppelt mit einem Diffusionsreaktionsmodell zeigten eindeutig mikrobielle Fe(III)-Reduktion über eine Distanz von 2 cm in Gegenwart von AQDS oder NOS als Elektronenshuttle, unabhängig von der Art der Fe(III)-reduzierenden Bakterien. Weiterhin wurde anhand des Cyclovoltammogramms von AQDS eine lineare Korrelation zwischen der heterogenen Elektronentransferratenkonstante und dem Diffusionskoeffizienten von AQDS festgestellt. Diese lineare Korrelation stimmt gut mit dem „Diffusions-Elektronensprung"-Modell, das in früheren Studien vorgeschlagen wurde, überein, was darauf hindeutet, dass der Elektronentransfer via AQDS durch eine Kombination von Diffusion und Elektronenspringen zwischen AQDS Molekülen erreicht wurde. Deswegen nehmen wir an, dass Elektronenspringen auch in der Umwelt eine kritische Rolle spielt, wo es die Geschwindigkeit des Elektronentransfers durch NOS Moleküle erhöht.

Insgesamt haben die Studien in dieser Arbeit gezeigt, dass mikrobielle Fe(III)-Reduktion mit NOS als Elektronenshuttles durch Diffusion von NOS und Elektronenspringen zwischen NOS Molekülen über Zentimeter hinweg möglich ist. Die Ergebnisse in dieser Arbeit verbessern deswegen unser Verständnis von mikrobieller Fe(III)-Mineralreduktion mit NOS als Elektronenshuttles in der Umwelt.

2. Introduction

2.1 Iron in the environment

Iron (Fe) widely exists in almost all aquatic and terrestrial environments and is one of the essential nutrients for almost all living organisms (Cornell and Schwertmann, 2006). In the environment, iron mostly presents in the form of ferrous (Fe(II)) or ferric iron (Fe(III)) (Cornell and Schwertmann, 2006). The redox cycling between Fe(II) and Fe(III) can be mediated either chemically or by Fe(II)-oxidizing and Fe(III)-reducing bacteria (Kappler and Straub, 2005). Because of the large surface area, iron minerals are strong sorbents for soil nutrients, contaminants and organic matters (Borch et al., 2010; Cornell and Schwertmann, 2006). Therefore, the redox cycle of iron has significant impact on other geological and environmental processes such as the preservation of organic matter and nutrients (Canfield, 1994; Wang et al., 2019), the remobilization of toxic metals (Muehe et al., 2016; Sundman et al., 2020) and the degradation of organic pollutants (Zhou et al., 2018).

2.2 Microbial Fe(III)-mineral reduction

Microbes undergo respiration processes to convert energy from nutrients to adenosine triphosphate (ATP) through a series of redox reactions that couple the oxidation of an electron donor (nutrients such as organic matter and H_2, *etc.*) to the reduction of an electron acceptor (Gray and Winkler, 2010). Under anoxic conditions, Fe(III) minerals are often the terminal electron acceptor for the microbial respiration process (Roden, 2006; Weber et al., 2006). However, unlike other electron acceptors such as dissolved nitrates or sulfates that can be taken up by microbes, the solubility of Fe(III) minerals is very low under typical environmental pH conditions (Cornell and Schwertmann, 2006). Therefore, in order to gain energy by transferring respiratory electrons to Fe(III) minerals, microbes have to develop strategies for extracellular electron transfer (Hernandez and Newman, 2001).

2.3 Extracellular electron transfer

Dissimilatory metal-reducing bacteria, including *Shewanella* spp. and *Geobacter* spp., are known to be capable of conducting extracellular electron transfer, thus reducing Fe(III) minerals (Lovley and Phillips, 1988; Myers and Nealson, 1988). The strategies employed for extracellular electron transfer, although differs between *Shewanella* spp. and *Geobacter* spp., fall into two broad categories: endogenous and exogenous. Whereas endogenous indicates that microbes transfer electrons by self-produced electron shuttles, exogenous represents that microbes exploit redox-active electron shuttles that already exist in the environment (Glasser et al., 2017).

Endogenous electron-transfer strategy

1.   *c*-type cytochromes

Extracellular electron transfer requires the transportation of respiratory electrons from the inner membrane, through the periplasm and outer membrane to the surface of cells. And this step can be achieved by cell-produced *c*-type cytochromes. There are two well-studied dissimilatory metal-reducing bacteria, *Shewanella oneidensis* MR-1 and *Geobacter sulfurreducens*, which are known to produce *c*-type cytochromes (Shi et al., 2007). However, as shown in Figure 2.1, these *c*-type cytochromes participate in the extracellular electron transfer process very differently between the two species. For *Shewanella oneidensis* MR-1, the respiratory electron is first transferred to an inner-membrane *c*-type cytochrome CymA, which is capable of reducing another *c*-type cytochrome MtrA that is located at the periplasm (Lies et al., 2005; Myers and Myers, 1997). MtrA might interact with the outer membrane protein MtrB. Although it is not a *c*-type cytochrome, MtrB is speculated to facilitate the electron transfer across the outer membrane to MtrC, which is associated with OmcA. The MtrC-OmcA complex can directly transfer electrons to a solid electron acceptor such as Fe(III) minerals (Beliaev and Saffarini, 1998; Beliaev et al., 2001; Myers and Myers, 2001). In contrast

to *Shewanella oneidensis* MR-1 that directly uses *c*-type cytochromes for extracellular electron transfer to the Fe(III) minerals, it has been suggested that *Geobacter sulfurreducens* uses porin-cytochrome complex to transfer electrons from the inner membrane to the Fe(III) minerals (Lovley, 2006; Reardon and Mueller, 2013). In *Geobacter sulfurreducens*, the respiratory electrons are first transferred to *c*-type cytochromes ImcH and CbcL in the cytoplasmic membrane (Seidel et al., 2012). These *c*-type cytochromes then donate electrons to PpcA in the periplasm, which is able to transfer electrons to another two porin-cytochrome complexes that are located in the outer membrane: OmaB-OmbB-OmcB and OmaC-OmbC-OmcC (Ding et al., 2006), which eventually transfer electrons to the Fe(III) minerals (Mehta et al., 2005).

Although *c*-type cytochromes can successfully transfer electrons from the inner membrane to the surface of cell, it has been shown that the largest distance an electron can 'hop' between cytochromes and a solid electron acceptor, such as Fe(III) minerals, is around 2 nm (Gray and Winkler, 2003). Therefore, for dissimilatory metal-reducing bacteria that are spatially separated from Fe(III) minerals by a distance that is longer than 2 nm, other electron transfer pathways may have to be employed.
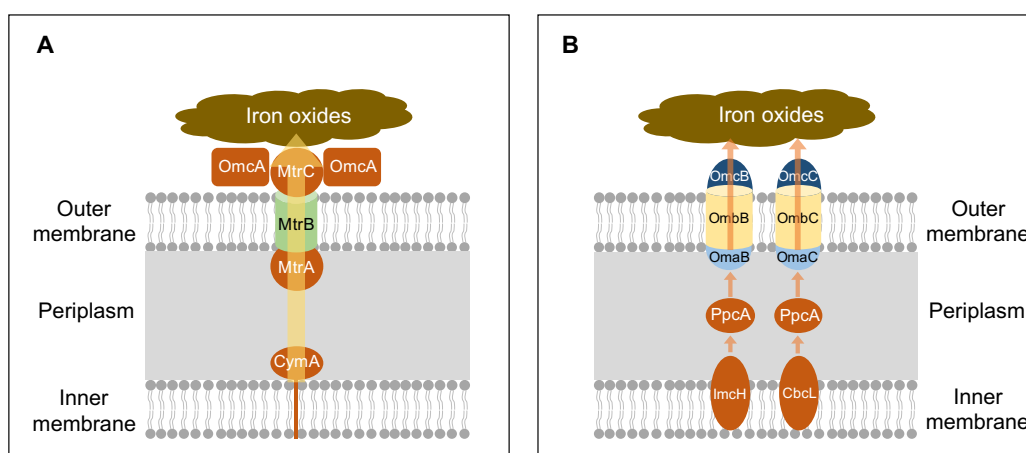

Figure 2.1. Proposed models depicting electron transfer pathways from inner membrane to the outer membrane by *c*-type cytochromes for (A) *Shewanella oneidensis* MR-1 and (B) *Geobacter sulfurreducens* (modified from Shi et al. 2007).

2.   Redox-active riboflavin

The production of riboflavin was first observed in *Shewanella* strains (Marsili et al., 2008; Newman and Kolter, 2000; von Canstein et al., 2008) and later also discovered in *Geobacter* species (Huang et al., 2018; Okamoto et al., 2014). Experimental results showed significantly faster ferrihydrite reduction in setups with the amendment of riboflavin compare to setups where the cell-produced riboflavin was removed, and the removal of riboflavin resulted in the decrease of the electron transfer rate by > 70% (Marsili et al., 2008). Riboflavin is redox-active and it can undergo oxidation-reduction reactions by either accepting/donating one electron in a two-step process or two electrons at once, as shown in Figure 2.2. Therefore, riboflavin can act as a recyclable electron shuttle between *Shewanella* or *Geobacter* and Fe(III) minerals. It has been shown that the diffusion-based recycling of riboflavin allows *Shewanella oneidensis* MR-1 to access Fe(III) minerals up to 60 micrometers (μm) distance (Michelson et al., 2019).
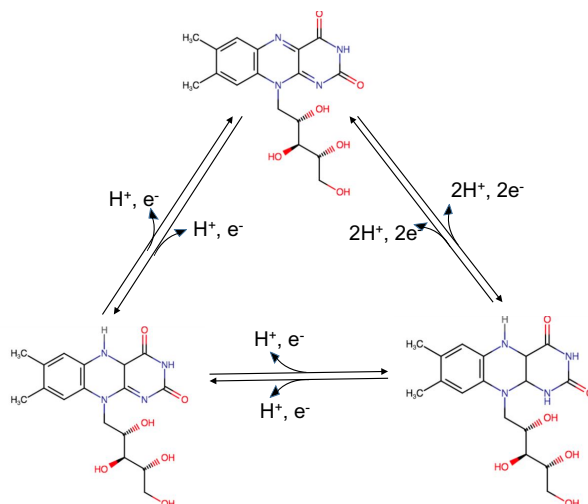

Figure 2.2. The conversions between reduced and oxidized riboflavin.

3.   Conductive pili/nanowires

When conducting extracellular electron transfer, both *Geobacter* spp. and *Shweanella* spp. can produce a nanometer scale diameter and micrometer scale long proteinaceous filaments, referred to as pili or microbial nanowires (Gorby et al., 2006; Reguera et al., 2005). Under

atomic force microscopy, pili/nanowire produced by *Geobacter* and *Shweanella* showed high conductivity, confirming their significant role in the electron transfer process from bacteria to the electron acceptor (Leung et al., 2013; Malvankar et al., 2014). The utility of conductive pili/nanowires can i) facilitate electron transfer from bacteria to metal oxides over distance, ii) significantly increase the reactive surface area and iii) help to deliver electrons to metal oxides that are confined in micro-pore environments that may otherwise be inaccessible (Cologgi et al., 2011; Lovley and Walker, 2019). However, it has been reported in several recent studies that the reduction of metal oxides by conductive pili/nanowires is only possible with redox co-factors, such as riboflavin and *c*-type cytochromes, which are closely attached to the conductive pili/nanowires (Leang et al., 2010; Michelson et al., 2017; Snider et al., 2012). So far, the longest electron transfer distance by redox-co-factor-coated conductive pili/nanowire is 15 μm (Michelson et al., 2017).

Exogenous electron transfer strategy

Exogenous electron transfer strategies depend on the redox-active compounds that already exist in the environments. It has been shown that dissolved and solid-phase humic substances (HS) (Jiang and Kappler, 2008; Lovley et al., 1996; Roden et al., 2010), biochar (Kappler et al., 2014; Yang et al., 2020) and some inorganic compounds such as sulfur species can all undergo redox cycles and act as electron shuttles between *Shewanella/Geobacter* and Fe(III) minerals (Flynn et al., 2014).

2.4 Natural organic matter (NOM) and humic substances (HS)

Definition, classification and isolation

Natural organic matter (NOM) consists of plant and animal detritus at various stages of decomposition, cells and tissues of microbes and microbes-synthesized substances (Sparks, 2003). NOM typically has a very high specific surface (up to 800-900 m^2 g^{-1}) and abundant redox-active functional groups (Chiou et al., 1990; Sparks, 2003), thus, it is an important

sorbent for macro-and micro-nutrients (Impellitteri et al., 2002; Krosshavn et al., 1993), heave metals and organic contaminants (Karapanagiotis et al., 1991; Shi et al., 2010; Zeng et al., 2011). Understanding the chemical composition and redox properties of NOM can help us to predict the nutrient cycling and the fate of heavy metals and organic contaminants in the environment. However, studying NOM is challenging because it needs to be separated from other components before any laboratory experiments; therefore, an extractable fraction defined as "humic substances (HS)" has been used as a proxy for NOM (Lehmann and Kleber, 2015).

HS is defined as a series of relatively high-molecular-weight, brown- to black-colored substances, formed by a secondary synthesis reaction recognized as "humidification" (Aiken, 1985). HS contains a variety of functional groups, including COOH, phenolic OH, enolic OH, quinone, lactone, ether and alcoholic OH. It is amorphous, aromatic and polyelectrolyte, with the average molecular weight ranging from 500 to 5000 Da (Stevenson, 1994). HS can be further divided into humic acid (HA), fulvic acid (FA) and humin. Humin is the fraction that is not soluble in bases and acids and is rich in OH groups. HA usually has dark brown to black color, and it is soluble in bases but not in acid. HA is the high-molecular-weight fraction of HS with a large content of quinone functional group, whereas FA is made out of much smaller molecules with an orange to light-brown color, and has abundant carboxyl and phenolic groups (Stevenson, 1994). As shown in Figure 2.3, HA and FA can be isolated from soil with an extraction method using sodium hydroxide (NaOH) and hydrochloride (HCl) to adjust pH of the soil suspension solution to either very alkaline (pH=12) or extremely acidic (pH=2) (Aiken, 1985).
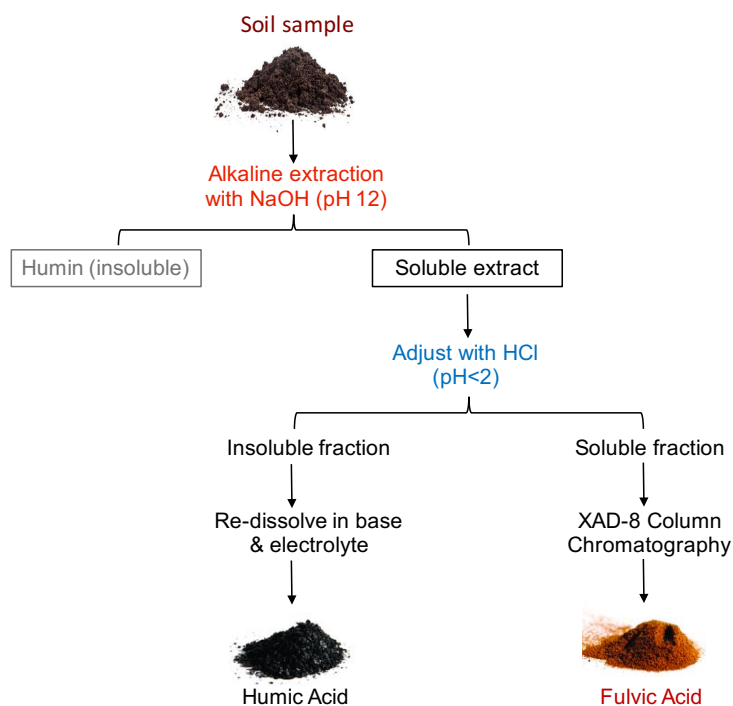
Figure 2.3. The isolation procedure of humic substances from soil.

Redox properties of HS

HS is the composition of heterogeneous, redox-active organic compounds; thus, it processes a certain capacity of taking up electrons by the oxidized functional groups (electron accepting capacity, EAC) or releasing electrons from the reduced functional groups (electron donating capacity, EDC). By applying a novel electrochemical method, Aeschbacher and co-authors analyzed the EAC and EDC of 15 FA and HA samples from either terrestrial or aquatic systems (Aeschbacher et al., 2012). They found that, although the EAC and EDC vary between aquatic and terrestrial samples, all of the analyzed FA and HA had EACs ranging from 0.8 to 2 mmol e$^-$ (g$_{sample}$)$^{-1}$, and EDCs from 0.5 to 2.8 mmol e$^-$ (g$_{sample}$)$^{-1}$ at pH 7. Moreover, a strong correlation between the EAC of the samples and their aromaticity (analyzed by nuclear magnetic resonance (NMR)) was observed (R^2= 0.82), indicating that the EAC of HA and FA samples is majorly contributed by aromatic reducible moieties such as quinones.

Because of its heterogeneous structure, no defined reduction potential can be assigned to HS but rather a range of reduction potentials at which the HS can accept or donate electrons.

Using the same electrochemical analysis, Aeschbacher and co-authors measured the reduction potential distribution of three HA samples from different source at pH 7 (Aeschbacher et al., 2010). They found that the reduction potential of the three samples ranged between -0.4 to +0.2 V, with a peak at around -0.3 V. Compared to the standard reduction potential of other biogeochemical redox couples at pH 7, part of the reducible moieties of HA have more negative reduction potential than redox couples such as $Fe(OH)_3$-Fe^{2+} and α-$FeOOH$-Fe^{2+}, as shown in Figure 2.4. Therefore, HA contains moieties with sufficiently low reduction potential (E_h^0, pH 7) to reduce some typical iron minerals.
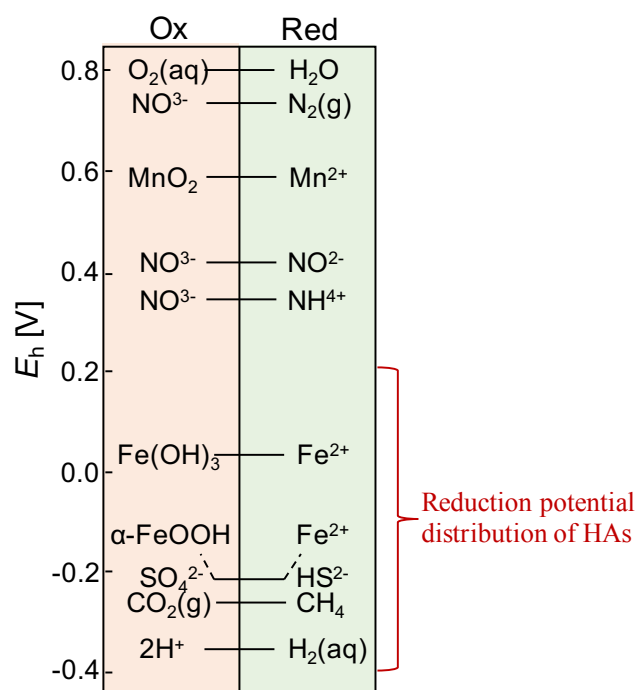
Figure 2.4. Estimated reduction potential distribution of HA at pH 7 (analyzed electrochemically), compared to the standard reduction potential E_h^0 (pH 7) of selected biogeochemical redox couples (modified from Aeschbacher et al 2011).

HS as electron shuttles

In 1996, Lovley and co-authors reported for the first time that the addition of HA could significantly increase the extent and rate of Fe(III)-mineral reduction compared to the experiments with *Geobacter metallireduces* or *Shewanella alga* only (Lovley et al., 1996). The

initially explanation for this observed stimulation effect was that HA acted as chelator and dissolved Fe(III) minerals to release Fe^{3+}; therefore, making it more accessible to microbes. However, Lovley and co-authors only detected around 200 μmol L^{-1} dissolved Fe^{3+} in the experiment with HA amendment, and this amount of Fe^{3+} is too low to explain for the 2.75 mmol L^{-1} more reduced Fe(III)-minerals in the experiment with HA than with *Geobacter metallireduces* only. Therefore, Lovley and co-authors suggested that instead of a chelator, HA might serve as an electron shuttle between microbes and Fe(III) minerals. They further proposed that HA stimulated the Fe(III) reduction as electron shuttles in a two-steps process, as shown in Figure 2.5: (i) *Geobacter metallireduces* or *Shewanella alga* couples the oxidation of organic substrates to the reduction of HA and (ii) the reduced HA donate electrons to Fe(III) minerals. The stimulation effects of HS on the microbial Fe(III) reduction as electron shuttles were also observed by many other studies using different HS, dissimilatory metal-reducing bacteria and Fe(III) minerals (Behrends and Van Cappellen, 2007; O'Loughlin, 2008; Wolf et al., 2009). And the study of Jiang and Kappler (Jiang and Kappler, 2008) showed that *Geobacter sulfurreducens* transfers electrons to HS at least 27 times faster than to Fe(III) minerals, and the microbial-reduced HS transfer electrons to Fe(III) minerals at least seven times faster than *Geobacter sulfurreducens* to Fe(III) minerals. These results further confirmed that Fe(III) can be reduced at a higher rate when electron shuttling occurs. Moreover, Jiang and Kappler also showed that the stimulation effects of HS as electron shuttles on the microbial Fe(III)-mineral reduction can be observed with a HS concentration as low as 5 mg L^{-1}. Since this concentration is related to the dissolved organic matter concentration in many aquifers (Aiken, 1985), this discovery indicates the potentially important role of HS electron shuttling in natural systems.
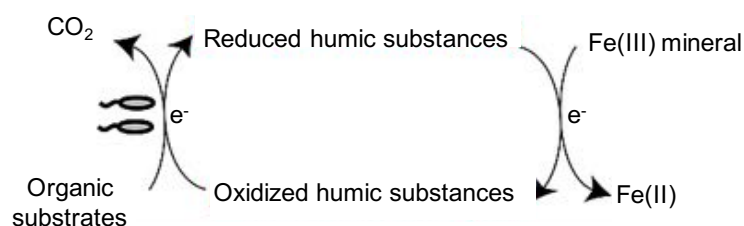
Figure 2.5. Schematic diagram of HS as electron shuttles to stimulate microbial Fe(III)-mineral reduction (modified from Lovley et al 1996).

Anthraquinone-2,6-disulfonate (AQDS)

It has been believed that quinone moieties that widely exist in HS are the functional groups that undergo redox cycles, therefore enabling HS to be electron shuttles between dissimilatory metal-reducing bacteria and Fe(III) minerals (Newman and Kolter, 2000; Piepenbrock and Kappler, 2013; Scott et al., 1998; Wolf et al., 2009). Therefore, anthraquinone-2,6-disulfonate (AQDS), a model quinone compound, has been used as a proxy for the quinone functional groups in HS in many electron shuttling studies (Lovley et al., 1998; Piepenbrock and Kappler, 2013). As shown in Figure 2.6, AQDS can undergo electrochemically reversible reduction-oxidation reaction, with the highly-reactive semiquinone radical as an intermediate product (Rosso et al., 2004).
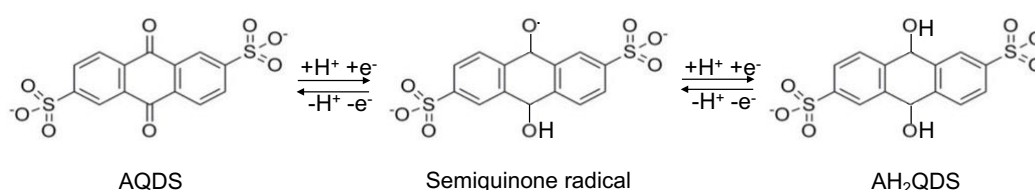
Figure 2.6. Redox reactions between AQDS and AH_2QDS.

It was showed that with 100 μmol L^{-1} AQDS amendment, the rate of Fe(III) mineral reduction was 50 times higher than with dissimilatory metal-reducing bacteria only (Lovley et al., 1996). The importance of quinone functional groups in HS on the stimulation effect of the Fe(III)-mineral reduction was also confirmed by many other studies. For example, in 2003,

Chen and co-authors discovered the formation of semiquinone radicals during the microbial reduction of HS (Chen et al., 2003), and later in 2007, Ratasuk and Nanny identified three groups of reactive sites in a variety of HS, among which, two had a quinoid nature (Ratasuk and Nanny, 2007). However, some other functional groups, such as sulfuryl groups, aromatic constituents and complexed metal ions have also been suggested to participate in redox cycles of HS (Chen et al., 2003; Einsiedl et al., 2008).

Mechanism of electron shuttling

Diffusion of the reduced electron shuttle to the Fe(III) mineral and oxidized electron shuttle back to the Fe(III)-reducing bacteria has been considered as one of the main mechanisms of electron shuttling (Murray and Jackson, 1992; Nauman et al., 2007; Phalak et al., 2016; Picioreanu et al., 2007). A previous study adapting a three-dimensional diffusion model that comprising an inner sphere of anoxic cells and an outer shell of electron acceptors showed that, for any shuttle compound that has a diffusion coefficient higher than 10^{-10} m^2 s^{-1} and concentration more than 10 μmol L^{-1}, diffusion of the shuttles can drive sufficient flux of oxidized shuttle molecules to support the survival of the cells. However, with the distance limitation up to 100 μm (Glasser et al., 2017). An alternative mechanism of longer distance electron shuttling is electron hopping (Boyd et al., 2015; Ing et al., 2018; Snider et al., 2012). Electron hopping requires a very high density of the electron-transfer sites (Gray and Winkler, 2009); with a high concentration of electron shuttles, the distance between two electron-transfer sites might get close enough for an electron to hop (2 nm), and the multi-step electron hopping can facilitate electron transfer over a longer distance and with a faster rate compare to diffusion (Gray and Winkler, 2009; Pirbadian and El-Naggar, 2012). So far, it has been shown that electrons were transferred by hopping through the conductive pili of *Geobacter sulfurreducens* (Lovley and Walker, 2019; Michelson et al., 2017) and the extracellular polymeric substances

(EPS) of *Shewanella oneidensis* MR-1 (Xiao et al., 2017), but it remains unknown whether electron hopping also plays a role in the electron shuttling of NOM.

Concerns of the chemically extracted HS

The idea of using HS extracted chemically under extreme pH conditions as the proxy for NOM has been questioned for almost 180 years (Kleber and Lehmann, 2019). It has been shown in many studies that the chemical extraction of HS with NaOH and HCl alters the elemental composition, ash content and fraction of organic carbon, the size class distribution and the frequency of functional groups of the extracted material (de Souza and Bragança, 2018; Dick et al., 1999; Piepenbrock et al., 2014; Sanchez-Monedero et al., 2002). Recent studies also suggested a much higher electron accepting capacity (EAC) of chemically-extracted HS compared to NOM samples extracted under neutral pH conditions with reverse osmosis (RO) and electrodialysis (ED) method (Olk et al., 2019; Li et al., 2016). However, because the HS and NOM samples were extracted from different origins in these studies, it was difficult to evaluate to which extent the different EAC of the HS and NOM was resulted from the extraction method.

Participation in redox reactions is one of the key properties of NOM, and it is relevant for many biogeochemical reactions in the environment, such as the microbial Fe(III) reductions. However, most of the Fe(III) reduction experiments so far have applied chemically extracted HS as the representor of NOM (Bauer and Kappler, 2009; Klupfel et al., 2014; Lovley et al., 1996; Lovley et al., 1998; Stern et al., 2018; Wolf et al., 2009; Zhou et al., 2018). Therefore, a study is needed to compare the redox properties of the HS and NOM extracted from the same origin with different extraction methods and to determine how the different redox property (e.g. electron accepting and electron donating capacity) influence the stimulation effects of the extracted HS/NOM on the microbial Fe(III) reduction as electron shuttles.

2.5 Objectives of this study

So far, most of the mediated Fe(III) reduction experiment with HS as an electron shuttle have been done in batch setups where bacteria, Fe(III) minerals and HS are mixed together (Bauer and Kappler, 2009; Klupfel et al., 2014; Lovley et al., 1996; Lovley et al., 1998; Stern et al., 2018; Wolf et al., 2009; Zhou et al., 2018). In a mixed system, HS is not only the electron shuttle, but it can also impact the rate and extent of Fe(III) mineral reduction by being the chelator for the produced Fe^{2+}, thus increasing the thermodynamic driving force for Fe(III) reduction (Roden and Urrutia, 1999). HS can also adsorb on the surface of Fe(III) minerals and potentially block the surface sites (Kaiser and Guggenberger, 2003) and induce aggregation (Amstaetter et al., 2012). Due to the various interactions between HS and Fe(III) minerals, it is difficult to evaluate to what extent HS stimulates microbial Fe(III) reduction by acting as an electron shuttle. Furthermore, the longest distance that electrons can be transferred from the dissimilatory metal-reducing bacteria to the Fe(III) minerals is not known yet. Although it has been shown that AQDS as electron shuttles can transfer electrons in the range of μm distance (Michelson et al., 2017), we suspect that in natural systems with high organic matter content, the electron shuttle can happen over a much longer distance in centimeter (cm) scale, as shown in a previous study that the electric currents running through defaunated sediment can couple the oxygen consumption and the oxidation of hydrogen sulfide over cm distance (Nielsen et al., 2010). Furthermore, although it is known that the electron shuttle over μm distance is achieved by the diffusion of electron shuttles, the mechanism of electron shuttling over a longer distance remains unknown. Finally, chemically-extracted HS have been used as the proxy for NOM, and it remains unclear how the chemical extraction influences the redox properties of the HS compare to NOM. Therefore, the objectives of this study are:

1. Identifying the effects of the chemical extraction on the redox properties of the extracted HS (Chapter 3).

2. Comparing the stimulation effects of NOM and HS extracted with different methods from the same soil on the microbial Fe(III) reduction as electron shuttles (Chapter 3).

3. Demonstrating that microbial Fe(III)-mineral reduction can happen over cm distance with NOM as electron shuttles (Chapter 4).

4. Evaluating the potential mechanisms of the electron shuttling process over cm distance (Chapter 4, Chapter 5).

2.6 References

Aeschbacher, M., Graf, C., Schwarzenbach, R. P. and Sander, M. (2012) Antioxidant properties of humic substances. *Environ. Sci. Technol.* **46**, 4916-4925.

Aeschbacher, M., Sander, M. and Schwarzenbach, R. P. (2010) Novel electrochemical approach to assess the redox properties of humic substances. *Environ. Sci. Technol.* **44**, 87-93.

Aiken, G.R. (1985) Humic substances in soil, sediment, and water: geochemistry, isolation, and characterization. Wiley, New York.

Amstaetter, K., Borch, T. and Kappler, A. (2012) Influence of humic acid imposed changes of ferrihydrite aggregation on microbial Fe(III) reduction. *Geochim. Cosmochim. Acta* **85**, 326-341.

Ayuke, F. O., Brussaard, L., Vanlauwe, B., Six, J., Lelei, D. K., Kibunja, C. N. and Pulleman, M. M. (2011) Soil fertility management: Impacts on soil macrofauna, soil aggregation and soil organic matter allocation. *Appl. Soil. Ecol.* **48**, 53-62.

Bauer, I. and Kappler, A. (2009) Rates and extent of reduction of Fe(III) compounds and O_2 by humic substances. *Environ. Sci. Technol.* **43**, 4902-4908.

Behrends, T. and Van Cappellen, P. (2007) Transformation of hematite into magnetite during dissimilatory iron reduction- Conditions and mechanisms. *Geomicrobiol. J.* **24**, 403-416.

Beliaev, A. S. and Saffarini, D. A. (1998) *Shewanella putrefaciens* mtrB encodes an outer membrane protein required for Fe(III) and Mn(IV) reduction. *J. Bacteriol.* **180**, 6292-6297.

Beliaev, A. S., Saffarini, D. A., McLaughlin, J. L. and Hunnicutt, D. (2001) MtrC, an outer membrane decahaem *c*-cytochrome required for metal reduction in *Shewanella putrefaciens* MR-1. *Mol. Microbiol.* **39**, 722-730.

Borch, T., Kretzschmar, R., Kappler, A., Van Cappellen, P., Ginder-Vogel, M., Voegelin, A. and Campbell, K. (2010) Biogeochemical redox processes and their impact on contaminant dynamics. *Environ. Sci. Technol.* **44**, 15-23.

Boyd, D. A., Snider, R. M., Erickson, J. S., Roy, J. N., Strycharz-Glaven, S. M. and Tender, L. M. (2015) Theory of redox conduction and the measurement of electron transport rates through electrochemically active biofilms. In Beyenal, H. and Babauta, J. (Ed.), *Biofilms in bioelectrochemical systems: From laboratory practice to data interpretation*, pp. 177-209.

Canfield, D. E. (1994) Factors influencing organic-carbon preservation in marine-sediments. *Chem. Geol.* **114**, 315-329.

Chen, J., Gu, B. H., Royer, R. A. and Burgos, W. D. (2003) The roles of natural organic matter in chemical and microbial reduction of ferric iron. *Sci. Total Environ.* **307**, 167-178.

Chiou, C. T., Lee, J. F. and Boyd, S. A. (1990) The surface-area of soil organic-matter. *Environ. Sci. Technol.* **24**, 1164-1166.

Cologgi, D. L., Lampa-Pastirk, S., Speers, A. M., Kelly, S. D. and Reguera, G. (2011) Extracellular reduction of uranium via *Geobacter* conductive pili as a protective cellular mechanism. *P. Natl. Acad. Sci. USA* **108**, 15248-15252.

Cornell, R. M. and Schwertmann, U. (2006) The iron oxides: structure, properties, reactions, occurrences and uses. Wiley-VCH, Weinheim.

de Souza, F. and Bragança, S. R. (2018) Extraction and characterization of humic acid from coal for the application as dispersant of ceramic powders. *J. Mater. Res. Technol.* **7**, 254-260.

Demir, Y. and Demir, A. D. (2019) The effect of organic matter applications on the saturated hydraulic conductivity and available water-holding capacity of sandy soils. *Appl. Ecol. Env. Res*. **17**, 3137-3146.

Dick, D. P., Burba, P. and Herzog, H. (1999) Influence of extractant and soil type on molecular characteristics of humic substances from two Brazilian soils. *J. Brazil. Chem. Soc.* **10**, 140-145.

Ding, Y. H. R., Hixson, K. K., Giometti, C. S., Stanley, A., Esteve-Nunez, A., Khare, T., Tollaksen, S. L., Zhu, W. H., Adkins, J. N., Lipton, M. S., Smith, R. D., Mester, T. and Lovley, D. R. (2006) The proteome of dissimilatory metal-reducing microorganism *Geobacter*

sulfurreducens under various growth conditions. *Biochim. Biophys. Acta. Proteins and proteomics* **1764**, 1198-1206.

Einsiedl, F., Mayer, B. and Schafer, T. (2008) Evidence for incorporation of H_2S in groundwater fulvic acids from stable isotope ratios and sulfur K-edge X-ray absorption near edge structure spectroscopy. *Environ. Sci. Technol.* **42**, 2439-2444.

Flynn, T. M., O'Loughlin, E. J., Mishra, B., DiChristina, T. J. and Kemner, K. M. (2014) Sulfur-mediated electron shuttling during bacterial iron reduction. *Science* **344**, 1039-1042.

Glasser, N. R., Saunders, S. H. and Newman, D. K. (2017) The colorful world of extracellular electron shuttles. *Annu. Rev. Microbiol.* **71**, 731-751.

Gorby, Y. A., Yanina, S., McLean, J. S., Rosso, K. M., Moyles, D., Dohnalkova, A., Beveridge, T. J., Chang, I. S., Kim, B. H., Kim, K. S., Culley, D. E., Reed, S. B., Romine, M. F., Saffarini, D. A., Hill, E. A., Shi, L., Elias, D. A., Kennedy, D. W., Pinchuk, G., Watanabe, K., Ishii, S., Logan, B., Nealson, K. H. and Fredrickson, J. K. (2006) Electrically conductive bacterial nanowires produced by *Shewanella oneidensis* strain MR-1 and other microorganisms. *P. Natl. Acad. Sci. USA* **103**, 11358-11363.

Gray, H. B. and Winkler, J. R. (2003) Electron tunneling through proteins. *Q. Rev. Biophys.* **36**, 341-372.

Gray, H. B. and Winkler, J. R. (2009) Electron flow through proteins. *Chem. Phys. Lett.* **483**, 1-9.

Gray, H. B. and Winkler, J. R. (2010) Electron flow through metalloproteins. *Biochim. Biophys. Acta. Bioenergetics* **1797**, 1563-1572.

Hernandez, M. E. and Newman, D. K. (2001) Extracellular electron transfer. *Cell. Mol. Life Sci.* **58**, 1562-1571.

Huang, L. Y., Tang, J. H., Chen, M., Liu, X. and Zhou, S. G. (2018) Two modes of riboflavin-mediated extracellular electron transfer in *Geobacter uraniireducens*. *Front. Microbiol.* **9**, 2886.

Hudson, B. D. (1994) Soil organic-matter and available water capacity. *J. Soil Water Conserv.* **49**, 189-194.

IHSS: Isolation of IHSS samples, available at: http: //humic-substances.org/isolation-of-ihss-samples/, last access: 29th July 2019.

Impellitteri, C. A., Lu, Y. F., Saxe, J. K., Allen, H. E. and Peijnenburg, W. J. G. M. (2002) Correlation of the partitioning of dissolved organic matter fractions with the desorption of Cd, Cu, Ni, Pb and Zn from 18 Dutch soils. *Environ. Int.* **28**, 401-410.

Ing, N. L., El-Naggar, M. Y. and Hochbaum, A. I. (2018) Going the distance: Long-range conductivity in protein and peptide bioelectronic materials. *J. Phys. Chem. B.* **122**, 10403-10423.

Jiang, J. and Kappler, A. (2008) Kinetics of microbial and chemical reduction of humic substances: Implications for electron shuttling. *Environ. Sci. Technol.* **42**, 3563-3569.

Kaiser, K. and Guggenberger, G. (2003) Mineral surfaces and soil organic matter. *Eur. J. Soil Sci.* **54**, 219-236.

Kappler, A. and Straub, K. L. (2005) Geomicrobiological cycling of iron. *Rev. Mineral Geochem.* **59**, 85-108.

Kappler, A., Wuestner, M. L., Ruecker, A., Harter, J., Halama, M. and Behrens, S. (2014) Biochar as an electron shuttle between bacteria and Fe(III) minerals. *Environ. Sci. Tech. Let.* **1**, 339-344.

Karapanagiotis, N. K., Sterritt, R. M. and Lester, J. N. (1991) Heavy-metal complexation in sludge-amended soil- the role of organic-matter in metal retention. *Environ. Technol.* **12**, 1107-1116.

Kleber, M. and Lehmann, J. (2019) Humic substances extracted by alkali are invalid proxies for the dynamics and functions of organic matter in terrestrial and aquatic ecosystems. *J. Environ. Qual.* **48**, 207.

Klupfel, L., Piepenbrock, A., Kappler, A. and Sander, M. (2014) Humic substances as fully regenerable electron acceptors in recurrently anoxic environments. *Nat. Geosci.* **7**, 195-200.

Krosshavn, M., Steinnes, E. and Varskog, P. (1993) Binding of Cd, Cu, Pb and Zn in soil organic-matter with different vegetational background. *Water Air Soil Poll.* **71**, 185-193.

Leang, C., Qian, X. L., Mester, T. and Lovley, D. R. (2010) Alignment of the *c*-type cytochrome OmcS along pili of *Geobacter sulfurreducens*. *Appl. Environ. Microb.* **76**, 4080-4084.

Lehmann, J. and Kleber, M. (2015) The contentious nature of soil organic matter. *Nature* **528**, 60-68.

Leung, K. M., Wanger, G., El-Naggar, M. Y., Gorby, Y., Southam, G., Lau, W. M. and Yang, J. (2013) *Shewanella oneidensis* MR-1 bacterial nanowires exhibit *p*-type, tunable electronic behavior. *Nano. Lett.* **13**, 2407-2411.

Li, Y., Harir, M., Lucio, M., Kanawati, B., Smirnov, K., Flerus, R., Koch, B. P., Schmitt-Kopplin, P. and Hertkorn, N. (2016) Proposed guidelines for solid phase extraction of Suwannee river dissolved organic matter. *Anal. Chem.* **88**, 6680-6688.

Libohova, Z., Seybold, C., Wysocki, D., Wills, S., Schoeneberger, P., Williams, C., Lindbo, D., Stott, D. and Owens, P. R. (2018) Reevaluating the effects of soil organic matter and other properties on available water-holding capacity using the national cooperative soil survey characterization database. *J. Soil. Water. Conserv.* **73**, 411-421.

Lies, D. P., Hernandez, M. E., Kappler, A., Mielke, R. E., Gralnick, J. A. and Newman, D. K. (2005) *Shewanella oneidensis* MR-1 uses overlapping pathways for iron reduction at a distance and by direct contact under conditions relevant for biofilms. *Appl. Environ. Microb.* **71**, 4414-4426.

Lovley, D. R. (2006) Bug juice: harvesting electricity with microorganisms. *Nat. Rev. Microbiol.* **4**, 797-797.

Lovley, D. R., Coates, J. D., BluntHarris, E. L., Phillips, E. J. P. and Woodward, J. C. (1996) Humic substances as electron acceptors for microbial respiration. *Nature* **382**, 445-448.

Lovley, D. R., Fraga, J. L., Blunt-Harris, E. L., Hayes, L. A., Phillips, E. J. P. and Coates, J. D. (1998) Humic substances as a mediator for microbially catalyzed metal reduction. *Acta. Hydroch. Hydrob.* **26**, 152-157.

Lovley, D. R. and Phillips, E. J. P. (1988) Novel mode of microbial energy-metabolism-organic-carbon oxidation coupled to dissimilatory reduction of iron or manganese. *Appl. Environ. Microb.* **54**, 1472-1480.

Lovley, D. R. and Walker, D. J. F. (2019) *Geobacter* Protein Nanowires. *Front. Microbiol.* **10**, 2078.

Malvankar, N. S., Yalcin, S. E., Tuominen, M. T. and Lovley, D. R. (2014) Visualization of charge propagation along individual pili proteins using ambient electrostatic force microscopy. *Nat. Nanotechnol.* **9**, 1012-1017.

Marsili, E., Baron, D. B., Shikhare, I. D., Coursolle, D., Gralnick, J. A. and Bond, D. R. (2008) *Shewanella* Secretes flavins that mediate extracellular electron transfer. *P. Natl. Acad. Sci. USA* **105**, 3968-3973.

Mehta, T., Coppi, M. V., Childers, S. E. and Lovley, D. R. (2005) Outer membrane *c*-type cytochromes required for Fe(III) and Mn(IV) oxide reduction in *Geobacter sulfurreducens*. *Appl. Environ. Microb.* **71**, 8634-8641.

Michelson, K., Alcalde, R. E., Sanford, R. A., Valocchi, A. J. and Werth, C. J. (2019) Diffusion-based recycling of flavins allows *Shewanella oneidensis* MR-1 to yield energy from metal reduction across physical separations. *Environ. Sci. Technol.* **53**, 3480-3487.

Michelson, K., Sanford, R. A., Valocchi, A. J. and Werth, C. J. (2017) Nanowires of *Geobacter sulfurreducens* require redox cofactors to reduce metals in pore spaces too small for cell passage. *Environ. Sci. Technol.* **51**, 11660-11668.

Muehe, E. M., Morin, G., Scheer, L., Pape, P. L., Esteve, I., Daus, B. and Kappler, A. (2016) Arsenic(V) incorporation in vivianite during microbial reduction of arsenic(V)-bearing biogenic Fe(III) (oxyhydr)oxides. *Environ. Sci. Technol.* **50**, 2281-2291.

Murphy, B. W. (2015) Impact of soil organic matter on soil properties- a review with emphasis on Australian soils. *Soil Res.* **53**, 605-635.

Murray, A. G. and Jackson, G. A. (1992) Viral dynamics- a model of the effects of size, shape, motion and abundance of single-celled planktonic organisms and other particles. *Mar. Ecol. Prog. Ser.* **89**, 103-116.

Myers, C. R. and Myers, J. M. (1997) Cloning and sequence of cymA a gene encoding a tetraheme cytochrome *c* required for reduction of iron(III), fumarate, and nitrate by *Shewanella putrefaciens* MR-1. *J. Bacteriol.* **179**, 1143-1152.

Myers, C. R. and Nealson, K. H. (1988) Microbial reduction of manganese oxides- interactions with iron and sulfur. *Geochim. Cosmochim. Ac.* **52**, 2727-2732.

Myers, J. M. and Myers, C. R. (2001) Role for outer membrane cytochromes OmcA and OmcB of *Shewanella putrefaciens* MR-1 in reduction of manganese dioxide. *Appl. Environ. Microb.* **67**, 260-269.

Nauman, J. V., Campbell, P. G., Lanni, F. and Anderson, J. L. (2007) Diffusion of insulin-like growth factor-I and ribonuclease through fibrin gels. *Biophys. J.* **92**, 4444-4450.

Newman, D. K. and Kolter, R. (2000) A role for excreted quinones in extracellular electron transfer. *Nature* **405**, 94-97.

Nielsen, L. P., Risgaard-Petersen, N., Fossing, H., Christensen, P. B. and Sayama, M. (2010) Electric currents couple spatially separated biogeochemical processes in marine sediment. *Nature* **463**, 1071-1074.

O'Loughlin, E. J. (2008) Effects of electron transfer mediators on the bioreduction of lepidocrocite (γ-FeOOH) by *Shewanella putrefaciens* CN32. *Environ. Sci. Technol.* **42**, 6876-6882.

Okamoto, A., Saito, K., Inoue, K., Nealson, K. H., Hashimoto, K. and Nakamura, R. (2014) Uptake of self-secreted flavins as bound cofactors for extracellular electron transfer in *Geobacter* species. *Energ. Environ. Sci.* **7**, 1357-1361.

Olk, D. C., Bloom, P. R., Perdue, E. M., McKnight, D. M., Chen, Y., Farenhorst, A., Senesi, N., Chin, Y. P., Schmitt-Kopplin, P., Hertkorn, N. and Harir, M. (2019) Environmental and agricultural relevance of humic fractions extracted by alkali from soils and natural waters. *J. Environ. Qual.* **48** (2), 217-232.

Phalak, P., Chen, J., Carlson, R. P. and Henson, M. A. (2016) Metabolic modeling of a chronic wound biofilm consortium predicts spatial partitioning of bacterial species. *Bmc. Syst. Biol.* **10**, 90.

Picioreanu, C., Head, I.M., Katuri, K. P., van Loosdrecht, M. C. M. and Scott, K. (2007) A computational model for biofilm-based microbial fuel cells. *Water Res.* **41**, 2921-2940.

Piepenbrock, A. and Kappler, A. (2013) Humic substances and extracellular electron transfer. In: Gescher, J. and Kappler, A., (Ed.), *Microbial metal respiration*, pp. 107-128.

Piepenbrock, A., Schroder, C. and Kappler, A. (2014) Electron transfer from humic substances to biogenic and abiogenic Fe(III) oxyhydroxide minerals. *Environ. Sci. Technol.* **48**, 1656-1664.

Pirbadian, S. and El-Naggar, M. Y. (2012) Multistep hopping and extracellular charge transfer in microbial redox chains. *Phys. Chem. Chem. Phys.* **14**, 13802-13808.

Quansah, C., Drechsel, P., Yirenkyi, B. B. and Asante-Mensah, S. (2001) Farmers' perceptions and management of soil organic matter- a case study from West Africa. *Nutr. Cycl. Agroecosys.* **61**, 205-213.

Ratasuk, N. and Nanny, M. A. (2007) Characterization and quantification of reversible redox sites in humic substances. *Environ. Sci. Technol.* **41**, 7844-7850.

Reardon, P. N. and Mueller, K. T. (2013) Structure of the type IVa major pilin from the electrically conductive bacterial nanowires of *Geobacter sulfurreducens*. *J. Biol. Chem.* **288**, 29260-29266.

Reguera, G., McCarthy, K. D., Mehta, T., Nicoll, J. S., Tuominen, M. T. and Lovley, D. R. (2005) Extracellular electron transfer via microbial nanowires. *Nature* **435**, 1098-1101.

Roden, E. E. (2006) Geochemical and microbiological controls on dissimilatory iron reduction. *Cr. Geosci*. **338**, 456-467.

Roden, E. E., Kappler, A., Bauer, I., Jiang, J., Paul, A., Stoesser, R., Konishi, H. and Xu, H. F. (2010) Extracellular electron transfer through microbial reduction of solid-phase humic substances. *Nat. Geosci.* **3**, 417-421.

Roden, E. E. and Urrutia, M. M. (1999) Ferrous iron removal promotes microbial reduction of crystalline iron(III) oxides. *Environ. Sci. Technol.* **33**, 2492-2492.

Rosso, K. M., Smith, D. M. A., Wang, Z. M., Ainsworth, C. C. and Fredrickson, J. K. (2004) Self-exchange electron transfer kinetics and reduction potentials for anthraquinone disulfonate. *J. Phys. Chem. A.* **108**, 3292-3303.

Sanchez-Monedero, M. A., Roig, A., Cegarra, J., Bernal, M. P. and Paredes, C. (2002) Effects of HCl-HF purification treatment on chemical composition and structure of humic acids. *Eur. J. Soil Sc.* **53**, 375-381.

Scott, D. T., McKnight, D. M., Blunt-Harris, E. L., Kolesar, S. E. and Lovley, D. R. (1998) Quinone moieties act as electron acceptors in the reduction of humic substances by humics-reducing microorganisms. *Environ. Sci. Technol.* **32**, 2984-2989.

Seidel, J., Hoffmann, M., Ellis, K. E., Seidel, A., Spatzal, T., Gerhardt, S., Elliott, S. J. and Einsle, O. (2012) MacA is a second cytochrome *c* peroxidase of *Geobacter sulfurreducens*. *Biochemistry* **51**, 2747-2756.

Shi, L., Squier, T. C., Zachara, J. M. and Fredrickson, J. K. (2007) Respiration of metal (hydr)oxides by *Shewanella* and *Geobacter*: a key role for multihaem *c*-type cytochromes. *Mol. Microbiol.* **65**, 12-20.

Shi, X., Ji, L. L. and Zhu, D. Q. (2010) Investigating roles of organic and inorganic soil components in sorption of polar and nonpolar aromatic compounds. *Environ. Pollut.* **158**, 319-324.

Snider, R. M., Strycharz-Glaven, S. M., Tsoi, S. D., Erickson, J. S. and Tender, L. M. (2012) Long-range electron transport in *Geobacter sulfurreducens* biofilms is redox gradient-driven. *P. Natl. Acad. Sci. USA* **109**, 15467-15472.

Sparks, D. L. (2003) Environmental soil chemistry. Academic Press, Amsterdam; Boston.

Stern, N., Mejia, J., He, S. M., Yang, Y., Ginder-Vogel, M. and Roden, E. E. (2018) Dual role of humic substances as electron donor and shuttle for dissimilatory iron reduction. *Environ. Sci. Technol.* **52**, 5691-5699.

Stevenson, F. J. (1994) Humus chemistry: genesis, composition, reactions, 2nd ed. Wiley, New York.

Sundman, A., Vitzthum, A. L., Adaktylos-Surber, K., Figueroa, A. I., van der Laan, G., Daus, B., Kappler, A. and Byrne, J. M. (2020) Effect of Fe-metabolizing bacteria and humic substances on magnetite nanoparticle reactivity towards arsenic and chromium. *J. Hazard Mater.* **384**, 121450.

von Canstein, H., Ogawa, J., Shimizu, S. and Lloyd, J. R. (2008) Secretion of flavins by *Shewanella* species and their role in extracellular electron transfer. *Appl. Environ. Microb.* **74**, 615-623.

Wang, P., Wang, J. D., Zhang, H., Dong, Y. and Zhang, Y. C. (2019) The role of iron oxides in the preservation of soil organic matter under long-term fertilization. *J. Soil Sediment* **19**, 588-598.

Weber, K. A., Achenbach, L. A. and Coates, J. D. (2006) Microorganisms pumping iron: Anaerobic microbial iron oxidation and reduction. *Nat. Rev. Microbiol.* **4**, 752-764.

Wolf, M., Kappler, A., Jiang, J. and Meckenstock, R. U. (2009) Effects of humic substances and quinones at low concentrations on ferrihydrite reduction by *Geobacter metallireducens*. *Environ. Sci. Technol.* **43**, 5679-5685.

Xiao, Y., Zhang, E. H., Zhang, J. D., Dai, Y. F., Yang, Z. H., Christensen, H. E. M., Ulstrup, J. and Zhao, F. (2017) Extracellular polymeric substances are transient media for microbial extracellular electron transfer. *Sci. Adv.* **3** (7), e1700623.

Yang, Z., Sun, T., Subdiaga, E., Obst, M., Haderlein, S. B., Maisch, M., Kretzschmar, R., Angenent, L.T. and Kappler, A. (2020) Aggregation-dependent electron transfer via redox-active biochar particles stimulate microbial ferrihydrite reduction. *Sci. Total Environ.* **703**, 135515.

Zeng, F. R., Ali, S., Zhang, H. T., Ouyang, Y. B., Qiu, B. Y., Wu, F. B. and Zhang, G. P. (2011) The influence of pH and organic matter content in paddy soil on heavy metal availability and their uptake by rice plants. *Environ. Pollut.* **159**, 84-91.

Zhou, C., Wang, H. Q., Si, Y. B., Wu, K. and Yousaf, A. (2018) Electron shuttles enhance the degradation of sulfamethoxazole coupled with Fe(III) reduction by *Shewanella oneidensis* MR-1. *Environ. Toxicol. Phar.* **62**, 156-163.

Chapter 3-Personal contribution

Experiments in this chapter were conceptually designed by myself, together with Prof. Andreas Kappler and Prof. Stefan B. Haderlein. The soil samples used in this study were taken from Schönbuch forest with the help of Prof. Thomas Scholten. The soil organic matter (SOM) and humic substances (HS) extraction were performed by myself, as well as the microbial Fe(III) reduction experiments. Dr. Edisson Subdiaga helped me with the electrochemical analyses of the SOM and HS samples. Prof. Heike Knicker performed the nuclear magnetic resonance (NMR) measurement and analyzed the NMR data. Other data analyses were done by myself, with the help of Dr. Edisson Subdiaga, Dr. Silvia Orsetti, Prof. Andreas Kappler and Prof. Stefan B. Haderlein. The manuscript was written by myself, Dr. Edisson Subdiaga, Dr. Allison Enright, Dr. Zhe Zhou, Prof. Andreas Kappler and Prof. Stefan B. Haderlein revised the manuscript.

3. High-pH and anoxic conditions during soil organic matter extraction increases its electron-exchange capacity and ability to stimulate microbial Fe(III) reduction by electron shuttling

Yuge Bai[1], Edisson Subdiaga[2], Stefan B. Haderlein[2], Heike Knicker[3], Andreas Kappler[1]

[1]Geomicrobiology, Center of Applied Geosciences, University of Tübingen, Germany

[2]Environmental Mineralogy and Chemistry, Center of Applied Geosciences, University of Tübingen, Germany

[3]Instituto de Recursos Naturales y Agrobiología de Sevilla, Consejo Superior de Investigaciones Científicas, Spain

3.1 Abstract

Soil organic matter (SOM) is redox-active, can be microbially reduced, and transfers electrons in an abiotic reaction to Fe(III) minerals, thus serving as an electron shuttle. The standard procedure to isolate organic matter (OM) from soil involves the use of alkaline and acidic solutions and the separation of humic acid (HA) and fulvic acid (FA). This process potentially leads to unwanted changes in SOM chemical and redox properties. To determine the effects of extraction conditions on the redox and electron shuttling properties of SOM extracts, we prepared HA, FA, and water-extractable organic matter (OM) extracts, applying either a combination of 0.1 M NaOH and 6 M HCl or ultrapure water (pH 7), from soil samples collected from the subsoil (0–15 cm, A horizon, pH 6.5–6.8) in Schönbuch forest, Baden-Württemberg, Germany. Both chemical extractions (NaOH/HCl) and water extractions were done in separate experiments under either oxic or anoxic conditions. Furthermore, we applied the NaOH/HCl treatment to a subsample of the water-extractable OM to separate HA and FA from the water-extractable OM. When comparing the amount of carbon extracted from soil by different extraction methods, we found that FA and HA chemically extracted from the soil can make up to 34%–40% of the soil organic carbon pool while the water-extractable OM only represents 0.41%–2.74% of the total soil organic carbon. The higher extraction efficiency of the chemical extraction is probably due to the deprotonation of carboxyl and phenol functional groups under high pH. Anoxic extraction conditions also led to more extracted carbon. For water-extractable OM, seven times more C was extracted under anoxic conditions compared to oxic conditions. This difference was probably due to the occurrence of microbial reduction and dissolution of Fe(III) minerals in soil during the anoixc water extraction and thus the concomitant release of Fe(III) mienral-cound organic matter. To compare the redox activity of different SOM extracts, the electron-exchange capacity (EEC) of all extracted HA, FA, and water-extractable OM was analyzed and our results showed that, under anoxic extraction conditions, the HA chemically isolated from the water-extractable OM had 2 times higher EEC

values compare to the water-extractable OM itself, suggesting the potential formation of redox-active aromatic functional groups during the extraction with NaOH under anoxic conditions by condensation reactions between amino acids, aldehydes, and hydroxyl- and catechol-containing molecules. We also performed a microbial Fe(III) reduction experiment with all extracts and found that higher EEC of extracts in turn resulted in a higher stimulation of microbial Fe(III) mineral reduction by electron shuttling, i.e., faster initial Fe(III) reduction rates, and in most cases also in higher reduction extents. Our findings suggest that OM extracted with water at neutral pH should be used to better reflect environmental SOM redox processes in lab experiments and that potential artefacts of the chemical extraction method and anoxic extraction condition need to be considered when evaluating and compairing abiotic and microbial SOM redox processes.

3.2 Introduction

Soil organic matter (SOM) contains more organic carbon than the sum of the atmosphere and living plants (Fischlin et al., 2007) and can influence greenhouse gas emission, plant growth, and water quality (Lal, 2004; Marin- Spiotta et al., 2014). Studying SOM is challenging because it needs to be separated from other soil components before doing laboratory experiments (Lehmann and Kleber, 2015). One of the most commonly used methods is a chemical extraction of humic substances (HS) at pH> 12 (Achard, 1786). Although the concept of HS as high-molecular-weight molecules formed by degradation and re-polymerization of biomolecules has been challenged by seeing SOM as a continuum progressively decomposing organic compounds (Lehmann and Kleber, 2015), HS extraction is still applied by many laboratories and the extracted HS are still widely used as a proxy for SOM. Briefly, HS are extracted by adjusting the pH to > 12 using NaOH, followed by acidification of the alkaline extract to pH< 2 to separate humic acids (HA) from fulvic acids (FA) (Achard, 1786). Ion exchange resins, dialysis, and even hydrofluoric acid (HF) treatment are used to

further purify the extracts (IHSS, 2019). Concerns regarding the effectiveness of this harsh chemical extraction method were already raised in 1888 (van Bemmelen, 1888) and have lasted until today (Lehmann and Kleber, 2015; Kleber and Lehmann, 2019).

It has been shown that alkaline extraction influences the chemical composition and the content of redox-active quinoid moieties of the extracted SOM (Piccolo, 1988; Engebretson and von Wandruszka, 1999). Participation in redox reactions is a key property of SOM and relevant for many biogeochemical processes in the environment (Murphy, 2014). For example, under anoxic conditions, SOM can accept electrons from microorganisms, transfer electrons to other electron acceptors such as Fe(III) minerals, and be reoxidized to accept electrons again from microorganisms (Lovley et al., 1996; Kappler et al., 2004; Bauer and Kappler, 2009; Wolf et al., 2009). This electron-shuttling process, which is facilitated by SOM, can significantly increase microbial reduction rates of poorly soluble Fe(III) minerals (Lovley et al., 1996; Jiang and Kappler, 2008), enable microbial reduction of otherwise inaccessible Fe(III) minerals (Lovley et al., 1998) and stimulate indirect reduction of minerals that are spatially separated from the bacteria (Lies et al., 2005). Highly purified FA and HA are used in most electron-shuttling studies to represent SOM (Lovley et al., 1998; Lovley and Blunt-Harris, 1999; Lies et al., 2005; Bauer and Kappler, 2009; Wolf et al., 2009; Klupfel et al., 2014). However, currently it is not known if and to which extent the SOM electron-shuttling capacity is based on protocol induced changes caused by the harsh chemical isolation procedure. Therefore, studies that compare the stimulating effects of SOM extracted with either the traditional chemical extraction method or with water at neutral pH conditions on the microbial Fe(III) reduction are needed.

Piepenbrock and co-authors extracted SOM from a forest soil at circumneutral pH using water (Piepenbrock et al., 2014). Compared to chemically extracted Pahokee Peat humic acids (PPHA), the extracted SOM had a significantly lower reducing capacity (μeq g C^{-1}), which was calculated from the concentration of reduced Fe(II) after the abiotic reaction of PPHA and SOM with Fe(III) citrate. This potentially indicates different types and proportions of functional

groups in these samples. However, due to the different origin of the extracted soils, it remains unclear whether and to which extent the differences in reducing capacities of the SOM extract and PPHA was caused by the chemical extraction methods. Furthermore, in this study the water extraction was conducted only under oxic conditions. Although it is known that the presence of O_2 causes oxidation of certain organic compounds under alkaline conditions and therefore chemical extraction with NaOH should be conducted under anoxic conditions (Bauer and Kappler, 2009; Maurer et al., 2010), it remains unclear whether and how the presence of O_2 influences the abundance of different (redox-active) functional groups and therefore the redox activity of the water-extracted organic compounds under neutral pH.

To determine the effect of these chemicals on the SOM redox properties, we extracted OM from a forest soil using several methods (Figure 3.1). The first was the traditional chemical extraction method (1 M NaOH followed by 6 M HCl) yielding HA and FA under either oxic or anoxic conditions. The second was OM extraction by ultrapure water at neutral pH (water-extractable OM) under either oxic or anoxic conditions. Additionally, we treated the water-extractable OM with NaOH and HCl to further separate HA and FA from the water-extractable OM (also under either oxic or anoxic conditions). We analyzed the electron accepting capacity (EAC, i.e., the number of electrons that can be accepted), the electron donating capacity (EDC, i.e., the number of electrons that can be donated by the OM), and the electron exchange capacity (the sum of EAC and EDC) of all extracted water-extractable OM, FA, and HA fractions. To further compare their electron-shuttling capacity, we performed a microbial Fe(III) mineral reduction experiment with all of the different extracts. The goals of this study were, first, to identify the effects of alkali and oxygen on the EEC values of the water-extractable OM, FA, and HA samples and, second, to compare the rates and extents of microbial ferrihydrite reduction in the presence of the different extract.
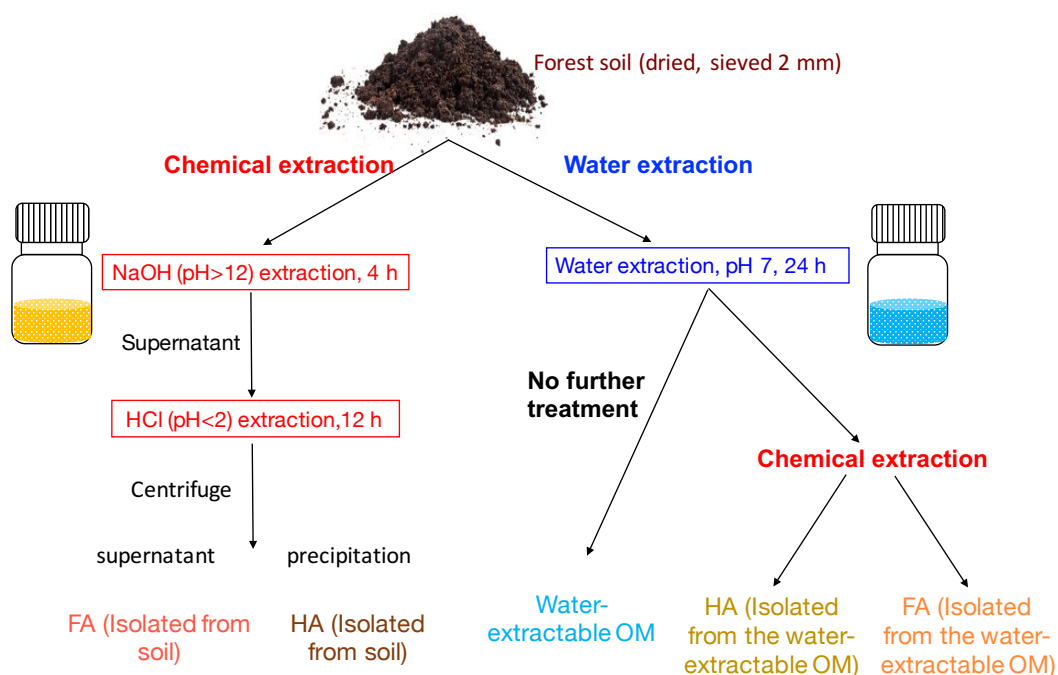
Figure 3.1. Schematic diagram of the soil organic matter (SOM) extraction process.

3.3 Materials and methods

Soil organic matter (SOM) extraction

Top soil (0–15 cm) without leaf litter from the A horizon was collected from the Schönbuch forest, Baden-Württemberg, Germany. The forest is dominated by beech with populations of oak, spruce, and bald cypress and the soil is qualified as vertic cambisol (World Reference Base for Soil, WRB, Schad et al., 2014). Soil was dried (30 °C), ground to pass through a 2 mm sieve by an automatic soil grinder (ball mill, Fritsch, Germany) and stored in the dark at 4 °C. Chemical extraction of FA and HA was modified from the IHSS protocol (IHSS, 2019) as follows. In the IHSS protocol, soil samples are incubated with 0.1M HCl with a ratio of 10 mL of liquid per gram of dry soil, and after 1 h of extraction and XAD-8 resin separation, a fraction called "FA_extract_1" is collected. In our experiment, we did not extract this fraction to avoid using XAD-8 separation. As shown in Figure 3.1, 100 g of soil was incubated with 400 mL of 0.1 M NaOH (pH 12) for 4 h (overhead shaker, 90 rpm, 25 °C) . The slurry was centrifuged (3528 $\times g$, 30 min) and the supernatant was acidified (pH 2) by 6 M HCl

to separate FA (dissolved in the supernatant) and HA (precipitated). Within the present study we define these extracts as FA (isolated from soil) and HA (isolated from soil). Water-extractable OM was prepared following Piepenbrock et al. (2014) (Figure 3.1). 100 g of soil was incubated with 400 mL of ultrapure water (resistivity = 18.2MΩcm, 25 °C; Milli-Q, Millipore) at a pH of 7 (pH was monitored during the extraction and it ranged between 7.02 and 7.33). The pH of the water extraction was adjusted to 7 to avoid any possible artefacts resulting from further pH adjustment prior to analyses and experiments that require the sample pH to be 7 such as the electrochemical analysis or the microbial Fe(III) reduction. The slurry was centrifuged after 24 h; we collected and defined the supernatant as water-extractable OM. A 200 mL aliquot of the supernatant containing the water-extractable OM was amended with 0.1 M NaOH until a pH of 12. After 4 h of incubation, the pH of the solution was adjusted to < 2 by 6M HCl to precipitate HA and to separate FA; this FA and HA are defined as FA (isolated from water-extractable OM) and HA (isolated from water-extractable OM). Anoxic chemical extractions (NaOH/HCl) and water extractions were performed in a N_2-filled anoxic glove box; filtration (0.45 μm, polyethersulfone membrane (PES), Millipore, Germany) was used instead of centrifugation to remove remaining soil after the extraction. All collected extracts were freeze-dried under oxic conditions and stored at 4 °C in dark until use.

Organic carbon quantification

Dissolved organic carbon (DOC) of water-extractable OM and FA isolated from soil was quantified using a DOC analyzer (model 2100S, Analytik Jena, Germany) directly from the extracted solutions after passing through a 0.45 μm syringe filter (polyethersulfone membrane (PES), Millipore, Germany). The total organic carbon (TOC) of all extracted HA and the FA isolated from the water-extractable OM were quantified using a TOC analyzer (model 2100S, Analytik Jena, Germany) from the freeze-dried powders.

Nuclear magnetic resonance (NMR) measurements

NMR analysis was conducted from freeze-dried water-extractable OM, HA, and FA samples. Solid-state ^{13}C NMR spectra were obtained with a Bruker AVANCE III HD 400 MHz wide board operating at a frequency of 100.63 MHz using zirconium rotors of 4 mm OD with Kel-F caps. The cross-polarization magic-angle spinning (CPMAS) technique was applied during magic-angle spinning of the rotor at 14 kHz. A ramped ^{1}H pulse was used in order to circumvent spin modulation of Hartmann–Hahn conditions. A contact time of 1 ms and a 90° ^{1}H-pulse width of 2.2 μs were used for all spectra. The ^{13}C-chemical shifts were calibrated to tetramethylsilane (0 ppm) and were calibrated with glycine (176.04 ppm). The aromaticity of samples was calculated following a previous study (Abelmann et al., 2005).

Specific UV absorbance at 254 (SUVA$_{254}$) analysis

SUVA$_{254}$ analysis was conducted from water-extractable OM, HA, and FA solutions dissolved in Milli-Q water at concentrations of 10 mg C L^{-1}. All solutions were filtered with a 0.45 μm syringe filter (polyethersulfone membrane (PES), Millipore, Germany), and the dissolved organic carbon (DOC) concentration of all samples was analyzed prior to the SUVA$_{254}$ analysis (DOC analyzer, model 2100S, Analytik Jena, Germany). The SUVA$_{254}$ values of all samples were measured in a 1 cm rectangular quartz cuvette with a fluorescence spectrophotometer (FluoroMax-4, Jobin Yvon– SPEX instruments, New Jersey, USA). The final SUVA$_{254}$ values of all extracts were calculated with Equation (1):

$$SUVA_{254=} UV_{254}/DOC \tag{1}$$

where UV$_{254}$ is the absorbance at 254 nm and there is a 1 cm optical path length.

Microwave plasma atomic emission spectrometer (MP-AES) analysis

Metal contents were analyzed by a microwave plasma atomic emission spectrometer (MP-AES) (4100, Agilent Inc., Santa Clara, CA, USA) in the extracted water-extractable OM, HA, and FA samples. Prior to the MP-AES analysis, a 0.5 g sample was digested with 10 mL

2% HNO_3 in a microwave oven at 190 °C (800 W) for 10 min; after cooling down to room temperature, it was centrifuged for 10 min at 28 649 $\times g$ and the supernatant was used for the analysis. The data for FA (isolated from soil, oxic) and HA (isolated from water-extractable OM, oxic) are missing due to the lack of enough samples. The unit of all metal concentrations is milligrams per kilogram, blank means the concentration of the corresponding metal is too low to be detected.

Electrochemical analysis

Electrochemical analysis followed the method described by Aeschbacher et al. (2010). Freeze-dried extracts (powders) were dissolved in 100 mM of phosphate buffer (pH 7) at a concentration of 100 mg C L^{-1}, After overnight agitation at 300 rpm at room temperature, samples were filtered through 0.22 μm syringe filters (mixed cellulose ester (MCE), Millipore, Germany). All preparations and measurements were conducted in an anoxic glove box. The number of electrons transferred to and from all extracts was quantified by integration of reductive and oxidative current responses after baseline correction in mediated electrochemical reduction (MER; at E_h = -0.49 V) and mediated electrochemical oxidation (MEO; E_h = +0.61 V) with 1'1-ethylene-2,2'-bipyridyldiylium di-bromide (DQ) and 2,2'-azino-bis (3-ethylbenzothiazoline-6-sulfonic acid) (ABTS) as electron transfer mediators, respectively. To obtain the EAC and EDC values, the integrated current response was normalized to the measured DOC of all extracts prior to the EEC analysis ($DOC_{SOM/FA/HA}$ (mg C L^{-1}), DOC analyzer, model 2100S, Analytik Jena, Germany) as shown in Equation. (2) and (3):

$$EAC = I_{red}dt/(F \times DOC_{SOM/FA/HA}) \tag{2}$$

$$EDC = \int I_{ox}dt/(F \times DOC_{SOM/FA/HA}) \tag{3}$$

Where I_{red} and I_{ox} ([A]) are baseline-corrected reductive and oxidative currents in MER and MOR, respectively (F = Faraday constant).

Microbial Fe(III) reduction experiment and calculation of microbial Fe(III) reduction rate

Solutions of organic matter extracts for the microbial Fe(III) reduction experiment were prepared by dissolving freeze-dried powders in 50 mM phosphate buffer (pH 7.0-7.2) at 500 mg C L^{-1}, agitation overnight (300 rpm, room temperature), filtration and sterilization (0.22 μm syringe filters, mixed cellulose ester (MCE), Millipore, Germany), as described before (Jiang and Kappler, 2008). Although the chosen phosphate concentration is higher than typically observed in nature and can potentially lead to the formation of Fe(II) phosphate minerals (e.g., vivianite) during our microbial Fe(III) reduction experiment, this phosphate buffer was chosen to enable comparison of our study to previous studies (Bauer and Kappler, 2009; Jiang and Kappler, 2008; Klupfel et al., 2014; Piepenbrock et al., 2014). All solutions were deoxygenated 3 times (each time 3 min vacuum and 3 min N_2-flushing) and stored in dark bottles to avoid photochemical reactions. Ferrihydrite was prepared as described before (Amstaetter et al., 2012) and stored no more than 2 months (4 °C) before use.

Shewanella oneidensis MR-1 cells from a frozen stock were streaked on oxic lysogeny broth (LB) agar plates (10 g L^{-1} peptone, 5 g L^{-1} yeast extract, 10 g L^{-1} NaCl and 15 g L^{-1} agar). Colonies were transferred to liquid LB medium and incubated at 30 °C for 14 h, harvested by centrifugation (10 min, 8602 $\times g$) and then washed three times with anoxic SBM medium (0.225 g L^{-1} K_2HPO_4, 0.225 g L^{-1} KH_2PO_4, 0.46 g L^{-1} NaCl, 0.225 g L^{-1} $(NH_4)_2SO_4$, 2.18 g L^{-1} Na-lactate, 0.117 g L^{-1} $MgSO_4 \cdot 7H_2O$, 2.38 g L^{-1} HEPES, pH 7.2-7.5). For the Fe(III) reduction experiments, washed cells were added at a final concentration of 10^7 cells mL^{-1} to solutions of water-extractable OM, FA, HA (50 mg C L^{-1}) and ferrihydrite (15 mM Fe(III)) in SBM medium, (phosphate in the SBM medium was 5 mmol L^{-1}). AQDS, i.e. 2,6-anthraquinone disulphonate, a quinone model compound commonly used in electron shuttling studies that can significantly increase the rates of microbial Fe(III) reduction, was used as 100 μmol L^{-1} in our experiments as a reference for a significant stimulation of Fe(III) reduction by our extracted OM via electron

shuttling. The headspace was flushed with N_2 and the bottles were incubated in the dark (30 °C). At each sampling point, an 100 μl aliquot was taken from each bottle, acidified and incubated with 900 μl of 1 M HCl for 1 h to facilitate mineral dissolution, centrifuged (28649 ×g, 5 min), and the total Fe(II) concentration was quantified with the spectrophotometric ferrozine assay in a microtiterplate (Hegler et al., 2008; Stookey, 1970). The fastest reduction rates of the microbial Fe(III) reduction experiments were calculated as shown and explained in the Figure S3.1.

3.3 Results

Quantity of soil organic carbon extracted by different methods and characterization of extracted OM, HA and FA

Comparison of different extraction methods revealed that the amount of soil-extracted carbon varied depending on the presence or absence of O_2 during the extraction and on the type of extraction liquid (Table 3.1). Extraction with H_2O at neutral pH under oxic conditions followed by NaOH and HCl treatment to separate HA and FA in the water-extractable OM yielded 0.036, 0.021 and 0.014 g C in the water-extractable OM, FA and HA fractions, respectively, corresponding to 0.41%, 0.24% and 0.15% of the total carbon present in the soil. In contrast, anoxic water extraction significantly increased the fraction of extracted carbon to 0.234, 0.146, and 0.079 g C in the water-extractable OM, FA and HA fractions, respectively, corresponding to 2.74%, 1.69% and 0.90% of the total soil C. Chemical extraction directly from soil using NaOH and HCl under oxic conditions yielded 1.451 g in the extracted FA (17.0% of the total carbon present in the soil) and 1.450 g C in HA (17.0% of the total carbon present inthe soil). Conducting the same chemical extraction from soil under anoxic conditions led to a higher percentage of extracted carbon for FA (20.7%) and HA (22%) than under oxic conditions.

Specific UV absorbance at 254 nm ($SUVA_{254}$) indicates the aromaticity of the extracted OM, FA and HA (Table 3.1). Water-extractable OM showed a $SUVA_{254}$ value of 0.018 mg^{-1} C cm^{-1} under oxic conditions and the value increased to 0.027 mg^{-1} C cm^{-1} when extracted under anoxic conditions. Similarly, for both FA isolated from water-extractable OM and FA isolated from soil, the $SUVA_{254}$ values were higher under anoxic conditions than under oxic conditions. HA extracts isolated from the water-extractable OM under oxic conditions showed a $SUVA_{254}$ value of 0.068 mg^{-1} C cm^{-1}, higher than the 0.018 mg^{-1} C cm^{-1} of the water-extractable OM itself obtained under oxic conditions. A higher $SUVA_{254}$ value for the HA isolated from the water-extractable OM (0.207 mg^{-1} C cm^{-1}) than for the water-extractable OM itself (0.027 mg^{-1} C cm^{-1}) was also found under anoxic extraction conditions. A 2-way ANOVA statistical analysis revealed that both oxic versus anoxic conditions and the extraction method (neutral pH water versus chemical extraction) resulted in different $SUVA_{254}$ values at a significance level of $P < 0.05$ (Table S3.1). In general, anoxic conditions and the chemical extraction method led to higher $SUVA_{254}$ values of the extracts, suggesting that these extracts had higher degree of aromaticity (Korshin et al., 1997). ^{13}C-NMR analysis of extracted OM, FA and HA (Figure 3.2) confirmed higher contents of aromatic carbon in samples subject to chemical extraction or anoxic conditions.

Table 3.1. The dissolved organic carbon (DOC) concentration of the water-extractable OM and FA isolated from soil, the total organic carbon in all extracted OM, HA and FA fractions, the calculated percentage of carbon extracted from the soil, as well as the specific absorbance value of all extracts at 254 nm wavelength ($SUVA_{254}$). Values are means±standard deviation (SD) of triplicates.

	Water-extractable OM		FA				[a]HA			
	Water-extracted, oxic	Water-extracted, anoxic**	[a]Isolated from water-extractable OM, oxic	[a]Isolated from water-extractable OM, anoxic**	Isolated from soil, oxic	Isolated from soil, anoxic**	Isolated from water-extractable OM, oxic	Isolated from water-extractable OM, anoxic**	Isolated from soil, oxic	Isolated from soil, anoxic**
DOC concentration in extract (mg C L^{-1})	0.149± 0.036	0.890± 0.041	–	–	5.800± 0.025	6.320± 0.071	–	–	–	–
[b]Total organic carbon in extract (g)	0.036± 0.012	0.234± 0.015	0.021± 0.002	0.146± 0.013	1.451± 0.008	1.770± 0.028	0.014± 0.003	0.079± 0.000	1.450± 0.002	1.881± 0.029
[c]Percentage of carbon extracted from soil (%)	0.41±0.14	2.74±0.18	0.24± 0.02	1.69± 0.15	17.0± 0.09	20.7± 0.32	0.15± 0.03	0.90± 0.00	17.0± 0.02	22.0± 0.34
[d]$SUVA_{254}$ (mg^{-1} C cm^{-1})	0.018	0.027	0.017	0.029	0.023	0.042	0.068	0.207	0.083	0.265

[a]TOC of all HA extracts and of the FA isolated from the water-extractable OM was directly quantified from the freeze-dried powders. The carbon content of all other liquid samples was determined as DOC, measured directly from the solutions after passing through 0.45 μm syringe filter

[b]Total organic carbon content in the extract was directly quantified form the freeze-dried samples of FA isolated from the water-extractable OM (oxic, anoxic) and all of the HA extracts. For the other extracts, the total organic carbon was calculated by DOC (mg C L^{-1}) $\times$ volume of the extracted solution (L)

[c]Percentage of carbon extracted from soil = Total carbon extracted (mg)/soil carbon content (8.54 mg)

[d]Specific UV absorbance 254 nm ($SUVA_{254}$) = $UV_{254} \times$ DOC (mg C L^{-1}), b is the optical path length in centimeter (1 cm in this experiment)

**The percentage of carbon extracted from soil of the samples are significantly different (n=2, two-sided t-test, P< 0.05)
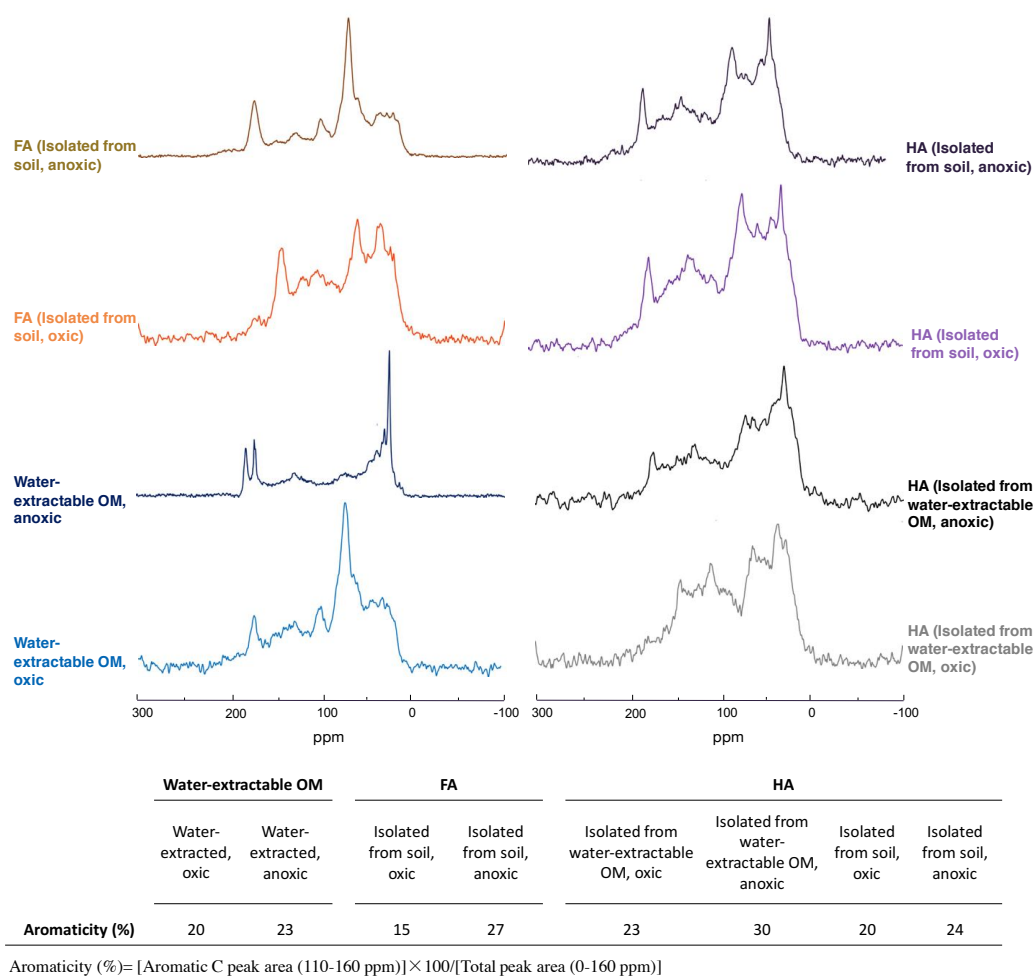
	Water-extractable OM		FA		HA			
	Water-extracted, oxic	Water-extracted, anoxic	Isolated from soil, oxic	Isolated from soil, anoxic	Isolated from water-extractable OM, oxic	Isolated from water-extractable OM, anoxic	Isolated from soil, oxic	Isolated from soil, anoxic
Aromaticity (%)	20	23	15	27	23	30	20	24

Aromaticity (%)= [Aromatic C peak area (110-160 ppm)]×100/[Total peak area (0-160 ppm)]

Figure 3.2. ^{13}C-NMR spectra of water-extractable OM, FA and HA. All spectra were collected from freeze-dried extracts and the aromaticity of samples was calculated as the percentage of aromatic C peak area to the total peak area. The relative intensity distributions of specific chemical shifts are shown in Table S3.2. Spectra for FA isolated from water-extractable OM cannot be presented due to the lack of an adequate amount of sample for analysis.

Furthermore, after 24 h water extraction of OM, we found a maximum Fe(II) concentration of 3 mmol L^{-1} in the water-extractable OM solution. Although, as shown in Table S3.3, more than 90% of the Fe was removed by filtration (0.22 μm, mixed cellulose ester (MCE), Millipore, Germany) and around 30% of the remaining Fe(II) was oxidized to Fe(III) during the oxic freeze drying process, there was still 15-123 μmol L^{-1} total Fe present in the water-extractable OM and FA or HA isolated from it. This Fe is potentially redox-active and can contribute to the redox properties of the extracted OM. For example, a previous study showed

that 4 mg L^{-1} of Fe(III) yielded an absorbance value of 0.65 cm^{-1} at 254 nm wavelength (Weishaar et al., 2003). Therefore, we believe that the high $SUVA_{254}$ value of HA isolated from the water-extractable OM compared to $SUVA_{254}$ values of HA shown in previous studies could be caused by the presence of Fe(II) and Fe(III) in the sample due to the microbial Fe(III) reduction that occurred under the anoxic extraction conditions. However, since this Fe is an integral part of the OM in the environment and we were interested in determining the role of environmentally relevant OM extracts in electron shuttling, we decided not to further purify the extracts (also because this probably would have changed the properties of the present redox-active organic matter).

Redox properties of extracted water-extractable OM, FA and HA

We used mediated electrochemical reduction and oxidation to quantify the EAC, EDC and thus the EEC of all water-extractable OM, FA, and HA extracts (Figure 3.3). Based on the Fe content we calculated the contribution of the Fe to the redox properties of all extracts (Table S3.3). A 2-way ANOVA statistical analysis revealed that both the extraction condition (anoxic versus oxic) and the extraction method (neutral pH water versus NaOH) resulted in significantly different EEC values ($P<0.05$; Table S3.4). The EEC of water-extractable OM obtained under oxic conditions was 32 μmol e^- mmol C^{-1} (with ca. 4 μmol e^- mmol C^{-1} from Fe), whereas when extracted anoxically, it increased to 44 μmol e^- mmol C^{-1} (with 14.8 μmol e^- mmol C^{-1} from Fe). Higher EEC values under anoxic compared to oxic extraction conditions were also observed for all extracted FA: for FA isolated oxically from the water-extractable OM, the EEC was 13 μmol e- mmol C^{-1} (2.3 μmol e^- mmol C^{-1} from Fe), while it increased to 24 μmol e^- mmol C^{-1} (2.7 μmol e^- mmol C^{-1} from Fe) when FA was isolated anoxically from the water-extractable OM. The EEC of FA isolated from soil under anoxic conditions was 33 μmol e^- mmol C^{-1} higher than FA isolated from soil under oxic conditions. Similar to FA, for the HA isolated from water-extractable OM, the EEC values increased from 15 μmol e^- mmol C^{-1} (1.9 μmol e^- mmol C^{-1}

from Fe) under oxic conditions to 83 μmol e⁻ mmol C⁻¹ (7.3 μmol e- mmol C⁻¹ from Fe) under anoxic conditions. For HA isolated from soil, EEC values increased from 40 μmol e- mmol C⁻¹ under oxic conditions to 127 μmol e- mmol C⁻¹ under anoxic conditions.

The total number of electrons that can be exchanged (that means transferred from Fe(III)-reducing bacteria to the OM, or from the OM to Fe(III) minerals) by water-extractable OM before and after the chemical separation of FA and HA from this water-extractable OM was also calculated (the recovery of EEC) under both oxic and anoxic conditions (Figure 3.3). For the extracts obtained under anoxic conditions, the sum of total exchangeable electrons values of the FA and HA isolated from water-extractable OM (786 μmol e⁻) was almost identical to that of water-extractable OM itself (836 μmol e⁻). In contrast, under oxic conditions, the sum of the EEC values of the FA and HA separated from the water-extractable OM was 324 μmol e⁻, ca. 5-times higher than the EEC value of the water-extractable OM (64 μmol e⁻). This confirms that the traditional chemical extraction procedure conducted under oxic conditions strongly enhances the redox capacity of the samples.

In addition to the EEC that represents the total amount of electrons that can be stored by the extracted organic compounds, the individual EAC and EDC values can be used to characterize the redox state of the water-extractable OM, HA and FA. The EDC and EAC quantify how many electrons are already stored in the molecules (EDC) and how many electrons can still be taken up by functional groups that can be reduced (EAC) (Figure 3.3). Surprisingly, the EAC values were larger for all FA and HA extracts obtained under anoxic extraction conditions than under oxic conditions (Figure 3.3). The higher EAC under anoxic conditions suggests the presence of more functional groups that can be reduced in FA and HA extracted in the absence of oxygen, meaning that the additional amount of organic compounds that was extracted under anoxic conditions compared to oxic conditions contain more oxidized functional groups.
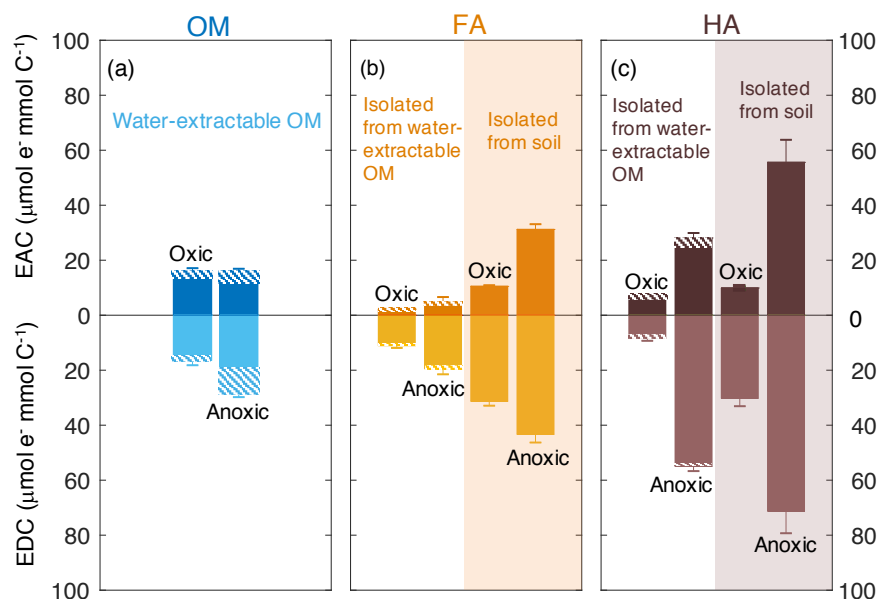
	EEC (mmol e⁻ mmol C⁻¹)	*Carbon content (mmol)	Total number of electrons that can be exchanged (mmol e⁻)
FA (Isolated from water-extractable OM, oxic)	13	3	39
HA (Isolated from water-extractable OM, oxic)	15	19	285
SUM			324
Water-extractable OM, oxic	32	2	64
FA (Isolated from water-extractable OM, anoxic)	24	12	288
HA (Isolated from water-extractable OM, anoxic)	83	6	498
SUM			786
Water-extractable OM, anoxic	44	19	836

*carbon content was calculated from the total organic carbon content in extracts in Table 3.1

Figure 3.3. Electron exchange capacity (EEC), the sum of EAC (electron accepting capacity) and EDC (electron donating capacity) of the extracted water-extractable OM (a), FA (b) and HA (c). Error bars indicate the standard deviation of 4 replicates. All EAC/EDC values were normalized to the DOC of the extracts.

Effects of different organic matter extracts on the rate and extent of microbial ferrihydrite reduction and mineral transformation during reduction

To determine the effects of water-extractable OM, FA and HA extracts on microbial Fe(III) reduction, the Fe(III) mineral- ferrihydrite was incubated with the Fe(III)-reducing bacteria *Shewanella oneidensis* MR-1 in experiments amended with our extracts and total Fe(II) concentration was monitored over time (Figure 3.4). The highest initial microbial Fe(III)

reduction rates were determined as shown in the supporting information (Figure S3.1). The presence of AQDS stimulated ferrihydrite reduction to Fe(II) with a maximum reduction rate of 3.12 ± 0.38 mM Fe(II) d^{-1} compared to experiments without electron shuttle with a rate of 0.79 ± 0.31 mM Fe(II) d^{-1} (Figure S3.1(a), (b)). The observed decrease of total Fe(II) after 5 days of incubation (from 14.67 mM to 6.87 mM) in the AQDS-amended setup was caused by Fe(II) loss due to sorption of Fe(II) or precipitation of Fe(II) (e.g. as Fe(II)-phosphate mineral due to the presence of phosphate buffer) at the wall of the glass bottles (Figure. S3.2). After the addition of oxic and anoxic water-extractable OM (Figure S3.1(c), (d)), Fe(III) was reduced at maximum rates of 1.53 ± 0.20 mM Fe(II) d^{-1} and 2.07 ± 0.43 mM Fe (II) d^{-1}, respectively, suggesting higher reduction rates than without any electron shuttle (0.79 ± 0.31 mM Fe(II) d^{-1}).

When comparing Fe(III) reduction in the presence of the different HA extracts (Figure S3.1(i)-(l)), we found that amendment with HA isolated from soil under anoxic conditions showed the fastest reduction rate (1.83 ± 0.03 mM Fe(II) d^{-1}) followed by HA isolated from water-extractable OM anoxically (1.70 ± 0.25 mM Fe(II) d^{-1}) and HA isolated from soil oxically (1.55 ± 0.08 mM Fe(II) d^{-1}). The reduction rate of the experiment amended with HA isolated oxically from the water-extractable OM was 0.82 ± 0.27 showing slight stimulation effect compare to the setup without electron shuttle (0.79 ± 0.31mM Fe(II) d^{-1}). Addition of FA increased Fe(III) reduction rates significantly in all cases (Figure S3.1(e)-(h)). In the presence of FA isolated oxically and anoxically from water-extractable OM, the fastest rates were 2.03 ± 0.54 and 2.22 ± 0.36 mM Fe(II) d^{-1}, respectively. After addition of FA isolated from soil under oxic and anoxic conditions, the maximum reduction rates were even faster with 2.31 ± 0.15 and 3.05 ± 0.07 mM Fe(II) d^{-1}. Control samples with only OM and ferrihydrite (without bacteria) did not show any ferrihydrite reduction (Figure S3.3). In addition to differences in reduction rates depending on the identity of the added organic extract, we also

found differences in reduction extents. In most cases, the reduction extent was higher in the presence of OM compared to OM-free experiments (3.87 mM of Fe(II) after 15 days). Specifically, experiments amended with FA showed higher microbial Fe(III) reduction extents than with HA. After 25 days of incubation, experiments with FA extracted chemically from soil under anoxic conditions reduced 10.87 mmol L^{-1} Fe(III) to Fe(II), while the maximum Fe(III) reduction extent in the presence of added HA (chemically isolated from anoxically water-extracted SOM) was about 7.08 mmol L^{-1} Fe(II) (Figure 3.4(c), (e)).

Since the used OM extracts contained some Fe(II) and Fe(III), we evaluated the contribution of these ions to the observed Fe(III) reduction (Table S3.3). First, the Fe(II) present in the water-extractable OM, FA and HA ranged from 7.2 (FA isolated from water-extractable OM, oxic) to 79.2 μmol L^{-1} (water-extractable OM, anoxic) (Table S3.3) and made up between 1-17.6% of the measured Fe(II) concentration after 30 minutes of incubation. With the increase of Fe(II) concentration over time, the percentage of Fe(II) present in the extracts to the measured Fe(II) concentration decreased to less than 0.1% and is therefore negligible. Second, the influence of Fe(III) initially present in the water-extracted SOM, FA and HA (Table S3.3) can be neglected as well, because the Fe(III) concentration of the extracted organic matter fractions ranged from 8.7-43.9 μmol L^{-1} (Table S3.3), but the ferrihydrite concentration used in the experiments was 15 mmol L^{-1}.
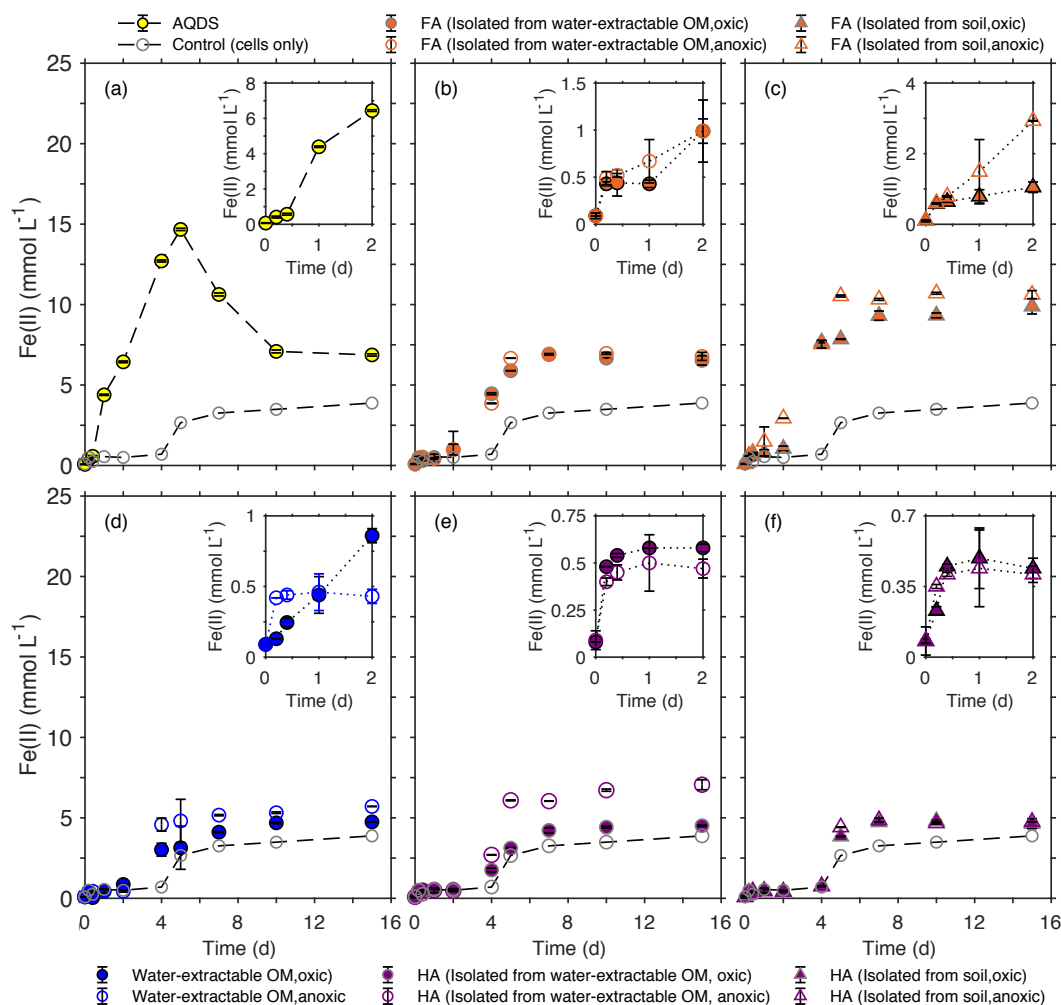
Figure 3.4. Microbial reduction of ferrihydrite (15 mmol L^{-1}) by *Shewanella oneidensis* MR-1 (10^7 cells mL^{-1}) in the presence of 15 mmol L^{-1} lactate as electron donor and 100 μmol L^{-1} AQDS (a), 50 mg C L^{-1} FA (b, c), water-extractable OM (d), and HA (e, f) as electron shuttles, presented as the formation of total Fe(II) over time. The inserts in panels a-f show the data points for the first 2 days of incubation. Control samples were incubated at the same condition in the absence of electron shuttles. Error bars represent standard deviations of triplicate bottles.

3.4 Discussion

Effects of the presence of oxygen on the amount and properties of SOM extracts

The presence and absence of oxygen impacted the amount of water-extractable OM. Under anoxic conditions, water at neutral pH extracted about 6.7 times more organic carbon

than under oxic conditions (Table 3.1). The presence of Fe(II) at the end of extraction in all anoxic extracts suggested that the higher amount of extracted OM is probably related to microbial Fe(III)-mineral reduction and the release of mineral-bound OM during mineral dissolution. A correlation between the dissolved organic carbon (DOC) concentration and the amount of Fe(II) in pore water was reported before for sediment samples that were incubated in the dark under anoxic conditions for 14 days (Dadi et al., 2017). In-situ monitoring of the DOC flux in pore water of marine sediment or freshwater wetland also suggested an increase in DOC with increasing microbial iron(III) mineral reduction (Burdige et al., 1992; Burdige et al., 1999; Chin et al., 1998). Other studies also suggested an increase in DOC under anoxic conditions due to the microbial iron(III) mineral reduction and dissolution and the concomitant release of organic carbon (OC) that was co-precipitated with and adsorbed to the iron(III) minerals (Gu et al., 1994; Riedel et al., 2013; Shimizu et al., 2013).

In addition to differences in the amount of extracted OM, the presence or absence of oxygen also influenced the aromaticity of the extracted SOM, as shown by the $SUVA_{254}$ values (Table 3.1) and ^{13}C -NMR data (Figure 3.2). Water-extractable OM extracted under anoxic conditions showed a higher aromaticity, suggesting that the additional organic matter mobilized by reductive dissolution of iron minerals possesses a higher degree of aromaticity. This is in line with findings described by other studies (Avneri-Katz et al., 2017; Coward et al., 2019; Gu et al., 1994; Lv et al., 2016). Kothawala and co-authors (Kothawala et al., 2012) incubated oxically-extracted soil solution with soils with different mineral composition. SUVA and fluorescence index analysis of the remaining non-sorbed organic matter showed that regardless of the soil type, the aromatic functional groups were preferentially adsorbed to the soil minerals.

Effects of extraction pH on the amount and properties of extracted organic matter

The practice of extracting and isolating HA and FA using NaOH and HCl under anoxic conditions has been the established standard protocol (IHSS, 2017). As early as in 1972, Swift

and Posner (Swift and Posner, 1972) showed that by incubating a peat HA with 1 M NaOH under oxic conditions for 30 days, more than half of the HA was degraded to low-molecular-weight molecules and amino acid N was lost from the HA. Later studies also reported the hydrolysis of esters in NOM to carboxylic acid groups when exposing NOM to NaOH under oxic conditions (Ritchie and Perdue, 2008). Consistent with previous studies, our SUVA$_{254}$ (Table 3.1), ^{13}C-NMR (Figure 3.2) and EEC (Figure 3.3) results showed that FA and HA isolated from soil under oxic conditions had lower aromaticity and EEC compared to the FA and HA isolated from soil under anoxic conditions. This indicates that degradation of aromatic structures and functional groups in the OM to smaller molecules occurs in the presence of O$_2$ under higher pH conditions.

However, we found that even under anoxic conditions, the chemical extraction extracted up to 100 times more carbon than the water extraction at neutral pH (Table 3.1), consistent with previous studies (Aiken, 1985). This higher extraction efficiency at high pH could be due to the deprotonation of carboxyl and phenol functional groups leading to both higher aqueous solubility and electrostatic repulsion of OM from negatively charged soil minerals (Kleber et al., 2015) or due to the hydrolysis of plant material and the formation of smaller oligo- and monomers (Sparks, 2003). Not only the amount of C extracted but also the properties of the extracted FA and HA are affected by the chemical extraction under anoxic conditions. Our results indicate that the HA isolated from soil have higher aromaticity than water-extractable OM under anoxic extraction conditions. On the one hand, the higher aromaticity in HA isolated from soil can probably be explained by the extra amount of C extracted from soil by the chemical extraction method. On the other hand, this cannot be the only explanation, since the HA isolated from the water-extractable OM also had higher aromaticity than the water-extractable OM itself. This suggests the formation of aromatic functional groups during the extraction with NaOH under anoxic conditions by condensation reactions between amino acids, aldehydes, hydroxyl-and catechol-containing molecules. Such condensation reactions could

result in larger molecules with a higher degree of aromaticity (Gieseking, 1975; Golchin et al., 1994; Kappler and Brune, 1999; Kappler and Haderlein, 2003). A recent study comparing OM extraction from a freshwater sediment using water (acidified to pH 2 with 1 M HCl), with an extraction using 0.1 M sodium pyrophosphate (pH 10) and 0.5 M NaOH (pH 12) also revealed a higher aromaticity in the alkali-extracted OM (Fox et al., 2017). Using Fourier-transform infrared spectroscopy (FTIR) and electrospray ionization Fourier-transform ion cyclotron resonance spectrometry (ESI-FTICR-MS), these authors showed that OM extracted by sodium pyrophosphate and NaOH had more condensed aromatic compounds.

Electron exchange capacity (EEC) of soil extracts determines their ability to stimulate microbial Fe(III) reduction

Our data showed that the rates of microbial ferrihydrite reduction differed in the presence of different OM extracts. The observed differences in Fe(III) reduction rates can either be a result of the differences in OM redox activity (e.g. number and redox potentials of redox-active functional groups) and the resulting function of the OM as electron shuttle or due to different secondary mineral phases that can form during ferrihydrite reduction. However, a previous microbial Fe(III) mineral reduction study of ferrihydrite (15 mM Fe(III)) in the presence of 50 mg C L^{-1} OM, 0.8 mM phosphate buffer and 2×10^5 cells mL^{-1} *Shewanella oneidensis* MR-1 showed no goethite or magnetite (based on ^{57}Fe-Moessbauer and XRD analysis) but vivianite as the major mineral phase produced (Amstaetter et al., 2012). The transformation of ferrihydrite to vivianite instead of goethite or magnetite in presence of phosphate buffer was also reported in other studies using similar concentration of OM, buffer, cells and ferrihydrite (Chen et al., 2003; Piepenbrock et al., 2011; Shimizu et al., 2013). The formation of more crystalline secondary mineral phases such as goethite was only observed during ferrihydrite reduction in the absence of phosphate (Borch et al., 2007; Hansel et al., 2003). Abiotic experiments showed that phosphate inhibits the transformation of ferrihydrite to

magnetite or goethite by blocking of surface sites of ferrihydrite, therefore prevents the sorption of the produced Fe(II) on the Fe(III) mineral, thus lowering the number of surface sites where conversion of ferrihydrite to magnetite or goethite can take place (Galvez et al., 1999). Therefore, the transformation of ferrihydrite to magnetite or goethite is not expected to happen in our experiments and the following discussion will focus on the influence of the redox activity of the extracted OM on the rate and extent of the microbial Fe(III) reduction.

As measures for the redox activity of the different extracted OM fractions, we determined their potential for accepting electrons (EAC) and for accepting and donating electrons (EEC). Correlating the EAC values of our different OM extracts and the maximum microbial ferrihydrite reduction rates showed that the higher the EAC values of the extracted OM, FA and HA, the faster the microbial Fe(III) reduction rates are (Figure 3.5). As shown before (Aeschbacher et al., 2012), (hydro)quinone functional groups contribute mainly to the measured EAC values in OM and these quinone moieties are thought to be the major functional group responsible for electron transfer between Fe(III)-reducing bacteria and Fe(III) minerals during electron shuttling. Scott et al. (1998) reported a direct correlation between OM oxidation capacity and the stable free-radical content in the OM, stemming from semiquinone radicals (Lovley et al., 1996; Scott et al., 1998). However, we also found a correlation between EEC values and the maximum microbial ferrihydrite reduction rates in the presence of water-extractable OM, HA and FA. Since higher EEC values reflects higher contents of aromatic/polycondensed aromatic compounds in the OM (Aeschbacher et al., 2012), our results also indicate that, apart from quinones, also other aromatic functional groups were involved in the microbial Fe(III) reduction with OM as electron shuttles and these functional groups also influence the electron transfer efficiency between the Fe(III)-reducing bacteria, the OM and the Fe(III) minerals. Support for the participation of non-quinone groups in such OM electron

transfer studies also comes from previous analyses of redox properties and stable free-radical

concentrations in OM (Chen et al., 2003; Struyk and Sposito, 2001).
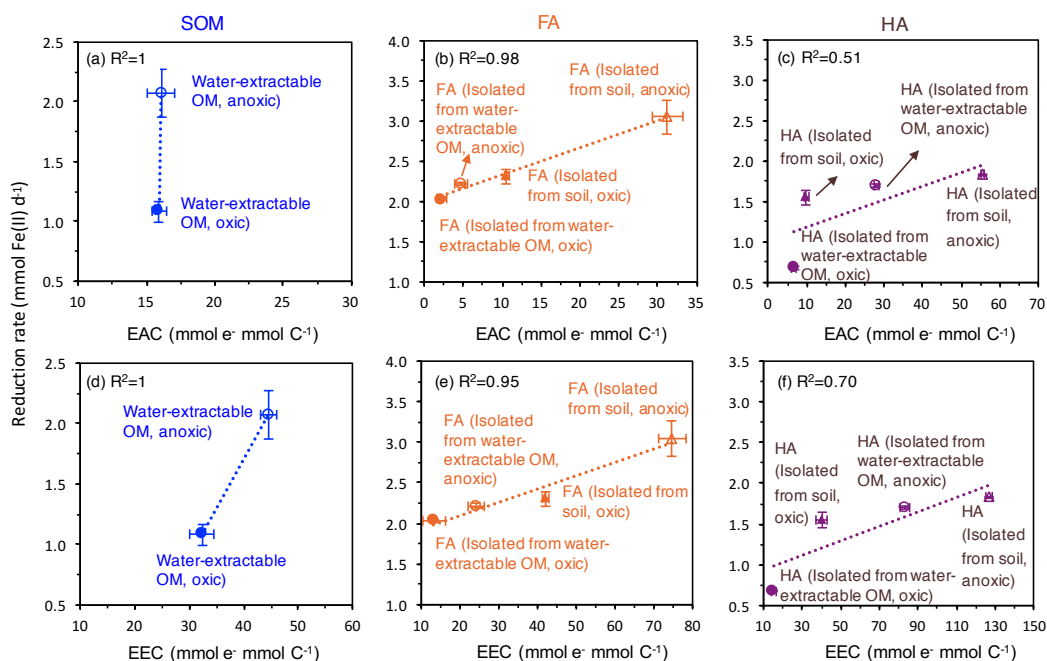

Figure 3.5. Correlation of the electron accepting capacity (EAC) (top) and electron exchange

capacity (EEC) (bottom) and with the fastest microbial ferrihydrite reduction rates in the

presence of oxically and anoxically prepared SOM (a, d), FA (b, e) and HA (c, f). EEC and

EAC are re-plotted from Figure 3.2. Horizontal error bars represent standard deviation of the

measured EAC/EEC; vertical error bars are standadr deviation of the reduction rates calculated

as shown in Figure S3.1.

Faster Fe(III) mineral reduction rates in the presence of more aromatic functional

groups (including quinones) was demonstrated previously in experiments with increasing

concentrations of AQDS or HA (Glasser et al., 2017; Jiang and Kappler, 2008; Wolf et al.,

2009). It was suggested that the microbial turnover of substrate (lactate as electron source) is

limited by the availability of the electron acceptor, i.e. either by the Fe(III) in the absence of

shuttles or by the OM when OM serves as electron shuttling compound (Jiang and Kappler,

2008; Poggenburg et al., 2018). Thus, with the same concentration of OM electron shuttle, the

OM with more redox-active functional groups can accept more electrons per time from the microorganisms, therefore resulting in higher Fe(III) reduction rates. Additionally, when more quinone or other redox-active functional groups are present per shuttle molecule, the distance between redox-active functional groups is smaller, therefore, electron transfer within the shuttle molecule and between the shuttle molecules can occur faster, thus further increasing the electron transfer rate from the microbial cells to the shuttle molecules and further to the Fe(III) minerals (Boyd et al., 2015; Glasser et al., 2017). The different types and proportions of functional groups in the different OM extracts may also influence their adsorption onto the ferrihydrite surface, and therefore also impact the rates of microbial ferrihydrite reduction amended with different OM. However, due to the high concentration of lactate and HEPES buffer in our experiment, we could not quantify the amount of adsorbed OM vs. dissolved OM. It has to be noted, however, that in our extracted OM (Table S3.3) different amounts of redox-active Fe ions were present and that the redox-active OM-bound Fe can potentially also influence the rates of Fe(III) mineral reduction. The OM-bound Fe(III) can also be reduced by the Fe(III)-reducing bacteria or by reduced organic functional groups in the OM to Fe(II), which can then transfer electrons further to the ferrihydrite. The OM-bound Fe is subsequently reoxidized to Fe(III), and therefore contributes to electron shuttling between Fe(III)-reducing bacteria and ferrihydrite.

In addition to the differences in the reduction rates, we also observed that the extent of ferrihydrite reduction was influenced by the presence of different OM. Specifically, amendments with HA lead to lower extents of Fe(III) reduction than FA amendments. This difference could be caused by the higher content of aromatic functional groups in HA than in FA and the resulting differences in sorption properties. OM with higher aromaticity and larger molecular weight was shown to have a higher adsorption affinity to ferrihydrite (Coward et al., 2019; Lv et al., 2016). Since our HA extracted under all conditions were more aromatic than

the FA, the HA were probably preferentially adsorbed to ferrihydrite. On the one hand, the sorbed HA can block surface sites on the minerals and restrict the accessibility for bacteria. On the other hand, HA adsorption changes the net surface charge of ferrihydrite from positive to (partially) negative and thus leads to repulsion of negatively charged cells (Aeschbacher et al., 2012).

3.5 Conclusion

In summary, our results clearly show that the extraction method determines the concentration of redox-active (aromatic) functional groups and the EEC of the soil extracts and the EEC is a key factor for the electron shuttling capacity of soil extracts in microbial Fe(III) mineral reduction. Therefore, it has to be carefully decided which SOM extraction method to apply and which SOM fraction to use in biogeochemical experiments to obtain soil extracts that can represent natural SOM. Representative SOM is necessary to obtain meaningful results that will prevent overestimating the reactivity of SOM in redox processes in the environment. Based on our experimental results we suggest that firstly, the NaOH extraction method should be avoided in general because it alters the chemical and redox properties of SOM. Additionally, soil pH values typically range from 3.5-8.5 (Sparks, 2003), therefore the organic matter that is soluble only at pH>12 will not be dissolved under in-situ soil conditions and might react differently in biogeochemical processes compared to solid-phase soil OM (Kappler et al., 2014; Roden et al., 2010). Secondly, when extracting SOM with water at neutral pH, the redox milieu (oxic or anoxic) during extraction needs to be carefully controlled. When targeting oxic environmental systems with the goal of obtaining relevant OM matter that participates in biogeochemical processes under such redox conditions, short extraction times (<24 h), small batches, aeration, and thorough stirring is recommended for the OM extraction. Thus, anoxic conditions during the OM extraction should be avoided that would lead to reductive dissolution of iron minerals with concomitant mobilization of OM that would not be available under oxic

conditions (in the absence of microbial Fe(III) reduction). However, in case the target environmental systems undergo redox fluctuations or even permanent reducing conditions, yielding anoxic conditions with microbial Fe(III) mineral reduction during the OM extraction is appropriate.

3.6 Supporting information

Table S3.1. Two-way ANOVA statistical analysis of the measured specific UV absorbance values at 254 nm ($SUVA_{254}$) for all NOM extracts. The two-way ANOVA analysis was conducted using the SPSS software to test whether the extraction condition, the extraction method, or both of them have significant impact on the $SUVA_{254}$ values of the extracts. $P<0.05$ indicates the rejection of the null hypotheses, meaning that the corresponding condition has significant influence on the $SUVA_{254}$.

[a]Dependent Variable: $SUVA_{254}$

Conditions	Sum of Squares	[b]Degrees of freedom	[c]Mean Square	[d]F	P
Extraction condition (oxic *vs.* anoxic)	0.002	1	0.002	11.181 F (1.20) =4.35	<0.05
Extraction method (water *vs.* chemical)	0.125	4	0.031	166.808 F (4.20) =2.87	<0.05
Extraction condition and extraction method	0.077	4	0.019	103.209 F (4.20) =2.87	<0.05
Error (within group variances)	0.004	20	0.000 (0.00018)		

[a]Three null hypotheses of the two-way ANOVA analysis:

$Hypothesis_{n1}$: the extraction condition does not have significant impact on the measured $SUVA_{254}$ values of the extracts

$Hypothesis_{n2}$: the extraction method does not have significant impact on the measured $SUVA_{254}$ values of the extracts

$Hypothesis_{n3}$: the extraction condition and the extraction method together do not have any significant impact on the measured $SUVA_{254}$ values of the extracts

[b]Degree of Freedom was calculated based on the number of variables under each condition. For example, for the extraction condition, there are two variables, i.e., oxic condition or anoxic condition, so the degree of freedom is 2-1=1. For the extraction method, there are five variables, i.e., water-extracted SOM, FA isolated from the water-extracted SOM, FA isolated from soil, HA isolated from the water-extractable SOM, HA isolated from soil. Therefore, the degree of freedom is 5-1=4. The degree of freedom of both conditions (the third row: extraction condition and extraction method) was calculated by multiplying the degree of freedom of extraction condition and the degree of freedom of extraction method, therefore $1 \times 4 = 4$

[c]Mean Square = Sum of Square/Degree of Freedom

[d]F ratio = variance of the group means (Mean Square)/mean of the within group variances (Mean Square Error). The calculated F ratio should be compared to the critical F ratio based on the degree of freedom (as shown in the brackets), and in all cases, the F ratio is higher than the critical F ratio, indicating that the null hypotheses should be rejected.

Table S3.2. ^{13}C-NMR analysis of SOM, FA and HA. ^{13}C-NMR was conducted from freeze-dried extracts. The relative intensity of the signals was obtained by integration of the specific chemical shift range by an integration routine with MESTRE NOVA. Data for water-extracted FA cannot be presented due to the lack of an adequate amount of sample for analysis.

Percentage distribution of ^{13}C within indicated ppm regions (%)

Sample/**ppm range**	**0-45**	**55-60**	**60-90**	**90-110**	**110-140**	**140-160**	**160-185**	**185-225**	[a]Aromaticity (%)
	Alkyl C	*N*-Alkyl C	*O*-Alkyl C	*O*-Alkyl & *C/H*-Aryl C	*C/H*-Aryl C	O-Aryl C	Carbonyl C	Aldehyde & Ketone	
Water-extracted SOM, oxic	20	10	30	10	12	6	7	4	20
Water-extracted SOM, anoxic	35	10	14	6	13	6	15	1	23
Chem.-extracted FA, oxic	21	9	32	9	9	4	11	3	15
Chem.-extracted FA, anoxic	22	10	19	8	14	8	12	6	27
Water-extracted HA, oxic	31	11	19	7	13	7	7	2	23
Water-extracted HA, anoxic	23	9	17	8	15	9	10	8	30
Chem.-extracted HA, oxic	24	11	22	8	15	8	9	3	20
Chem.-extracted HA, anoxic	27	11	21	8	14	7	8	3	24

[a]Aromaticity (%)= [Aromatic C peak area (110-160 ppm)]×100/[Total peak area (0-160 ppm)

Table S3.3. Total phosphate-leachable Fe, Fe(II) and Fe(III) in the isolated SOM, FA and HA samples. Iron concentrations were quantified in the extracts solution after filtration with 0.22 µm syringe filter (mixed cellulose ester (MCE), Millipore, Germany). Errors represent the standard deviation calculated from 3 parallels. The data for FA and HA isolated from soil is missing because the Fe(II) and Fe(III) concentrations in these samples are below the detection limit.

	Fe total (µmol L^{-1})	Fe(II) (µmol L^{-1})	Fe(III) (µmol L^{-1})	[1]Contribution of Fe(II) to electron donating capacity (EDC) (µmol e$^-$ mmol C^{-1})/%	[2]Contribution of Fe(III) to electron accepting capacity (EAC) (µmol e$^-$ mmol C^{-1})/%	[3]Total contribution of Fe to electron exchange capacity (EEC) (µmol e$^-$ mmol C^{-1})/%
SOM (water-extractable, oxic)	32.8±1.8	17.4±1.6	15.4±1.3	2.1±0.19/11.7-14.0	1.9±0.16/10.9-12.9	4.0±0.21/11.8-13.0
SOM (water-extractable, anoxic)	123.1±0.8	79.2±0.8	43.9±0.9	9.5±0.10/33.4-33.7	5.3±0.11/32.3-33.7	14.8±0.10/33.0-33.4
FA (isolated from the water-extractable OM, oxic)	18.8±1.3	7.2±0.4	11.6±0.7	0.9±0.05/7.7-8.6	1.4±0.08/59.6-66.8	2.3±0.16/16.1-18.5
FA (isolated from the water-extractable OM, anoxic)	22.6±1.0	10.0±1.0	12.6±1.6	1.2±0.12/5.5-6.8	1.5±0.19/27.5-35.4	2.7±0.12/10.6-11.6
HA (isolated from the water-extractable OM, oxic)	15.9±2.1	7.2±0.3	8.7±0.5	0.9±0.04/1.6-1.7	1.0±0.06/14.1-15.9	1.9±0.25/2.0-2.6
HA (isolated from the water-extractable OM, anoxic)	60.7±2.6	27.8±0.4	32.9±0.6	3.3±0.05/38.5-39.7	3.9±0.07/13.6-14.1	7.3±0.31/46.3-50.4

[1]Calculation of the contribution of Fe(II) to the EDC:

Take water-extractable SOM, oxic as an example, Fe(II) concentration = 17.4 µmol L^{-1}

The volume of SOM solution used for EDC analysis is 200 µL

Mole quantity of Fe(II) = 17.4 µmol L^{-1} × 200 µL = 0.00348 µmol Fe(II)

1 mol Fe(II) can donate 1 mol e$^-$, so 0.00348 µmol Fe(II) can donate 0.00348 µmol e$^-$

Mole quantity of C = 100 mg C L^{-1} × 200 µL ÷12 g mol^{-1} = 0.00167 mmol C

Therefore, the contribution of Fe(II) to the EDC = 0.00348 μmol e$^-$÷0.00167 mmol C = 2.1 μmol e$^-$ mmol C^{-1}

[2]**Calculation of the contribution of Fe(III) to the EAC:**

Take water-extracted SOM, oxic as an example, Fe(III) concentration = 15.4 μmol L^{-1}

The volume of SOM solution used for EAC analysis is 200 μL

Mole quantity of Fe = 15.4 μmol L^{-1} $\times$ 200 μL = 0.00308 μmol Fe

1 mol Fe(III) can accept 1 mol e$^-$, so 0.00308 μmol Fe(III) can accept 0.00308 μmol e$^-$

Mole quantity of C = 100 mg C L^{-1} $\times$ 200 μL ÷12 g mol^{-1} = 0.00167 mmol C

Therefore, the contribution of Fe(III) to the EAC = 0.00308 μmol e$^-$÷0.00167 mmol C =1.9 μmol e$^-$ mmol C^{-1}

[3]**Calculation of the contribution of Fe to the EEC:**

Take water-extracted SOM, oxic as an example, Fe total concentration = 32.8 μmol L^{-1}

The volume of SOM solution used for EEC analysis is 200 μL

Mole quantity of Fe total = 32.8 μmol L^{-1} $\times$ 200 μL = 0.00656 μmol Fe(II)

1 mol Fe(II) can exchange (either donate or accept) 1 mol e$^-$, so 0.00656 μmol Fe(II) can donate 0.00656 μmol e$^-$

Mole quantity of C = 100 mg C L^{-1} 10^{-3} $\times$ 200 μL ÷12 g mol^{-1} = 0.00167 mmol C

Therefore, the contribution of Fe(II) to the EDC = 0.00656 μmol e$^-$÷0.00167 mmol C = 4.0 μmol e$^-$ mmol C^{-1}

Table S3.4. Summary table for the two-way ANOVA of the measured electron exchange capacity (EEC) of all extracts. The two-way ANOVA analysis was conducted using the SPSS software to test whether the extraction condition or the extraction method, or both of them have significant impact on the EEC values of the extracts. P<0.05 indicates the rejection of the null hypotheses, meaning that the corresponding condition has significant influence on the EEC.

[a]Dependent Variable: Electron exchange capacity (EEC)

Condition	Sum of Squares	[b]Degrees of freedom	[c]Mean Square	[d]F	P
Extraction condition (oxic *vs.* anoxic)	18073	1	18073.6	657.912 F (1.20) =4.35	<0.05
Extraction method (water *vs.* chemical)	21448	4	5362.1	195 F (4.20) =2.87	<0.05
Extraction condition and extraction method	9722	4	2430.8	88.477 F (4.20) =2.87	<0.05
Error (within group variances)	150	20	7.5		

[a]Three null hypotheses of the two-way ANOVA analysis:

Hypothesis[n1]: the extraction condition do not have significant impact on the measured EEC values of the extracts

Hypothesis[n2]: the extraction method does not have significant impact on the measured EEC values of the extracts

Hypothesis[n3]: the extraction condition and the extraction method together do not have any significant impact on the measured EEC values of the extracts

[b]Degree of Freedom was calculated based on the number of variables under each condition. For example, for the extraction condition, there are two variables, i.e., oxic condition or anoxic condition, so the degree of freedom is 2-1=1. For the extraction method, there are five variables, i.e., water-extracted SOM, FA isolated from the water-extracted SOM, FA isolated from soil, HA isolated from the water-extractable SOM, HA isolated from soil. Therefore, the degree of freedom is 5-1=4. The degree of freedom of both conditions (the third row: extraction condition and extraction method) was calculated by multiplying the degree of freedom of extraction condition and the degree of freedom of extraction method, therefore 1×4 =4

[c]Mean Square = Sum of Square/Degree of Freedom

[d]F ratio = variance of the group means (Mean Square)/mean of the within group variances (Mean Square Error). The calculated F ratio should be compared to the critical F ratio based on the degree of freedom

(as shown in the brackets), and in all cases, the F ratio is higher than the critical F ratio, indicating that the null hypotheses should be rejected.

Table S3.5. Metal content analyzed by Microwave Plasma-Atomic Emission Spectrometer (MP-AES) (4100, Agilent Inc., Santa Clara, CA, USA) in the extracted SOM, HA and FA samples. The data for FA (chemically-extracted, oxic) and HA (water-extracted, oxic) are missing due to the lack of enough samples. The unit of all metal concentrations is mg kg^{-1}, blank means the concentration of the corresponding metal is too low to be detected.

|	B	Zn	Ca	Mg	Cu	Ag	Ba	Mn	Pb	Al	Ga
SOM (water-extracted, oxic)	1.65	0.04	10.09	3.03	0.10	0.02	0.07	3.82	0.10	0.99	0.33
SOM (water-extracted, anoxic)	0.11	0.13	-	8.97	0.11	0.01	0.68	10.64	0.14	12.64	0.01
FA (water-extracted, oxic)	0.34	0.01	14.02	0.20	0.08	0.01	0.03	0.45	0.07	0.26	0.03
FA (water-extracted, anoxic)	0.06	0.01	0.84	-	0.05	0.01	0.01	0.31	0.03	0.82	0.02
FA (chemically-extracted, anoxic)	0.09	0.11	-	11.13	0.19	0.02	1.05	3.40	0.12	14.87	0.01
HA (water-extracted, anoxic)	0.03	0.03	6.41	2.78	0.01	0.01	0.26	2.07	0.10	19.64	0.02
HA (chemically-extracted, oxic)	0.08	0.04	0.03	7.91	3.92	0.09	0.02	0.32	1.6	0.15	64.12
HA (chemically-extracted, anoxic)	0.02	0.02	0.01	6.46	2.94	0.05	0.03	0.09	0.15	0.09	7.14
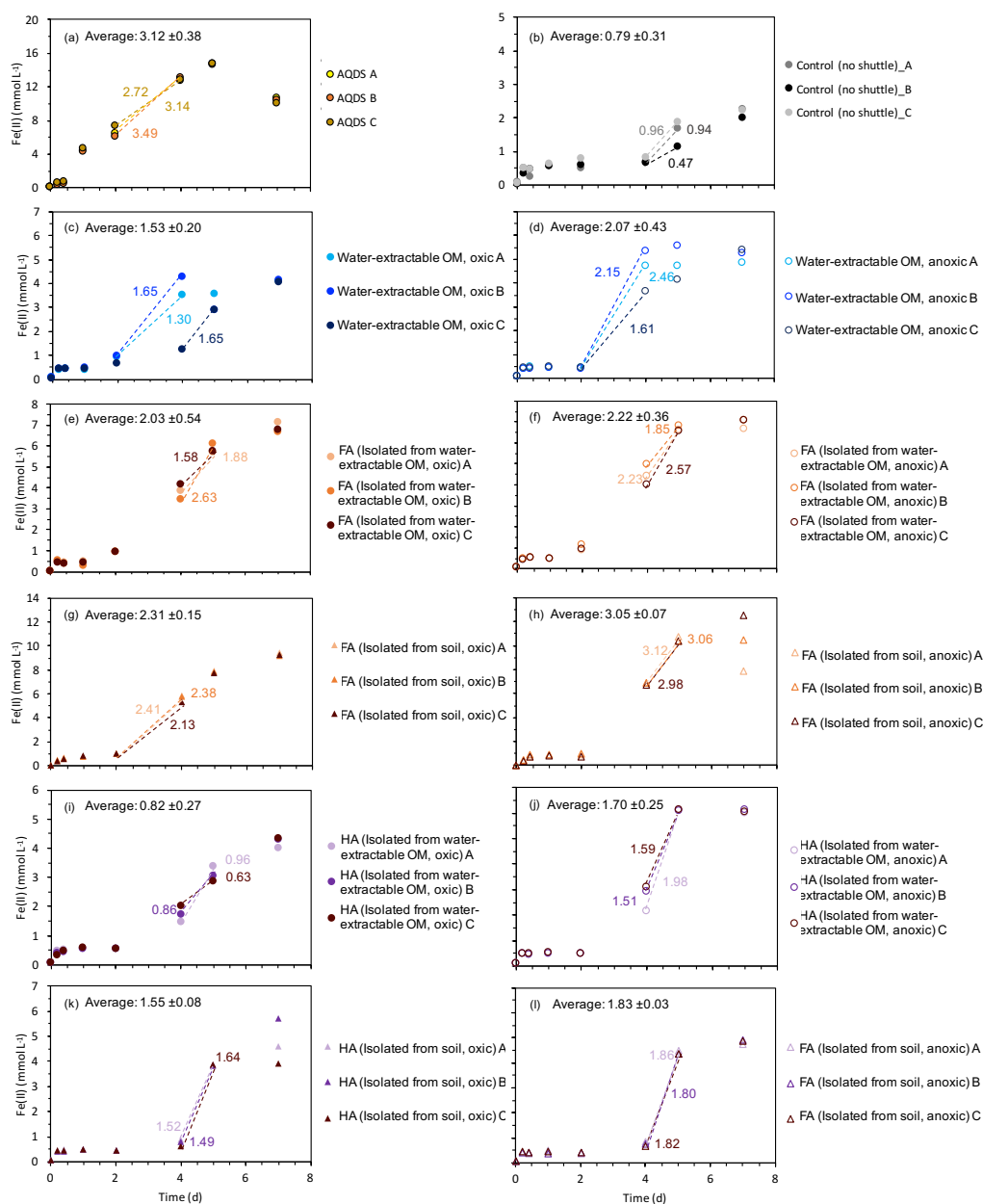
Figure S3.1. Calculation of the fastest initial microbial Fe(III) reduction rates in setups amended with AQDS (a), *Shewanella oneidensis* MR-1 only (control, b), water-extractable OM (c-d), FA(e-h), HA (i-l). The reduction rate was calculated separately for each of the triplicates. The standard deviation for the average of the three rates was calculated and indicated in each panel.
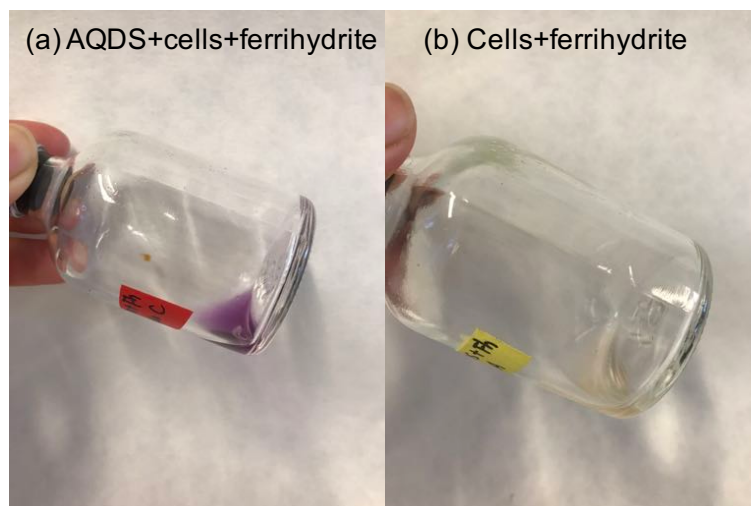
Figure S3.2. Addition of ferrozine to incubation bottles at the end of the experiment shows sorption or precipitation of Fe(II) at the glass walls of the experiments with *Shewanella oneidensis* MR-1 and ferrihydrite, in addition of AQDS (a) or absence of AQDS (b). Before adding ferrozine solution, original solutions in the bottles were discarded completely in the anoxic glovebox.
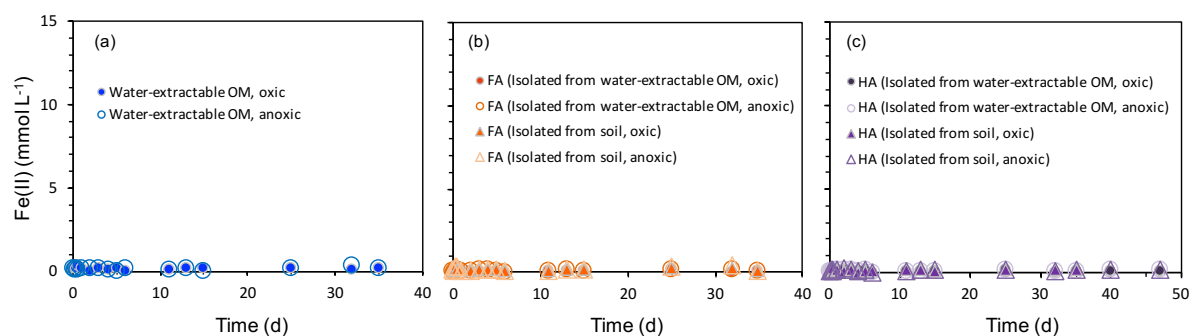
Figure S3.3. Abiotic reductions of ferrihydrite (15 mmol L^{-1}) in the presence of 50 mg C L^{-1} water-extractable OM (a), FA (b) and HA (c) and 15 mmol L^{-1} lactate, presented as total Fe(II) formed over time. All experiments were incubated in air-tight 100 mL glass serum bottles flushed with N_2 at 30 °C in the dark.

3.7 References

Abelmann, K., Kleineidam, S., Knicker, H., Grathwohl, P. and Koegel-Knabner, I. (2005) Sorption of HOC in soils with carbonaceous contamination: Influence of organic-matter composition. *J. Plant Nutr. Soil Sci.*, **168**, 293-306.

Achard, F. K. (1786) Chemische Untersuchung des Torfs, Chem. Ann. Freunde Naturlehre. *Arzneigel. Hausalt.* Manufact, **2**, 391-403.

Aeschbacher, M., Sander, M. and Schwarzenbach, R. P.(2010) Novel electrochemical approach to assess the redox properties of humic substances. *Environ. Sci. Technol.* **44**, 87-93.

Aeschbacher, M., Graf, C., Schwarzenbach, R. P. and Sander, M.(2012) Antioxidant properties of humic substances. *Environ. Sci. Technol.* **46**, 4916-4925.

Aiken, G. R. (1985) Humic substances in soil, sediment, and water: geochemistry, isolation, and characterization. Wiley, New York.

Amstaetter, K., Borch, T. and Kappler, A.(2012) Influence of humic acid imposed changes of ferrihydrite aggregation on microbial Fe(III) reduction. *Geochim. Cosmochim. Acta* **85**, 326-341.

Avneri-Katz, S., Young, R. B., McKenna, A. M., Chen, H., Corilo, Y. E., Polubesova, T., Borch, T. and Chefetz, B.(2017) Adsorptive fractionation of dissolved organic matter (DOM) by mineral soil: Macroscale approach and molecular insight. *Org. Geochem.* **103**, 113-124.

Bauer, I. and Kappler, A. (2009) Rates and extent of reduction of Fe(III) compounds and O_2 by humic substances. *Environ. Sci. Technol.* **43**, 4902-4908.

Borch, T., Masue, Y., Kukkadapu, R. K. and Fendorf, S. (2007) Phosphate imposed limitations on biological reduction and alteration of ferrihydrite. *Environ. Sci. Technol.* **41**, 166-172.

Boyd, D.A., Snider, R.M., Erickson, J.S., Roy, J.N., Strycharz-Glaven, S.M. and Tender, L.M. (2015) Theory of redox conduction and the measurement of electron transport rates through electrochemically active biofilms. In Beyenal, H. and Babauta, J. (Ed.), *Biofilms in bioelectrochemical systems: From laboratory practice to data interpretation*, pp. 177-209.

Burdige, D. J., Alperin, M. J., Homstead, J. and Martens, C. S. (1992) The role of Benthic fluxes of dissolved organic-carbon in oceanic and sedimentray carbon cycling. *Goephys. Res.* **19**, 1851-1854.

Burdige, D. J., Berelson, W. M., Coale, K. H., McManus, J. and Johnson, K. S. (1999) Fluxes of dissolved organic carbon from California continental margin sediments. *Geochim. Cosmochim. Acta* **63**, 1507-1515.

Chen, J., Gu, B. H., Royer, R. A. and Burgos, W. D. (2003) The roles of natural organic matter in chemical and microbial reduction of ferric iron. *Sci. Total Environ.* **307**, 167-178.

Chin, Y. P., Traina, S. J., Swank, C. R. and Backhus, D. (1998) Abundance and properties of dissolved organic matter in pore waters of a freshwater wetland. *Limno. Oceanogr*. **43**, 1287-1296.

Coward, E. K., Ohno, T. and Sparks, D. L. (2019) Direct evidence for temporal molecular fractionation of dissolved organic matter at the iron oxyhydroxide interface. *Environ. Sci. Technol.* **53**, 642-650.

Dadi, T., Harir, M., Hertkorn, N., Koschorreck, M., Schmitt-Kopplin, P. and Herzsprung, P. (2017) Redox conditions affect dissolved organic carbon quality in stratified freshwaters. *Environ. Sci. Technol.* **51**, 13705-13713.

Engebretson, R. R. and Von Wandruszka, R. (1999) Effects of humic acid purification on interactions with hydrophobic organic matter: Evidence from fluorescence behavior. *Environ. Sci. Technol.* **33**, 4299-4303.

Fischlin, A. M., Price, J., Leemans, R., Gopal, B., Turley, C., Rounsevell, M. D. A., Dube, P., Tarazona, J. and Velichko, A. A. (2007) Ecosystems, their properties, goods and services. In Parry, M. L., Canziani, O. F., Palutikof, J. P., van der Linden, P. J. and Hanson, C. E. (Ed.), *Climate Change 2007: Impacts, Adaptation and Vulnerability. Contribution of Working Group II on the Fourth Assessment Respot of the intergovernmental Panel on Climate Change*, pp. 211-272.

Fox, P. M., Nico, P. S., Tfaily, M. M., Heckman, K. and Davis, J. A. (2017) Characterization of natural organic matter in low-carbon sediments: Extraction and analytical approaches. *Org. Geochem.* **114**, 12-22.

Gieseking, J. E. (1975) Soil components. Volume 1, organic components, Springer, Heidelberg.

Glasser, N. R., Saunders, S. H. and Newman, D. K. (2017) The colorful world of extracellular electron shuttles. *Annu. Rev. Microbiol.* **71**, 731-751.

Golchin, A., Oades, J. M., Skjemstad, J. O. and Clarke, P. (1994) Soil structure and carbon cycling. *Aust. J. Soil. Res.* **32**, 1043-1068.

Gu, B. H., Schmitt, J., Chen, Z. H., Liang, L. Y. and McCarthy, J. F. (1994) Adsorption and desorption of natural organic-matter on iron-oxide- Mechanisms and models. *Environ. Sci. Technol.* **28**, 38-46.

Hansel, C. M., Benner, S. G., Neiss, J., Dohnalkova, A., Kukkadapu, R. K. and Fendorf, S. (2003) Secondary mineralization pathways induced by dissimilatory iron reduction of ferrihydrite under advective flow. *Geochim. Cosmochim. Acta* **67**, 2977-2992.

Hegler, F., Posth, N. R., Jiang, J. and Kappler, A. (2008) Physiology of phototrophic iron(II)-oxidizing bacteria: implications for modern and ancient environments. *Fems. Microbiol. Ecol.* **66**, 250-260.

IHSS: Isolation of IHSS samples, http://humic-substances.org/isolation-of-ihss-samples/, last access: 29th July, 2019.

Jiang, J. and Kappler, A. (2008) Kinetics of microbial and chemical reduction of humic substances: Implications for electron shuttling. *Environ.Sci. Technol.* **42**, 3563-3569.

Kappler, A. and Brune, A. (1999) Influence of gut alkalinity and oxygen status on mobilization and size-class distribution of humic acids in the hindgut of soil-feeding termites. *Appl. Soil. Ecol.* **13**, 219-229.

Kappler, A. and Haderlein, S. B. (2004) Natural organic matter as reductant for chlorinated aliphatic pollutants. *Environ. Sci. Technol.* **37**, 2714-2719.

Kappler, A., Benz, M., Schink, B. and Brune, A. (2004) Electron shuttling via humic acids in microbial iron(III) reduction in a freshwater sediment. *Fems. Microbiol. Ecol.* **47**, 85-92.

Kappler, A., Wuestner, M. L., Ruecker, A., Harter, J., Halama, M. and Behrens, S. (2014) Biochar as an electron shuttle between bacteria and Fe(III) minerals. *Environ. Sci. Tech. Let.* **1**, 339-344.

Kleber, M., Eusterhues, K., Keiluweit, M., Mikutta, C., Mikutta, R. and Nico, P. S. (2015) Mineral-organic associations: Formation, properties, and relevance in soil environments. *Adv. Agron.* **130**, 1-140.

Kleber, M. and Lehmann, J. (2019) Humic substances extracted by alkali are invalid proxies for the dynamics and functions of organic matter in terrestrial and aquatic ecosystems. *J. Environ.Qual.* **48**, 207.

Klupfel, L., Piepenbrock, A., Kappler, A. and Sander, M. (2014) Humic substances as fully regenerable electron acceptors in recurrently anoxic environments. *Nat. Geosci.* **7**, 195-200.

Korshin, G. V., Li, C. W. and Benjamin, M. M. (1997) Monitoring the properties of natural organic matter through UV spectroscopy: A consistent theory. *Water Res.* **31**, 1787-1795.

Kothawala, D. N., Roehm, C., Blodau, C. and Moore, T. R. (2012) Selective adsorption of dissolved organic matter to mineral soils. *Geoderma*, **189**, 334-342.

Lal, R. (2004) Soil carbon sequestration impacts on global climate change and food security. *Science* **304**, 1623-1627.

Lehmann, J. and Kleber, M. (2015) The contentious nature of soil organic matter. *Nature* **528**, 60-68.

Lies, D. P., Hernandez, M. E., Kappler, A., Mielke, R. E., Gralnick, J. A. and Newman, D. K. (2005) *Shewanella oneidensis* MR-1 uses overlapping pathways for iron reduction at a distance

and by direct contact under conditions relevant for biofilms. *Appl. Environ. Microb*. **71**, 4414-4426.

Lovley, D. R., Coates, J. D., BluntHarris, E. L., Phillips, E. J. P. and Woodward, J. C. (1996) Humic substances as electron acceptors for microbial respiration. *Nature* **382**, 445-448.

Lovley, D. R., Fraga, J. L., Blunt-Harris, E. L., Hayes, L. A., Phillips, E. J. P. and Coates, J. D. (1998) Humic substances as a mediator for microbially catalyzed metal reduction. *Acta. Hydroch. Hydrob*. **26**, 152-157.

Lovley, D. R. and Blunt-Harris, E. L. (1999) Role of humic-bound iron as an electron transfer agent in dissimilatory Fe(III) reduction. *Appl. Environ. Microb*. **65**, 4252-4254.

Lv, J. T., Zhang, S. Z., Wang, S. S., Luo, L., Cao, D. and Christie, P. (2016) Molecular-scale investigation with ESI-FT-ICR-MS on fractionation of dissolved organic matter induced by adsorption on iron oxyhydroxides. *Environ. Sci. Technol.* **50**, 2328-2336.

Marin-Spiotta, E., Gruley, K. E., Crawford, J., Atkinson, E. E., Miesel, J. R., Greene, S., Cardona-Correa, C. and Spencer, R. G. M. (2014) Paradigm shifts in soil organic matter research affect interpretations of aquatic carbon cycling: transcending disciplinary and ecosystem boundaries. *Biogeochemistry* **117**, 279-297.

Murphy, B. W. (2014) Soil organic matter and soil function- review of the literature and underlying data: effects of soil organic matter on functional soil properties, Department of Environment, Canberra, Austrilia.

Piccolo, A. (1988) Characteristics of soil humic extracts obtained by some organic and inorganic solvents and purified by HCl-HF treatment. *Soil Sci*. **146**, 418-426.

Piepenbrock, A., Dippon, U., Porsch, K., Appel, E. and Kappler, A. (2011) Dependence of microbial magnetite formation on humic substance and ferrihydrite concentrations. *Geochim. Cosmochim. Acta* **75**, 6844-6858.

Piepenbrock, A., Schroder, C. and Kappler, A. (2014) Electron transfer from humic substances to biogenic and abiogenic Fe(III) oxyhydroxide minerals. *Environ. Sci. Technol.* **48**, 1656-1664.

Poggenburg, C., Mikutta, R., Schippers, A., Dohrmann, R. and Guggenberger, G. (2018) Impact of natural organic matter coatings on the microbial reduction of iron oxides. *Geochim. Cosmochim. Acta* **224**, 223-248.

Riedel, T., Zak, D., Biester, H. and Dittmar, T. (2013) Iron traps terrestrially derived dissolved organic matter at redox interfaces. *P. Natl. Acad. Sci. USA* **110**, 10101-10105.

Ritchie, J. D. and Perdue, E. M. (2008) Analytical constraints on acidic functional groups in humic substances. *Org. Geochem*. **39**, 783-799.

Roden, E. E., Kappler, A., Bauer, I., Jiang, J., Paul, A., Stoesser, R., Konishi, H. and Xu, H. F. (2010) Extracellular electron transfer through microbial reduction of solid-phase humic substances. *Nat. Geosci.* **3**, 417-421.

Schad, P., van Huysteen, C. and Micheli, E. (Ed.) (2014) World reference base for soil rescouces 2014 – International soil classification system for naming soils and creating legends for soil maps, FAO, Rome, Italy.

Scott, D. T., McKnight, D. M., Blunt-Harris, E. L., Kolesar, S. E. and Lovley, D. R. (1998) Quinone moieties act as electron acceptors in the reduction of humic substances by humics-reducing microorganisms. *Environ. Sci. Technol.* **32**, 2984-2989.

Shimizu, M., Zhou, J., Schröder, C., Obst, M., Kappler, A. and Borch, T. (2013a) Dissimilatory reduction and transformation of ferrihydrite-humic acid coprecipitates. *Environ. Sci. Technol*. **47**, 13375-13384.

Sparks, D. L. (2003) Environmental soil chemistry, Academic Press, Amsterdam; Boston.

Stookey, L. L. (1970) Ferrozine- A new spectrophotometric reagent for iron. *Anal. Chem*. **42**, 779-781.

Struyk, Z. and Sposito, G. (2001) Redox properties of standard humic acids. *Geoderma* **102**, 329-346.

Swift, R. S. and Posner, A. M. (1972) Autoxidation of humic acid under alkaline conditions. *J. Soil Sci.* **23**, 381-393.

van Bemmelen, J. M. (1888) Die Absorptionsverbindungen und das Absorptionsvermögen der Ackererde. *Landwirtschaftlichen Versychs-Stationen* **35**, 2228-2233.

Weishaar, J. L., Aiken, G. R., Bergamaschi, B. A., Fram, M. S., Fujii, R. and Mopper, K. (2003) Evaluation of specific ultraviolet absorbance as an indicator of the chemical composition and reactivity of dissolved organic carbon. *Environ. Sci. Technol.* **37**, 4702-4708.

Wolf, M., Kappler, A., Jiang, J. and Meckenstock, R. U. (2009) Effects of humic substances and quinones at low concentrations on ferrihydrite reduction by *Geobacter metallireducens*. *Environ. Sci. Technol.* **43**, 5679-5685.

Chapter 4-Personal contribution

Experiments in this chapter were conceptually designed by myself, together with Prof. Andreas Kappler and Prof. Stefan B. Haderlein. Ellen Röhm developed the agar-solidified setup and performed preliminary tests. The microbial Fe(III) reduction experiments were performed by myself, Paula Eisnecker helped with the experimental setup and sampling. The diffusion-reaction model was developed by Dr. Adrian Mellage, with the help from Prof. Olaf A. Cirpka. Dr. Tianran Sun helped with the electrochemical analyses to determine the diffusion coefficient of anthraquinone-2,6-disulfonate (AQDS) in agar. The manuscript was written by myself and Dr. Adiran Mellage, Prof. Andreas Kappler, Prof. Olaf A. Cirpka, Prof. Stefan B. Haderlein and Prof. Largus T. Angenent revised the manuscript.

4. AQDS and redox-active NOM enables Fe(III)-mineral reduction at cm-scales

Yuge Bai[1], Adrian Mellage[2], Olaf A. Cirpka[2], Tianran Sun[3], Largus T. Angenent[3], Stefan B. Haderlein[4], Andreas Kappler[1]

[1]Geomicrobiology, Center of Applied Geosciences, University of Tübingen, Germany

[2]Hydeogeology, Center of Applied Geosciences, University of Tübingen, Germany

[3]Environmental Biotechnology, Center of Applied Geosciences, University of Tübingen, Germany

[4]Environmental Mineralogy and Chemistry, Center of Applied Geosciences, University of Tübingen, Germany

4.1 Abstract

Redox-active organic molecules such as anthraquinone-2,6-disulfonate (AQDS) and natural organic matter (NOM) can act as electron shuttles thus facilitating electron transfer from Fe(III)-reducing bacteria (FeRB) to terminal electron acceptors such as Fe(III) minerals. In this research, we examined the length scale over which this electron shuttling can occur. We present results from agar-solidified experimental incubations, containing either AQDS or NOM, where FeRB were physically separated from ferrihydrite or goethite by 2 cm. Iron speciation and concentration measurements coupled to a diffusion-reaction model highlighted clear Fe(III) reduction in the presence of electron shuttles, independent of the type of FeRB. Based on our fitted model, the rate of ferrihydrite reduction increased from 0.07 to 0.19 μmol d^{-1} with a 10-fold increase in AQDS concentration, highlighting a dependence of the reduction rate on the on electron-shuttle concentration. To capture the kinetics of Fe(II) production, the effective AQDS diffusion coefficient had to be increased by a factor of 9.4. Thus, we postulate that the 2 cm electron transfer was enabled by a combination of AQDS molecular diffusion and an electron hopping contribution from reduced to oxidized AQDS molecules. Our results demonstrate that AQDS and NOM can drive microbial Fe(III) reduction across 2 cm distances, and shed light on the electron transfer process in natural anoxic environments.

4.2 Introduction

Fe(III) (oxyhydr)oxides are crucial mineral phases involved in major biogeochemical cycles in sediments and soils. Under anoxic conditions, dissimilatory Fe(III)-reducing bacteria (FeRB) can use Fe(III) minerals as terminal electron acceptors for respiration (Fredrickson et al., 1998; Nealson and Saffarini, 1994). Microbial reduction of Fe(III) minerals such as ferrihydrite or goethite results in their dissolution and thus in the release of sorbed or incorporated compounds such as arsenic or phosphate. The dissolved Fe(II) produced can re-precipitate forming new Fe(II)-bearing minerals such as magnetite, siderite, or vivianite,

depending on the rate of Fe(II) formation, pH, temperature and the presence of other species (Coker et al., 2006; Hansel et al., 2003). These processes can affect the environmental fate of toxic metals, radionuclides, and organic contaminants (Gadd, 2004; Lloyd et al., 2000; Newsome et al., 2014; Watts et al., 2015).

Under pH-neutral conditions, Fe(III) minerals exist as poorly soluble phases that cannot be taken up into cells for microbial respiration. While microbes can reside directly on Fe(III) mineral surfaces, they have also adapted strategies to access solid-phase electrons when separated from the mineral phase. FeRB can rely on extracellular electron transfer, rather than direct cell contact, to reduce Fe(III) minerals (Glasser et al., 2017). Different mechanisms for extracellular electron transfer at nanometer (nm) to micrometer (μm) separations have been reported. Among these are the formation of *c*-type-cytochrome-containing pili and nanowires (Gorby et al., 2006; Lovley and Malvankar, 2015; Speers et al., 2016; Subramanian et al., 2018), the excretion of Fe(III) chelators to induce the solubilization of Fe(III) minerals to use the dissolved Fe(III) as electron acceptor (Nevin and Lovley, 2002b), electron hopping via redox-active cofactors that are present in a biofilm (Snider et al., 2012), or the usage of electron shuttles between FeRB and Fe(III) minerals (Glasser et al., 2017).

Electron transfer by electron shuttles from FeRB to Fe(III) minerals involves two reaction steps. First, FeRB donate electrons to the shuttle, the reduced electron shuttle subsequently transports the electrons (either by diffusion of the shuttle or by electron-hopping) toward the Fe(III) mineral where it then transfers electrons abiotically, getting oxidized and transported back to the FeRB thus resetting the sequence (Scott et al., 1998). To be recyclable, the electron shuttle compound must contain redox-active functional groups, such as a quinone/hydroquinone moiety. A model quinone compound that has been widely used in electron-shuttling studies is anthraquinone-2,6-disulfonate (AQDS). Additional shuttling compounds include flavins (excreted by some FeRB), dissolved and solid-phase humic substances, biochar particles and natural organic matter (NOM) (Kappler et al., 2014; Lovley

et al., 1996; Marsili et al., 2008; Roden et al., 2010; von Canstein et al., 2008). Previous studies demonstrated that electron shuttling can facilitate microbial Fe(III) reduction over μm distances (Lies et al., 2005; Michelson et al., 2019). However, in the environment, the spatial separation between the FeRB and Fe(III) minerals can be out of the μm range, and whether electron shuttling can happen also over longer distances, e.g., over centimeters (cm), has remained unknown until now.

In this study, we incubated FeRB (*Shewanella oneidensis* MR-1 or *Geobacter sulfurreducens*) separated from Fe(III) minerals (ferrihydrite or goethite) by 2 cm in the presence of shuttling compounds. We also collected geochemical data and coupled them to reactive transport modelling to probe separation distance, shuttle type and shuttle concentration as controls modulating extracellular Fe(III) mineral reduction. Our findings shed new light on the feasibility and mechanisms of extracellular electron transfer, as a driver of Fe(III)-mineral reduction, in natural anoxic environments.

4.3 Materials and methods

Agar-solidified reactors

All preparation steps were performed under sterile conditions. To prepare the shuttling layer with AQDS or organic matter (OM, including Pahokee Peat humic acid (PPHA) and Suwannee River Natural Organic Matter (SRNOM)), the AQDS or OM solutions were added to the warm autoclaved agar solution (for preparation steps see section S1 in the supporting information (SI)) under vigorous shaking. Eighty mL of the shuttle-agar mix was poured into a 100 mL bottle in ice water (Figure S4.1). The Fe(III) mineral agar ball (preparation see section S1 in SI) was dropped into the agar when ~2 cm of the bottom and the side of the agar in the bottle were solidified, but the middle part was still liquid, to fix the Fe(III) mineral agar ball in the center of the agar layer. When the agar was completely solidified, the headspace of the bottle was flushed with N_2 gas, closed with a rubber stopper and a screw cap to make it air-

tight. A suspension of FeRB (1 mL) and 1 mL of growth medium, containing either acetate (for *Geobacter sulfurreducens*) or lactate (for *Shewanella oneidensis* MR-1) as an electron donor, were added on top of the agar in the bottle. The cultivation of FeRB, preparation of cell suspensions and AQDS/OM solution, and Fe(III) mineral synthesis are described in the SI (sections S2-4).
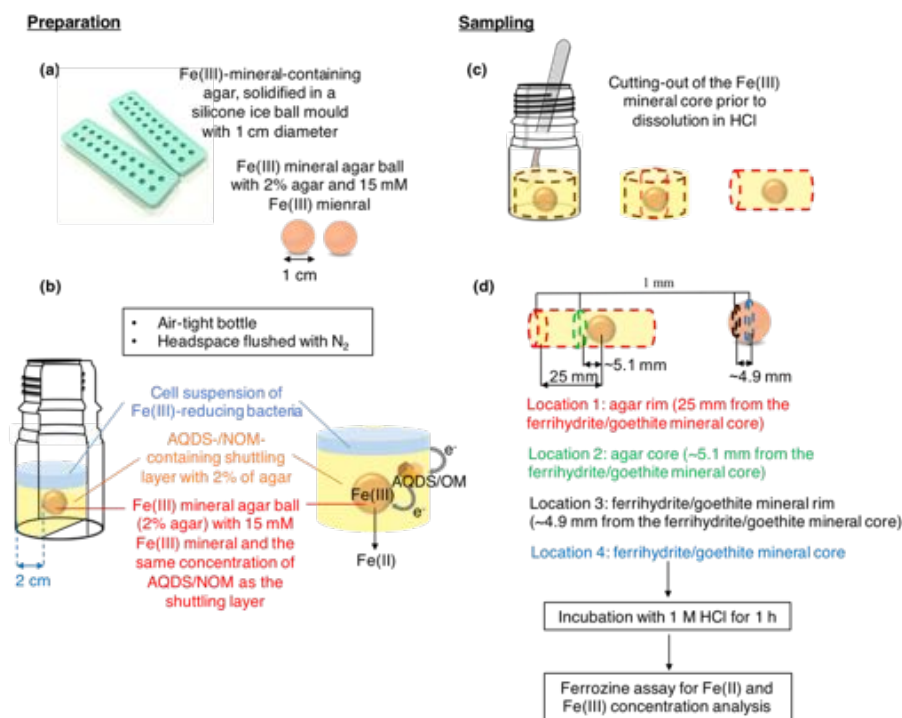

Figure 4.1. Preparation and sampling of agar-solidified electron shuttling experimental setup. (a) The Fe(III) mineral agar ball was prepared in a silicone mold with 1 cm diameter. (b) The core was located in the middle of an air-tight 100 mL glass bottle, surrounded by the AQDS- or NOM-containing shuttling layer. The suspension of Fe(III)-reducing bacteria (FeRB) was added on top of the agar with 2 cm distance from the Fe(III) mineral. The headspace of all setups was flushed with N_2 and the setups were incubated at 30 ºC in dark. (c) For sampling, a 1 cm diameter core was taken from the center of the agar containing the Fe(III) mineral core. (d) Four pieces of agar with an approximate thickness of 1 mm were sampled at different locations in the core.

Sampling and geochemical analyses

Sacrificial sampling was conducted anaerobically by placing triplicate bottles for each setup into a glovebox (100% N_2, with a copper bed for oxygen removal). The overlaying cell suspensions were removed with a pipette. A scalpel was used to cut the edge of the agar until it was small enough to be taken out of the bottle (Figure 4.1 (c)). A 10 mL syringe, cut at the top, was used to collect the solid agar sample (Figure 4.1 (c)). A 1-mm thick sample was taken at four different locations from the bottle (Figure 4.1 (d)), two from the OM-containing shuttling layer, one that was at the interface with the overlaying cell suspension (agar rim), and one that was in contact with the Fe(III) mineral agar ball. Two additional samples were taken from the Fe(III) mineral ball, one that was in contact with the AQDS-/OM-containing shuttling layer (ferrihydrite/goethite rim) and one from the center of the ball (ferrihydrite/goethite). The four agar samples were incubated in a 1 M HCl (for ferrihydrite) or 6 M HCl (for goethite) solution for 1 hour. At the end of the extraction, the agar became colorless indicating the complete dissolution of minerals from the agar to the HCl solution. After 10 min of centrifugation at 13,000 rpm, the Fe(II) and Fe(III) concentration was quantified using the spectrophotometric ferrozine assay in a microtiterplate assay (Hegler et al., 2008; Stookey, 1970; Viollier et al., 2000).

Diffusion-reaction model

We developed a numerical model, simulating reaction coupled to diffusive transport in radial coordinates, to help interpreting the measured iron dynamics in the AQDS incubations with ferrihydrite and *Shewanella oneidensis* MR-1. The experimental setup was approximated by a spherical domain, which we justify by the spherical shape of the ferrihydrite agar ball. The model considers that iron geochemistry is driven by abiotic dissimilatory ferrihydrite reduction via the reduced quinone, AH_2QDS, and that AH_2QDS is produced via the enzymatically catalyzed oxidation of lactate to acetate (assumed to only occur at the outer edge of the domain,

where the cells were situated), coupled to AQDS reduction. The products of ferrihydrite reduction include aqueous Fe^{2+} and solid-bound (adsorbed) Fe(II) and the reduced iron-phosphate mineral phase vivianite. We included the precipitation of vivianite because an immobile Fe(II) phase, measured in the experiment, accumulated at the fringe between the ferrihydrite ball and the clean agar. Aqueous Fe^{2+} would have otherwise diffused away from the source. Reactive transport of the dissolved chemical species i within the spherical domain is described by:

$$\frac{\partial C_i}{\partial t} = \frac{2D_e}{r}\frac{\partial C_i}{\partial r} + D_e\frac{\partial^2 C_i}{\partial r^2} + R_i \qquad (1)$$

in which C_i [mol L^{-1}] is the dissolved concentration of compound i, D_e [m^2 h^{-1}] is the effective diffusion coefficient, accounting for both molecular diffusion and electron hopping, R_i [mol L^{-1} h^{-1}] is the sum of all rates of reactions producing the chemical species minus those consuming it, and r and t are the radial distance and time, respectively. For a detailed description of rate expressions and coefficients that constitute the term R_i, refer to the SI (section S5). Transport and reaction were solved jointly, in MATLAB, by applying Finite-Volume discretization in space and integrating the nonlinear system of ordinary differential equations via the ordinary-differential-equation solver ode15s. The model was fitted to the experimental Fe(II) data using DREAM$_{ZS}$, a Markov-chain Monte Carlo-based (MCMC) method (Laloy and Vrugt, 2012; Vrugt, 2016), generating parameter distributions, conditioned on the measurements, and subsequent ranges of conditional parameter uncertainty. Model results are presented for the geometric-mean value of the fitted parameter distributions (see SI, Table S4.2, for calibrated parameter values and uncertainty ranges). The root mean square error (RMSE) was < 0.67 mM for all AQDS-treatments.

4.4 Results and discussion

AQDS-mediated ferrihydrite reduction

Using an agar-solidified experimental setup, *Shewanella oneidensis* MR-1 was spatially separated from the ferrihydrite-agar ball by 2 cm, with AQDS in the surrounding agar layer as the electron shuttle (Figure 4.1). Figure 4.2 presents time series of total Fe(II) and Fe(III) concentrations at different sampling locations (as shown in Figure 4.1) in the solid agar matrix for the 0.1 mM AQDS treatment inoculated with *Shewanella oneidensis* MR-1. After 5 days of incubation, the Fe(III) concentration at the rim of the ferrihydrite sphere decreased from its starting value of 15 mM to 4 mM (Figure 4.2 (b)). Concurrently, Fe(II) accumulated directly outside the ferrihydrite sphere, at sampling location 2 (agar core) until plateauing at 10.26 mM after 15 days of incubation (Figure 4.2 (a)). No accumulation of Fe(II) was measured in the ferrihydrite core or agar rim (locations 1 and 4). An increase of up to 3 mM and subsequent decrease of Fe(II) down to 0 mM, after 15 days, was measured at the ferrihydrite rim (location 3) (Figure 4.2 (a)). We attribute the dynamics in location 3 to sorption of Fe(II) onto ferrihydrite, which over time dissolved and yielded a re-release of dissolved Fe(II) with the inward progression of the dissolution front. The reductive dissolution of the ferrihydrite was observable from the color change of the agar (Figure 4.2 (c)). The Fe(II) produced from the reduction of Fe(III), at the ferrihydrite rim, diffused out to the agar core, but did not further diffuse to the agar rim, instead it accumulated at location 2, the agar core. The available phosphate (from the phosphate buffer used to prepare the AQDS solution) in the agar likely reacted with the newly reduced Fe(II) to precipitate vivianite, thus resulting in an immobile solid Fe(II) phase. The transformation of ferrihydrite to vivianite in the presence of phosphate buffer has been previously reported in studies with similar concentrations of OM, phosphate buffer, cells and ferrihydrite (Chen et al., 2003; Piepenbrock et al., 2011; Shimizu et al., 2013).
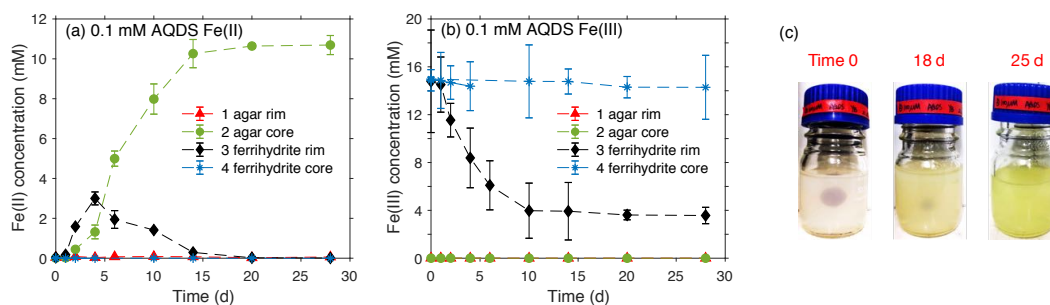
Figure 4.2. Fe(II) (a) and Fe(III) (b) concentrations measured at four locations of the agar of the microbial reduction experiment with ferrihydrite (15 mM) and *Shewanella oneidensis* MR-1 (10^8 cells mL^{-1}) in the presence of 15 mM lactate as electron donor and 0.1 mM AQDS as electron shuttle. Data are means from triplicate bottles ± standard deviation. (c) Gradual appearance of yellow color in the AQDS layer and the disappearance of the ferrihydrite core in the middle, indicating the progress of microbial Fe(III) reduction over time.

Figure 4.3 presents a comparison between experimental data and model-predicted vivianite accumulation, along with the model-computed cumulative Fe(III) reduction. The good agreement between the simulated and measured Fe(II) concentrations supports the inclusion of vivianite precipitation in the numerical model, which successfully captured the measured accumulation of an immobile Fe(II) solid phase. Figure S4.2 presents results of a model version without vivianite precipitation, which did not lead to Fe(II) accumulation at location 2 (the agar core), further supporting the inclusion of an immobile Fe(II) phase to fit the measured Fe(II) concentrations. Our Fe-concentration measurements suggest a slight spatial separation between the reductive dissolution front at sampling location 3 (ferrihydrite rim) and the accumulation of vivianite at location 2 (agar core) (Figure 4.2(a), 4.2(b)), while the model predicts that these would co-occur in closer proximity (data not shown). We attribute this to be an artifact of our sampling procedure which was partly driven by visually observing the boundary of the ferrihydrite-agar ball to the clean agar, and thus subject to slight spatial bias with the progression of the dissolution front. Fitted parameter values and their uncertainty ranges are

summarized in the supporting information, Table S4.2. The MCMC-based calibration considerably reduced the prior-distribution estimates for each parameter. Briefly, the two parameters controlling the kinetics of ferrihydrite reduction and lactate oxidation, k_{fh} and k_{lac} with calibrated geometric mean values of 5.4×10^4 L mmol^{-1} d^{-1} and 0.11 mmol L^{-1} d^{-1}, exhibited narrow uncertainty ranges: 3.5-8.4×10^4 L mmol^{-1} d^{-1} and 0.08-0.17 mM d^{-1}, respectively. The range of uncertainty for k_{lac} lies well within previously reported literature values (Bonneville et al., 2004; Mellage et al., 2018; Roden, 2003). Calibrated parameters with high uncertainty of estimation corresponded to half-saturation (Monod) constants (e.g., K_{lac}) and the rate coefficient for the sorption (k_{sorb}) linear-driving force approximation (equation 5 in the SI, see Table S4.2). Half-saturation coefficients are difficult to constrain under conditions where their magnitude is smaller than the concentration range of substrate. Overall, the parameters governing reaction kinetics and transport exhibit low uncertainty of estimation, and the agreement between the numerical model and the experimental data of all three treatments supports our conceptual understanding of the reactive system.

In a recent study, the addition of AQDS enabled the reduction of the Mn(IV) oxide birnessite over a distance of 40 μm, compared to successful reduction of Mn(IV) oxides over 15 μm in the absence of AQDS by *Geobacter sulfurreducens* with conductive nanowires and cell-excreted Riboflavin as cofactor (Michelson et al., 2017). Our study, with the amendment of 0.1 mM AQDS, showed microbial reduction of ferrihydrite that was initially 2 cm away from the microbial cells (Figure 4.2 (a)). Our control experiments in the agar-solidified setup, amended with only *Shewanella oneidensis* MR-1 or *Geobacter sulfurreducens* (in the absence of electron shuttles), showed no Fe(II) production within up to 50 days of incubation (Figure S4.3). Thereby, confirming that shuttling via FeRB-produced flavins, cytochromes, or conductive nanowires cannot shuttle electrons over 2 cm distances, and supporting AQDS-mediated extracellular reduction. Furthermore, fluorescence microscopy (Figure S4.4) did not detect the presence of cells in the agar of the AQDS setups throughout the incubation (Note: no

cells were detected in the agar of the PPHA and SRNOM amended treatments either.) The lack

of cells in the agar confirms previous reports that the pore size of 2% agar (100-200 nm) is too

dense for FeRB to penetrate (Caccavo et al., 1994; Hau and Gralnick, 2007; Narayanan et al.,

2006), and thus well-suited to prevent direct cell contact between the cells and the ferrihydrite.
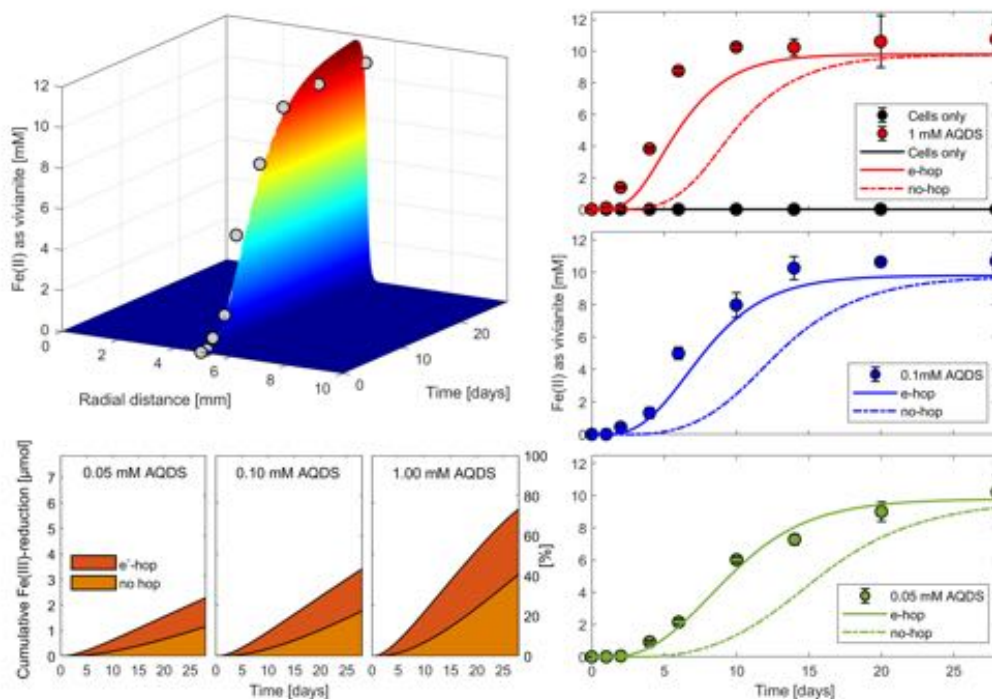

Figure 4.3. Comparison between measured and simulated concentrations. (a): simulated immobile Fe(II) accumulation, as vivianite, as function of radial distance from the center of the ferrihydrite core and time (surface plot) compared to measured values at the ferrihydrite-agar boundary (between sampling locations 2 and 3) (spheres), for the 0.1 mM AQDS treatment. (b-d): Comparison between 9.4-fold enhanced AQDS diffusion (e-hop) (solid line) and pure-diffusion (no e-hop) (dashed line) scenarios for Fe(II) production, at 5 mm from the center of the ferrihydrite (location 2, agar core), in all AQDS concentration treatments. (e-g): Computed cumulative Fe(III) reduction is shown for all scenarios.

Potential electron-transfer mechanisms

At the upper boundary, where the cells are in contact with the agar, AQDS is reduced

to AH$_2$QDS by *Shewanella oneidensis* MR-1, resulting in a localized drop in redox potential

(E_h) and thus more reducing conditions. Conversely, at the ferrihydrite boundary, the presence of the electron acceptor, Fe(III), re-oxidizes the AH_2QDS to AQDS, thus resulting in a relatively higher $AQDS/AH_2QDS$ ratio, and subsequently a more oxidizing E_h. Figure 4.4 shows the computed E_h for the $AQDS/AH_2QDS$ couple from the simulated $AQDS/AH_2QDS$ concentration ratios, along with the difference in E_h between the upper boundary, in contact with cells, and at the ferrihydrite edge, for the 0.1 mM AQDS concentration treatment. The redox gradient between the more reduced top boundary, in contact with *Shewanella oneidensis* MR-1 cells, and the ferrihydrite yields an electromotive force which drives electrons from the outer edge of the agar to the ferrihydrite (Figure 4.4).
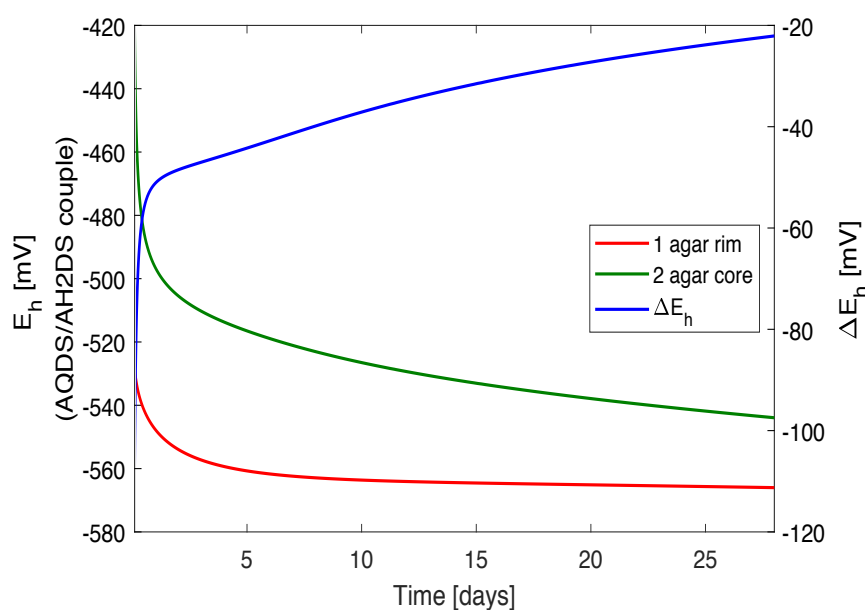
Figure 4.4. Redox potential (E_h) computed by the diffusion-reaction model for the $AQDS/AH_2QDS$ redox couple, at the agar rim that is in contact with the FeRB (red line) and the agar core, in contact with the ferrihydrite agar ball (green line), for the 0.1 mM AQDS treatment. The reduction potential difference (ΔE_h, blue line) is computed as the difference in E_h between the more reducing agar rim and the more oxidizing agar core, and is the electromotive force driving electrons from the outer edge of the agar to the ferrihydrite. An example calculation of the reduction potential is shown section S6 in the SI.

Huskinson et al. (Huskinson et al., 2014) and Liao et al. (Liao et al., 2016) reported an aqueous diffusion coefficient of AQDS of 4.80×10^{-10} m^2 s^{-1}. In our 2% agar medium we measured an effective diffusion coefficient, D_e^{AQDS}, of $5.76 (\pm 1.46) \times 10^{-11}$ m^2 s^{-1}, via cyclic voltammetry (for method details see supporting information section S7), one order of magnitude lower than in water. To capture the timing of Fe(II) accumulation, at location 2 in our experiment, we had to increase the magnitude of D_e^{AQDS} in the reactive-transport model by a calibrated factor (f_{hop}) of 9.41 (uncertainty range: 8.92-9.85). The almost 10-fold higher D_e^{AQDS} suggests the presence of a mechanism which increases the transport flux of reduced quinone, and thus electrons, to the Fe(III) mineral. We propose that this contribution arises from direct electron transfer (electron hopping/self-exchange reaction) between AH$_2$QDS and AQDS molecules (Rosso et al., 2004). Figures 4.3(b)-(d) show a comparison between model results with electron hopping (e$^-$-hop) and only by molecular diffusion of AQDS (no e-hop). Considering an electron hopping contribution successfully captured the timing of Fe(II) accumulation at location 2 (agar core), as observed in the experiments, without leading to Fe(II) appearing in the ferrihydrite core (sampling location 4), while the 'no e-hop' scenario lagged behind for all treatments (Figure 4.3(b)-(d)). (Note: faster lactate oxidation kinetics in the model were unable to capture the timing of Fe(II) accumulation without leading to significant Fe(II) accumulation at the ferrihydrite-core). Our parameterization of enhanced effective diffusion, however, does not account for a dependence on AQDS concentration. An enhancement factor was chosen as it best fits all three experimental results. Furthermore, it is calibrated for diffusion in an agar solidified medium and should be interpreted as an approximation of a hopping/self-exchange contribution. Further research is needed to more mechanistically parameterize enhanced electron transfer as a function of increasing AQDS concentration.

Considering electron hopping as the dominant electron transfer pathway of AQDS molecules, the simulated cumulative Fe(III) reduction shows that within the 28-day incubation

period, 14, 24, and 67% of the Fe(III) was reduced in the 0.05, 0.1 and 1 mM AQDS treatments, respectively (Figure 4.3(e)-(g)). The higher extent of reduction, with increasing AQDS concentration, is a direct result of increased shuttle availability to transport electrons to the ferrihydrite (Michelson et al., 2019). Because of the re-oxidation of AQDS, the model predicts that, with long enough incubation times, each concentration treatment will yield complete reduction of the bioavailable ferrihydrite. However, the overall rate of ferrihydrite reduction (total reduced divided by the incubation time) varies with the AQDS concentration. For an increasing AQDS concentration from 0.05, 0.1 to 1 mM, the ferrihydrite reduction rate increased from 0.04, 0.07 to 0.19 μmol d^{-1}, respectively. With increasing AQDS concentrations, the distance between these molecules is reduced, therefore, the time required for electron hopping is shorter, ultimately resulting in a faster Fe(III) reduction rate. We postulate that electron-carrying AH$_2$QDS molecules diffuse towards the ferrihydrite core, carrying with them electrons, which in addition, driven by the E$_h$-gradient, can hop between neighboring AQDS molecules and enhance the flux of electrons transported to the Fe(III).

Natural organic matter (NOM) as an Fe(III)-reducing electron shuttle

Figure 4.5 shows Fe(II) and Fe(III) concentration time series for agar-solidified incubation experiments with PPHA or SRNOM as the electron shuttle. PPHA amendment resulted in a decrease in Fe(III) concentration in the ferrihydrite rim from ~15 mM to 8 mM, within 20 days of incubation (Figure 4.5(b)). Concurrently, Fe(II) increased at the agar core from 0 to ~7 mM, and remained stable until the end of the experiment (Figure 4.5(a)). The production of Fe(II), mediated by electron transfer over 2 cm, was also found in the setups of ferrihydrite reduction with *Geobacter sulfurreducens* (Figure S4.5(a), (c), (e), (g)), goethite reduction with *Geobacter sulfurreducens* (Figure S4.5(b), (d), (f), (h)) or *Shewanella oneidensis* MR-1 (Figure S4.6), with both PPHA and SRNOM as electron shuttles. In general, goethite was reduced to a much smaller extent compared to ferrihydrite (Figure S4.5, S4.6) due

to the higher crystallinity of goethite than ferrihydrite. Most likely the formation of vivianite also occurred in the OM amended setups, evidenced by the accumulation of immobile Fe(II) in the agar core, and no detection of Fe(II) at the agar rim in all setups (Figure 4.5(a) and Figures S4.5, S4.6).
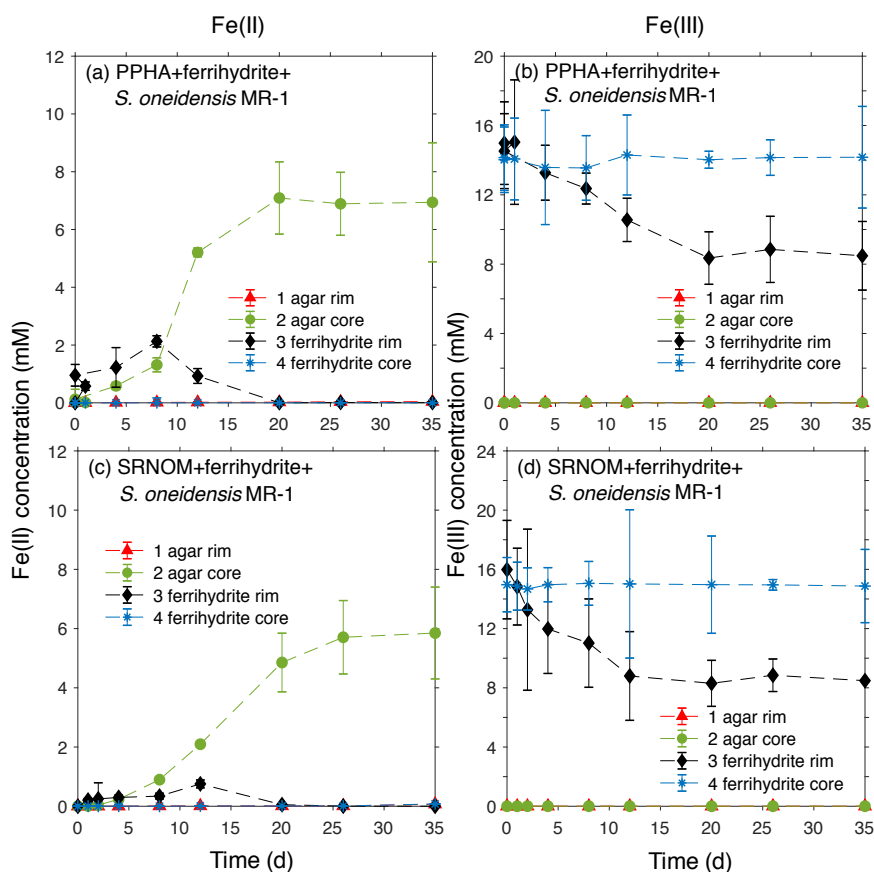

Figure 4.5. Microbial reduction of 15 mM ferrihydrite by 10^8 cells mL^{-1} of *Shewanella oneidensis* MR-1 in the presence of 15 mM lactate as electron donor, 100 mg L^{-1} Pahokee Peat Humic Acids (PPHA) ((a) and (b)) or Suwanee River Natural Organic Matter (SRNOM) ((c) and (d)) as electron shuttle. All experiments were conducted with the agar-solidified setup as shown in Figure 4.1 with 2 cm shuttling distance and incubated at 30 °C in the dark. Data are means from triplicate bottles ± standard deviation, shown as Fe(II) and Fe(III) concentration at four different locations of the agar.

Because of the lower molecular weight of SRNOM, we would expect a larger diffusion coefficient of SRNOM than PPHA, and thus a larger reduction extent of Fe(III) minerals. However, Figure 4.5, Figure S4.5 and S4.6 all show that, regardless of the identity of FeRB and Fe(III) mineral, PPHA always yields more Fe(II) for the same incubation time than SNROM. As discussed above, we postulate that the electron transfer pathway between shuttle molecules and the Fe(III) mineral is enhanced via electron hopping, therefore, instead of the molecular size, we expect the amount of quinone functional groups to influence the extent of ferrihydrite reduction. PPHA, with a higher electron accepting capacity (EAC) (Aeschbacher et al., 2012), therefore containing more quinone functional groups (Aeschbacher et al., 2012) and more electron hopping sites (Pirbadian and El-Naggar, 2012), can accept more electrons per unit molecule compared to SRNOM, and reduce more Fe(III) mineral within the same time.

Additionally, the lower extent of Fe(III) mineral reduction with SRNOM could also be caused by the more positive reduction potential of SRNOM compared to PPHA, as determined by mediated electrochemical analysis (Aeschbacher et al., 2012). At pH 7, the reduction potential of the redox couple FeOOH (synthesized ferrihydrite)-Fe^{2+} is +0.768 V, as measured by mediated potentiometry using a Pt ring combined redox electrode and expressed against the standard hydrogen electrode (SHE) (Gorski et al., 2016; Orsetti et al., 2013). Therefore, electron shuttles with reduction potentials negative enough (e.g., $E_h^{0'}$ of $AQDS_{ox}$-$AQDS_{red}$ is -0.186 V, pH 7) are able to reduce the ferrihydrite after being reduced by the FeRB. Thus, with a more positive reduction potential, reduced SRNOM may reduce ferrihydrite to a lesser extent than reduced PPHA (Bauer and Kappler, 2009).

In addition to its function as an electron shuttle, NOM can interact with both the Fe(III) minerals and Fe(II) without exchanging electrons. Complexation of Fe(II) by the NOM could have increased the thermodynamic driving force for Fe(III) reduction (Roden and Urrutia, 1999). However, previous studies have shown that phosphate can outcompete OM for Fe(II)

(Poggenburg et al., 2018), and the formation of vivianite in our experiments further supports that the complexation of Fe(II) by OM did not seem to exert a noticeable influence on the Fe(III) reduction. Moreover, the adsorption of OM to the Fe(III) mineral surfaces could potentially block surface sites (Kaiser and Guggenberger, 2003) and induce aggregation (Amstaetter et al., 2012). However, the starting state of the ferrihydrite/goethite agar ball was a ferrihydrite/goethite-OM aggregated agar ball because the same concentration of OM as in the shuttling agar was used in the ferrihydrite/goethite ball. Finally, although OM can act as a ligand promoting Fe(III) solubilization (Jones et al., 2009; Nevin and Lovley, 2002a, b), the highest Fe(III) concentration found outside of the ferrihydrite/goethite agar ball (sampling location 2, see Figure 4.1) was 0.02 mM, suggesting that the release of Fe(III) via chelation by OM was negligible during our experiment. In summary, we postulate that electron shuttling by OM, i.e., OM-facilitated electron transfers between the cells that were physically separated from the ferrihydrite, and the mineral, was the main mode of action of the added OM in our experiments.

4.5 Implications

Batch experiments have typically been used to study the effects of AQDS and OM as electron shuttles on microbial Fe(III) reduction (Amstaetter et al., 2012; Jiang and Kappler, 2008; Kappler et al., 2004; Lovley et al., 1996; Poggenburg et al., 2018; Roden et al., 2010; Wolf et al., 2009). However, due to various interactions between OM and Fe(III) minerals, it is challenging to evaluate to what extent OM stimulates microbial Fe(III) reduction by acting as an electron shuttle (Poggenburg et al., 2018). Our study showed that microbial Fe(III) reduction can occur over 2 cm distance with AQDS or OM only acting as the electron shuttle. Coupling our experimental data with a diffusion-reaction model shed light on an electron hopping contribution (in addition to molecular diffusion) as an electron transfer pathway between AQDS/OM. Although the organic carbon concentration used in our study (100 mg C L^{-1}) was much higher than in most natural settings (Sparks, 2003), our experiment with 0.05 mM AQDS

suggest that even a low concentration of redox-active organic molecules could stimulate microbial reduction of Fe minerals over cm distances. Furthermore, long enough time-scales, would result in the complete reduction of Fe(III) oxides, even at low concentrations of electron shuttles, due to the reversibility of the oxidation/reduction of quinone groups. Additionally, we showed that long-distance electron transfer is independent of the crystallinity of the Fe(III) mineral, the identity of the FeRB, and can be facilitated by multiple types of OM.

4.6 Supporting information

S1. Preparation of agar for the electron shuttling experiment

Agar powder (agar powder for bacteriology, VWR Chemicals, CAS: 9002-18-0, Germany) was washed three times with Milli-Q water before use to remove salts and impurities. The washed agar was re-suspended in Milli-Q water at a concentration of 2% (w/v), deoxygenated 3 times (each time 5 min vacuum and 5 min N_2-flushing) while stirring and autoclaved at 120 °C for 20 min. The autoclaved warm agar solution was used immediately before it cooled down.

The Fe(III) mineral agar core, with 15 mM ferrihydrite or goethite, and the same concentration of electron shuttle as in the shuttling agar layer was prepared in a sterile silicone mold with 1 cm diameter (Figure S4.1). To prepare the Fe(III) mineral agar core, a suspension of ferrihydrite or goethite, together with the electron shuttle solution, was added to the autoclaved warm agar, and it was vigorously shaken. A 0.52 mL volume of the warm agar mix was added to each hole of the mold. After 10 min of incubation on ice, the solidified Fe(III) mineral agar core was squeezed out of the hole and was stored in a sterilized bottle for no more than 2 hours before further use.

S2. Cultivation of Fe(III)-reducing bacteria

Shewanella oneidensis MR-1 cells from a frozen stock were streaked on oxic lysogeny broth (LB) agar plates (Hallberg and Johnson, 2001) (10 g/L peptone, 5 g/L yeast extract, 10 g/L NaCl and 15 g/L agar). Colonies were transferred to liquid LB medium and incubated at 30 °C for 14 h, cells were harvested by centrifugation (10 min, 8000 rpm) and then washed three times with and re-suspended in anoxic SBM medium (0.225 g/L K_2HPO_4, 0.225 g/L KH_2PO_4, 0.46 g/L NaCl, 0.225 g/L $(NH_4)_2SO_4$, 2.18 g/L Na-lactate, 0.117 g/L $MgSO_4 \cdot 7H_2O$, 2.38 g/L HEPES, pH 7.2-7.5). For *Geobacter sulfurreducens*, 10 mL of a culture were transferred with a syringe to a sterile, crimp-sealed 200 mL serum bottle with 100 mL anoxic mineral medium containing 15 mM acetate as the electron donor and 40 mM fumarate as electron acceptor. The mineral medium contained, per liter doubly-deionized water (<18.2 MΩ.cm; Milli-Q, Millipore): 0.6 g KH_2PO_4, 0.3 g NH_4Cl, 0.5 g $MgSO_4 \cdot 7H_2O$, 0.1 g $CaCl_2 \cdot 2H_2O$, 2.5 g $NaHCO_3$, 1 mL trace elements solution SL10 ($FeCl_2 \cdot 4H_2O$, $ZnCl_2$, $MnCl \cdot 4H_2O$, H_3BO_3, $CoCl_2 \cdot 6H_2O$, $CuCl_2 \cdot 2H_2O$, $NiCl_2 \cdot 6H_2O$, $Na_2MoO_4 \cdot 2H_2O$), 1 mL vitamin solution and 1 mL selenite solution. Cells were harvested by centrifugation (10 min, 8000 rpm) and re-suspended in the anoxic mineral medium as described above.

S3. Preparation of PPHA and SRNOM solutions

Pahokee Peat Humic Acid (PPHA, 1S103F) and Suwannee River natural organic matter (SRNOM, 1R101N) were purchased from the International Humic Substances Society. To prepare solutions for the shuttling experiment, PPHA and SRNOM powders were added to phosphate buffer (50 mM, pH 7) at a concentration of 1 g L^{-1}. Although the chosen phosphate concentration is higher than typically observed in nature and can potentially led to the formation of Fe(II) phosphate minerals (e.g., vivianite), this phosphate buffer was chosen to allow comparison of our study to previous studies (Bauer and Kappler, 2009; Jiang and Kappler, 2008;

Klupfel et al., 2014; Piepenbrock et al., 2014). The solutions were agitated overnight (>14 h) at room temperature, filtered and sterilized at the mean time by 0.22 μm syringe filters (mixed cellulose ester (MCE), Millipore, Germany) as described before (Jiang and Kappler, 2008). All solutions were deoxygenated 3 times (each time 3 min vacuum and 3 min N_2-flushing) and stored in dark bottles to avoid photochemical reactions. The dissolved organic matter (DOM) concentration of all solutions were measured after the preparation (TOC analyzer, model 2100S, Analytik Jena, Germany).

S4. Fe(III) mineral synthesis

Ferrihydrite was synthesized by neutralizing 200 mM $Fe(NO_3)_3$ with 1 M KOH; goethite was prepared by aging ferrihydrite at elevated temperature (70 °C) for 60 hours (Cornell and Schwertmann, 2006). Goethite was identified by μ-X-ray diffraction (μ-XRD). The synthesized minerals were washed four times with doubly-deionized water (<18.2 MΩ.cm; Milli-Q, Millipore), re-suspended in Milli-Q-water and stored at 4 °C. The ferrihydrite used in all experiments was freshly synthesized for each experiment and stored no longer than seven days before use.

S5. Diffusion-reaction model

Table S4.1 presents a list of the geochemical reactions considered in the diffusion-reaction model. *Shewanella oneidensis* MR-1, inoculated on top of the agar-solidified setup, were implicitly considered in the reaction rates outlined below. In the calculations, pH is kept constant at 7, that is the pH of the agar medium. Reactive transport of dissolved chemical species i within the spherical domain is described by:

$$\frac{\partial C_i}{\partial t} = \frac{2D_e}{r}\frac{\partial C_i}{\partial r} + D_e\frac{\partial^2 C_i}{\partial r^2} + R_i \tag{1}$$

in which C_i [mol L^{-1}] is the dissolved concentration of compound i, D_e [m^{-2} s^{-1}] is the effective diffusion coefficient in agar, R_i [mol L^{-1} h^{-1}] is the sum of all rates of reactions producing the chemical species minus those consuming it, and r and t are the radial distance and time, respectively.

The effective diffusion coefficient D_e summarizes the cumulative effects of molecular diffusion and electron hopping and is parameterized as the molecular diffusion coefficient D_m^{AQDS} measured by cyclic voltammetry (see section S7) multiplied by an enhancement factor f_{hop}:

$$D_e = f_{hop} \cdot D_m^{AQDS} \tag{2}$$

The reaction rate of microbially mediated lactate oxidation, r_{lac} [mmol L^{-1} d^{-1}], was simulated with dual-Monod kinetics, implicitly accounting for biomass:

$$r_{lac} = k_{lac} \cdot \frac{C_{Lac}}{C_{Lac} + K_{Lac}} \cdot \frac{C_{AQDS}}{C_{AQDS} + K_{AQDS}} \tag{3}$$

in which k_{lac} [d^{-1}] is the corresponding maximum reaction rate constant , C_{Lac} [mmol L^{-1}] is the lactate concentration, C_{AQDS} [mmol L^{-1}] the concentration of AQDS, K_{Lac} [mmol L^{-1}] is the half-saturation constant for lactate uptake, K_{AQDS} [mmol L^{-1}] is the half-saturation constant for AQDS.

The reaction rate of AH2QDS-mediated abiotic reduction of ferrihydrite was simulated with double-linear kinetics (Shi et al., 2012):

$$r_{FHRED} = k_{fh} \cdot C_{Fe(III)} \cdot C_{AH_2QDS} \tag{4}$$

where k_{fh} [mmol^{-1} L d^{-1}] is the rate constant of ferrihydrite reduction, $C_{Fe(III)}$ [mmol L^{-1}] is the bioavailable concentration of free Fe(III) as ferrihydrite, and C_{AH_2QDS} [mmol L^{-1}] is the aqueous concentration of AH2QDS. A fraction ferrihydrite of 0.2 was considered unavailable for reduction in the model, based on the consistently (across all experiments) remaining 3 mM

of Fe(III), of the initial 15 mM concentration. In addition, the model accounts for Fe(II) adsorption onto ferrihydrite. Sorption is computed via a first-order rate driven by the sorption disequilibrium, that is, the difference between equilibrium sorbed and actual sorbed Fe(II) concentrations at each simulation time-step.

$$C_{Fe(II)}^{EQ-sorb} = \alpha \cdot C_{Fe(III)}^{tot} \cdot \frac{C_{Fe(II)}}{K_{ads} + C_{Fe(II)}} \tag{5}$$

$$r_{sorb} = k_{sorb}\left(C_{Fe(II)}^{EQ-sorb} - C_{Fe(II)}^{ads}\right) \tag{6}$$

The equilibrium surface-associated Fe(II), $C_{Fe(II)}^{EQ-sorb}$, is computed as a function of dissolved Fe^{2+}, $C_{Fe(II)}$, assuming Langmuir sorption (equation 4), where the maximum sorption is the product of the moles of available sorption sites per mole of ferrihydrite, α, and the total concentration (bioavailable plus the non-available fraction) ferrihydrite, $C_{Fe(III)}^{tot}$, and K_{ads} [mmol L^{-1}] is the binding constant (Roden, 2018). The first-order kinetic sorption rate is given by equation 5 (analogous to the approach in Mikutta et al. (Mikutta et al., 2009), where k_{sorb} [d^{-1}] is the kinetic sorption rate constant, and $C_{Fe(II)}^{ads}$ [mmol L^{-1}] is the actual ferrihydrite-surface-associated Fe(II) concentration). Desorption of Fe(II) caused by ferrihydrite dissolution is computed as proportional to the rate of ferrihydrite reductive-dissolution:

$$r_{desorb} = \beta \cdot r_{FHRED} \tag{7}$$

where β corresponds to the number of moles of surface associated Fe(II) per mole of ferrihydrite.

The precipitation of vivianite was also simulated in separate equilibrium and kinetic steps. Phosphate concentrations were computed at each time step based on the acid-base chemistry of phosphoric acid (Priambodo et al., 2017) and the available total soluble phosphorus. The equilibrium Fe(II) concentration was computed from the solubility product ($K_{sp}=10^{-35.775}$) (Alborno and Tomson, 1994). Vivianite precipitation was simulated via a kinetic rate,

dependent on the difference between actual dissolved Fe^{2+} and the expected concentration in equilibrium with vivianite, $C_{Fe(II)}^{EQ-viv}$:

$$r_{precip} = k_{precip} \cdot \left(C_{Fe(II)} - C_{Fe(II)}^{EQ-viv} \right) \tag{8}$$

where k_{precip} [d^{-1}] is the first-order kinetic rate constant for vivianite precipitation.

With the above reaction rate expressions, the diffusion-reaction model yields the following system of equations governing the concentration changes of chemical species:

$$\frac{\partial C_{lac}}{\partial t} = \frac{2D_e}{r}\frac{\partial C_{lac}}{\partial r} + D_e\frac{\partial^2 C_{lac}}{\partial r^2} - r_{lac} \tag{9}$$

$$\frac{\partial C_{AQDS}}{\partial t} = \frac{2D_e}{r}\frac{\partial C_{AQDS}}{\partial r} + D_e\frac{\partial^2 C_{AQDS}}{\partial r^2} + \frac{1}{2}r_{FHRED} \tag{10}$$

$$\frac{\partial C_{AH_2QDS}}{\partial t} = \frac{2D_e}{r}\frac{\partial C_{AH_2QDS}}{\partial r} + D_e\frac{\partial^2 C_{AH_2QDS}}{\partial r^2} - \frac{1}{2}r_{FHRED} \tag{11}$$

$$\frac{\partial C_{Fe(II)}}{\partial t} = \frac{2D_e}{r}\frac{\partial C_{Fe(II)}}{\partial r} + D_e\frac{\partial^2 C_{Fe(II)}}{\partial r^2} + r_{FHRED} - r_{sorb} + r_{desorb} - r_{precip} \tag{12}$$

$$\frac{\partial C_{PO_4^{3-}}}{\partial t} = \frac{2D_e}{r}\frac{\partial C_{PO_4^{3-}}}{\partial r} + D_e\frac{\partial^2 C_{PO_4^{3-}}}{\partial r^2} - r_{precip} \tag{13}$$

$$\frac{dC_{Fe(III)}^{tot}}{dt} = -r_{FHRED} \tag{14}$$

$$\frac{dC_{Fe(II)}^{ads}}{dt} = r_{sorb} - r_{desorb} \tag{15}$$

$$\frac{dC_{Fe(II)}^{viv}}{dt} = r_{precip}$$

(16)

Equation 1 was discretized by the finite volume method, and the spherical domain was subdivided into n [−] shells of identical thickness. Transport and reaction (equations 8-15) were solved jointly, in MATLAB, by integrating the resulting nonlinear system of ordinary differential equations by the ordinary-differential-equation solver ode15s. Lactate oxidation, driven by r_{lac}, is microbially-catalyzed, and this only occurs at the outer edge of the domain, where the cells (which cannot penetrate the agar) are situated. Hence, equation 8 only holds true at the outermost shell of the domain. In all inner shells lactate was assumed to only undergo transport, that is, no reaction contribution by r_{lac}.

We fitted the model to the measured data using DREAM$_{ZS}$ (Laloy and Vrugt, 2012; Vrugt, 2016), a Markov-chain Monte Carlo method resulting in a posterior distribution of all fitted parameters. We fitted the logarithms of the model coefficients rather than the coefficients themselves which alleviates that the individual coefficients have nominal values differing by orders of magnitude. As objective function, we considered the sum of squared differences between the measured and simulated Fe(II) concentrations. We analyzed the posterior distribution of the delogarithmized parameters to obtain their geometric mean, median and standard deviations of estimation, $\hat{\sigma}_{p_i}$. Standard deviations were obtained by computing quantiles, namely, the 16th and 84th percentiles, which correspond to (±) one-standard deviation assuming a normal distribution for each parameter. Table S4.2 summarizes the list of the median, geometric mean, and best estimates (i.e., yielding the lowest value of the objective function) for all calibrated parameters. Standard deviations for the posterior parameter distributions are reported alongside, providing an estimated uncertainty range. The root mean square error of the fitted Fe(II) concentrations was 0.67, 0.46 and 0.66 mM for the 0.05, 0.1 and 1 mM AQDS concentration treatments, respectively, using the geometric mean parameter-

values. (Note: all model output in the SI and main manuscript are for forward runs with the geometric mean values.). Furthermore, an overview of the spatio-temporal model output for oxidized and reduced iron and quinone species is compared to experimental data, for the 0.1 mM AQDS concentration treatment, in Figure S4.7. Figure S4.8 shows histograms of the marginal estimated log-parameter distributions and bivariate scatter plots, considering the last 3000 model realizations of the MCMC sampler.

S6. Reduction potential (E_h) calculation of AQDS-AH$_2$QDS redox couple

We calculated the redox potential for the AQDS-AH$_2$QDS redox couple using the Nernst equation at 25 °C:

$$E_h = E^{0\prime}_{AQDS/AH2QDS} + \frac{2.3RT}{nF} log\left(\frac{AQDS}{AH_2QDS}\right) - \frac{0.059}{2} log(H^+) \qquad (17)$$

The $E^{0\prime}_{AQDS/AH_2QDS}$ at pH 7 and 25 °C was determined to be -184 mV (Cadena et al., 2007).

S7. Determination of the diffusion coefficient of AQDS in 2 % agar

The diffusion coefficient of AQDS in 2% agar was determined from the cyclic voltammetry of 5 mM AQDS in 2% agar. Although much higher than the concentration of AQDS used for the agar-solidified experiments, 5 mM was used for the cyclic voltammetry because of the undetectable signal of oxidation and reduction peaks of AQDS at lower concentrations. As shown in previous studies, the cyclic voltammetry measurement was performed in a three-electrode configured cell using a Bio-logic model VSP potentiostat controlled by the EC-lab platform at room temperature. Platinum wire, graphite rod, and Ag/AgCl saturated with KCl was used as working electrode, counter electrode and reference electrode, respectively (Sun et al., 2017; Sun et al., 2018). A 0.1 M KCl solution at pH 7 (buffered with phosphate) was used as the supporting electrolyte. At room temperature (25 °C), the relation between scan rate and the peak current is described by the Randles-Sevcik equation:

$$i_p = 268{,}600 \, n^{\frac{3}{2}} \, A D^{\frac{1}{2}} \, C v^{\frac{1}{2}} \tag{18}$$

Where i_p is the peak current [A], n is the number of electrons transferred in the redox event (n=2 for AQDS to AH_2QDS), A is the electrode area ($0.314 \, cm^2$), D is the diffusion coefficient [$m^2 \, s^{-1}$], C is the concentration [$mol \, cm^{-3}$] and v is the scan rate [$V \, s^{-1}$]. From equation 18, the diffusion coefficient of AQDS (D) can be determined from equation 19:

$$D = \left(\frac{i_p}{v^{\frac{1}{2}}} \times \frac{1}{268600 \times n^{\frac{3}{2}} \times AC} \right)^2 \tag{19}$$

in which $\frac{i_p}{v^{\frac{1}{2}}}$ can be obtained from the slope of Figure S4.9(b), which shows the correlation of peak current and the square root of scan rate [$(V \, s^{-1})^{0.5}$]. The peak current at different scan rate was directly measured from the cyclic voltammogram of 5mM AQDS, as shown in Figure S4.9(a). For calculation, we took the average value of the slopes from oxidation and reduction scan. The calculated (from duplicates) diffusion coefficient of AQDS $\left(D_e^{AQDS} \right)$ in 2% agar is $5.76 \pm 1.46 \times 10^{-11} \, m^2 \, s^{-1}$.

Table S4.1. Reactions that happen in the experiment of ferrihydrite reduction by *Shewanella oneidensis* MR-1, with AQDS as electron shuttle.

Lactate oxidation coupled to AQDS reduction	$C_3H_6O_3 + H_2O + 2AQDS \rightarrow CH_3COOH + CO_2 + 2AH_2QDS$
Fe(III) mineral reduction coupled to AH_2QDS oxidation	$2Fe(OH)_3 + 4H^+ + AH_2QDS \rightarrow 2Fe^{2+} + AQDS + 6H_2O$
Vivianite formation	$3Fe^{2+} + 2HPO_4^{2-} + 8H_2O \rightarrow Fe_3(PO_4)^{2} \cdot 8H_2O + 2H^+$

Table S4.2. Reaction parameters for the fitted diffusion reaction model and the corresponding uncertainty bounds. The median, geometric mean and best estimate calibrated parameter values are provided alongside the computed 16th and 84th percentile ranges which correspond to plus and minus one-standard deviation ($\pm\hat{\sigma}_{p_i}$).

	Parameter	Units	Median	Geometric mean	Best Estimate	Uncertainty range ($\pm\hat{\sigma}_{p_i}$)	Prior range
f_{hop}	hopping factor	[-]	9.51	9.41	8.72	8.92–9.85	1–10
k_{lac}	lactate oxidation max. reaction rate constant	[mmol L^{-1} d^{-1}]	0.12	0.11	0.26	0.08–0.17	0.008–0.78
K_{Lac}	lactate half-saturation coefficient	[mmol L^{-1}]	0.12	0.13	0.24	0.03–0.48	0.01–1
K_{AQDS}	AQDS half-saturation coefficient	[mmol L^{-1}]	0.31	0.32	0.65	0.23–0.44	0.01–1
k_{fh}	ferrihydrite reduction rate constant	[L mmol^{-1} d^{-1}]	6.0×10^4	5.4×10^4	5.7×10^4	$(3.5–8.4)\times10^4$	$(0.08–8.6)\times10^4$
K_{ads}	binding constant	[mmol L^{-1}]	3.3×10^{-3}	4.1×10^{-3}	2.8×10^{-3}	$(1.3–15)\times10^{-3}$	$(1-100)\times10^{-3}$
k_{sorb}	kinetic sorption constant	[d^{-1}]	2.8×10^3	5.4×10^3	1.9×10^4	$(0.8–114)\times10^3$	$(0.08–860)\times10^3$
α	max. sorption capacity	[-]	19.1	16.6	93.6	2.72–84.7	1–100
k_{precip}	kinetic precipitation constant	[d^{-1}]	1.5×10^5	1.3×10^5	8.6×10^5	2.8×10^5	$86–8.6\times10^5$
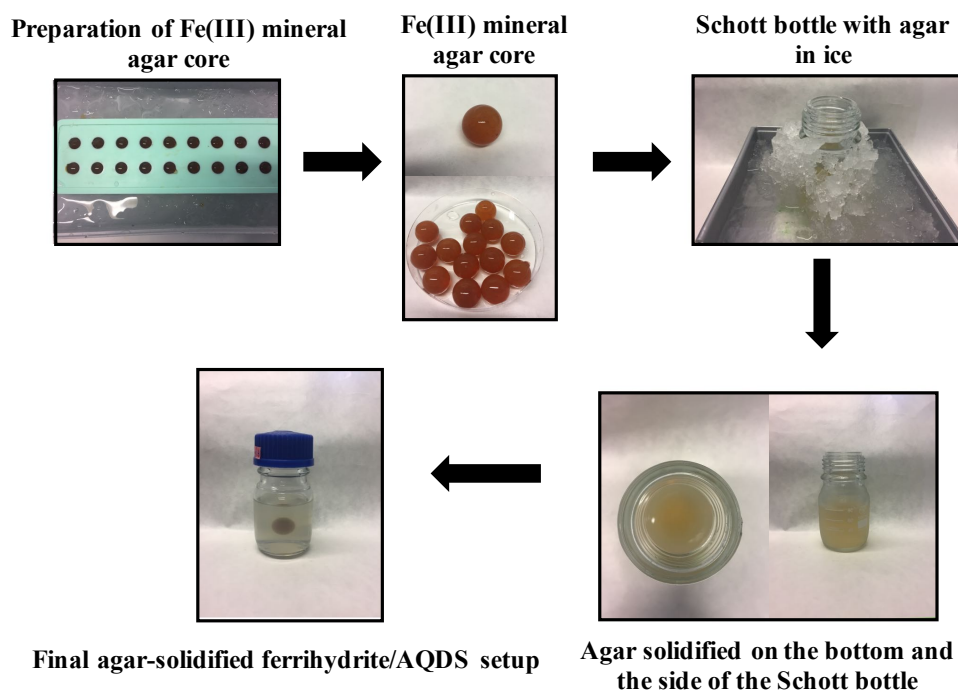
Figure S4.1. Preparation of the agar-solidified experimental setup. The Fe(III) mineral agar core with 15 mM ferrihydrite or goethite and the same concentration of electron shuttle as in the shuttling layer was prepared in a silicone mold with 1 cm diameter. 100 mL Schott bottles with the organic matter (OM)-containing agar solution was surrounded by ice water. When about 2 cm of the bottom and the edge of the agar were solidified, the Fe(III)-mineral-agar core was dropped into the bottle to be fixed in the center. Bottles stayed in ice until complete solidification of the agar.
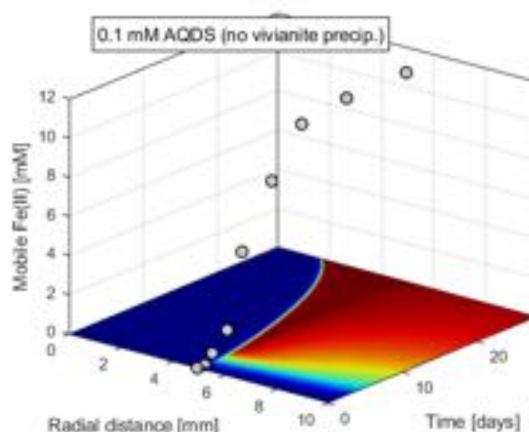
Figure S4.2. Simulated mobile Fe(II) concentration with the omission of vivianite precipitation in the presence of 0.1 mM AQDS, compared to Fe(II) measurements at location 2 (agar core).
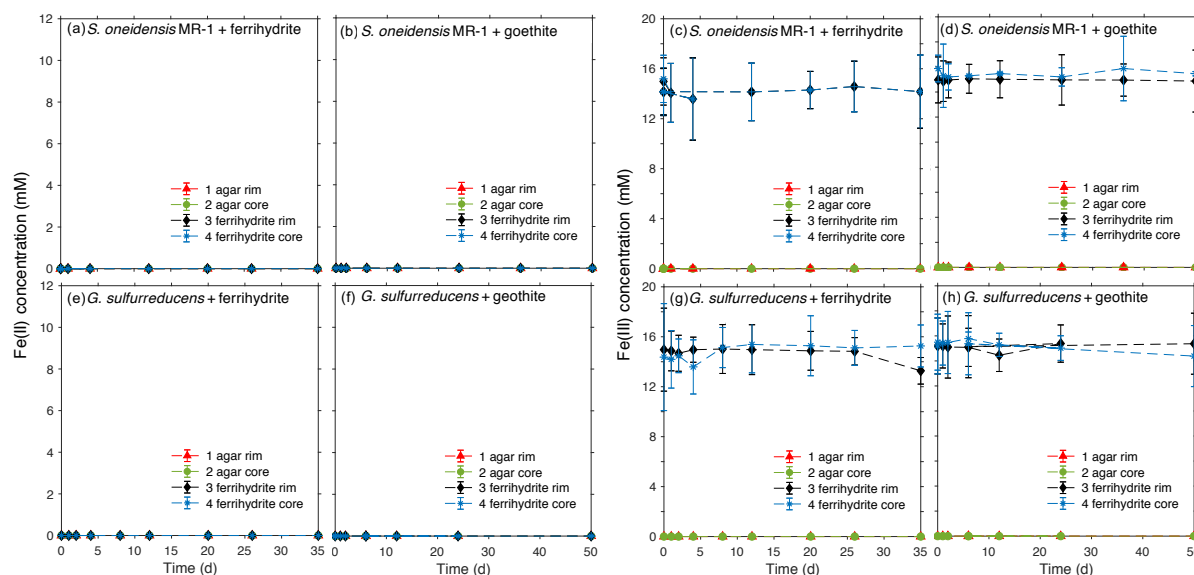
Figure S4.3. Experiments with 15 mM ferrihydrite ((a), (c), (e), (g)) or goethite ((b), (d), (f), (h)) by 10^8 cells mL^{-1} of *Shewanella oneidensis* MR-1 ((a)-(d)) or *Geobacter sulfurreducens* ((e)-(h)) in the presence of 15 mM lactate (for *S. oneidensis* MR-1) or acetate (for *G. sulfurreducens*) as electron donor. All experiments were conducted with the agar-solidified setup with 2 cm shuttling distance and incubated at 30 °C in the dark. Data are mean from triplicate bottles ± standard deviation, shown as Fe(II) and Fe(III) concentration at four different locations of the agar.
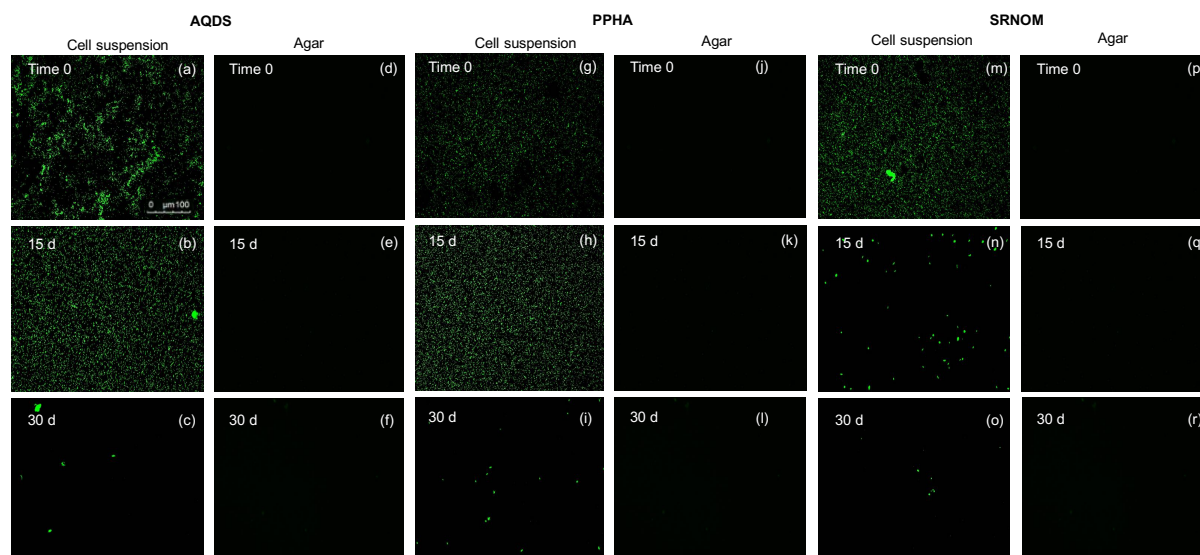
Figure S4.4. Fluorescence microscopy images of the cell suspension on top of the agar and in the agar of the experiments with 0.1 mM AQDS (a-f), PPHA (g-l) and SRNOM (m-r) and *Shewanella oneidensis* DKN308 cells. *Shewanella oneidensis* DKN308, on the one hand, contains the gene encoding the GFP mut3* fluorescent protein (Marin-Spiotta et al., 2014) and thus can be easily visualized using a 485/20 excitation filter and 528/20 emission filter (Teal et al., 2007). On the other hand, it has been tested and proven to behave exactly the same as *Shewanella oneidensis* MR-1 in biogeochemical reactions (Groh et al., 2005; Myers and Myers, 1997). The *Shewanella oneidensis* MR-1 cells were not used in the experiments for microscopy imaging due to the difficulties of successfully staining the cells when they are in agar. When using *Shewanella oneidensis* MR-1 cells it was impossible to evaluate whether the absence of cells in the agar (the absence of fluorescence signal) is due to the poor staining of the cells or because cells were indeed unable to penetrate into the agar. Instead, when using *Shewanella oneidensis* DKN308, green fluorescence indicates *Shewanella oneidensis* DKN308 cells at the beginning of the experiment (time 0), after 15 days of incubation and the end of the experiment. The absence of cell fluorescence signal in the agar shows that the 2% agar is solid enough to prevent cell penetration therefore the cells must use the provided AQDS, PPHA and SRNOM to transfer electrons to the Fe(III) mineral.
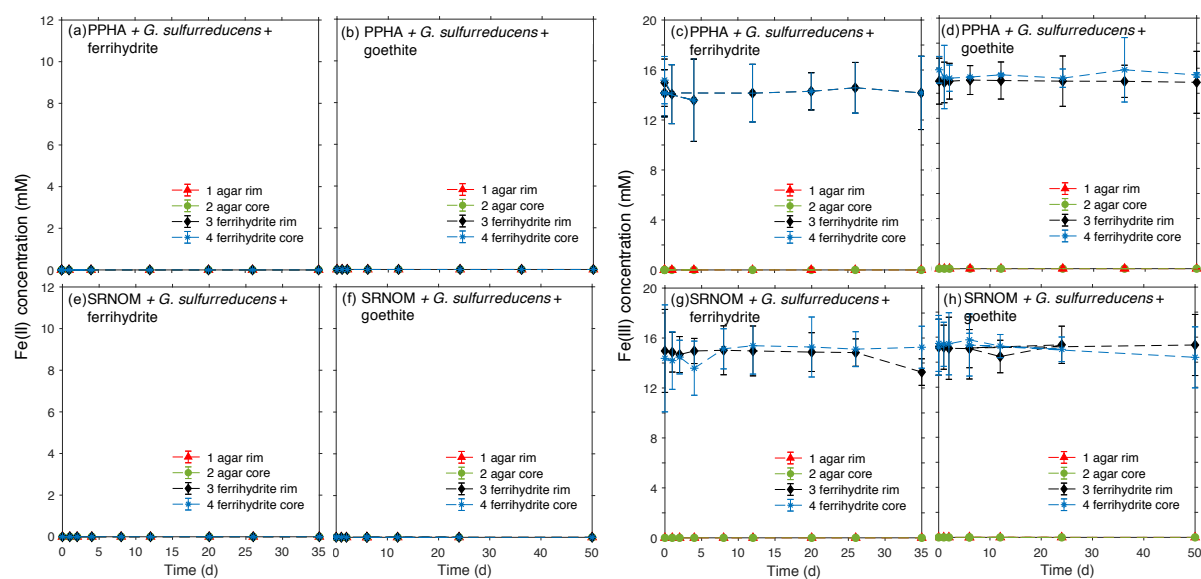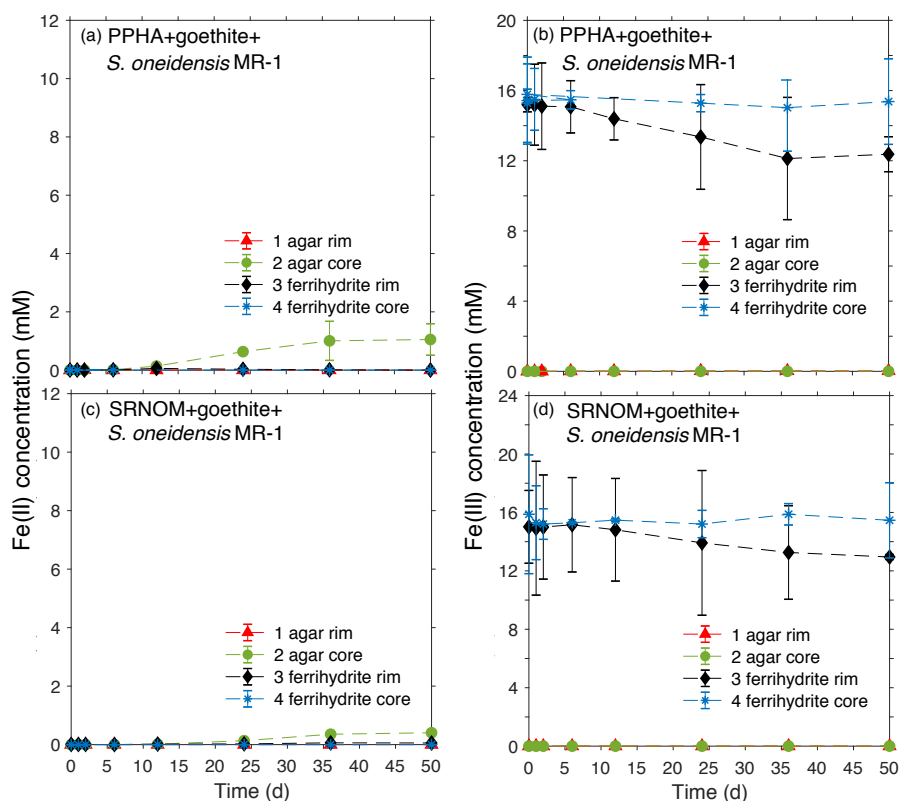
Figure S4.5. Microbial reduction of 15 mM ferrihydrite ((a), (c), (e), (g)) or goethite ((b), (d), (f), (h)) by 10^8 cells mL^{-1} of *Geobacter sulfurreducens* in the presence of 15 mM acetate as electron donor, 100 mg L^{-1} Pahokee Peat Humic Acids (PPHA) ((a)-(d)) or Suwanee River Natural Organic Matter (SRNOM) ((e)-(h)) as electron shuttle. All experiments were conducted with the agar-solidified setup with 2 cm shuttling distance and incubated at 30 °C in the dark. Data are mean from triplicate bottles ± standard deviation, shown as Fe(II) and Fe(III) concentration at four different locations of the agar.

Figure S4.6. Microbial reduction of 15 mM goethite by 10^8 cells mL^{-1} of *Shewanella oneidensis* MR-1 in the presence of 15 mM lactate as electron donor, 100 mg L^{-1} Pahokee Peat Humic Acids (PPHA) ((a)-(b)) or Suwanee River Natural Organic Matter (SRNOM) ((c)-(d)) as electron shuttle. All experiments were conducted with the agar-solidified setup with 2 cm shuttling distance and incubated at 30 °C in the dark. Data are mean from triplicate bottles ± standard deviation, shown as Fe(II) and Fe(III) concentration at four different locations of the agar.
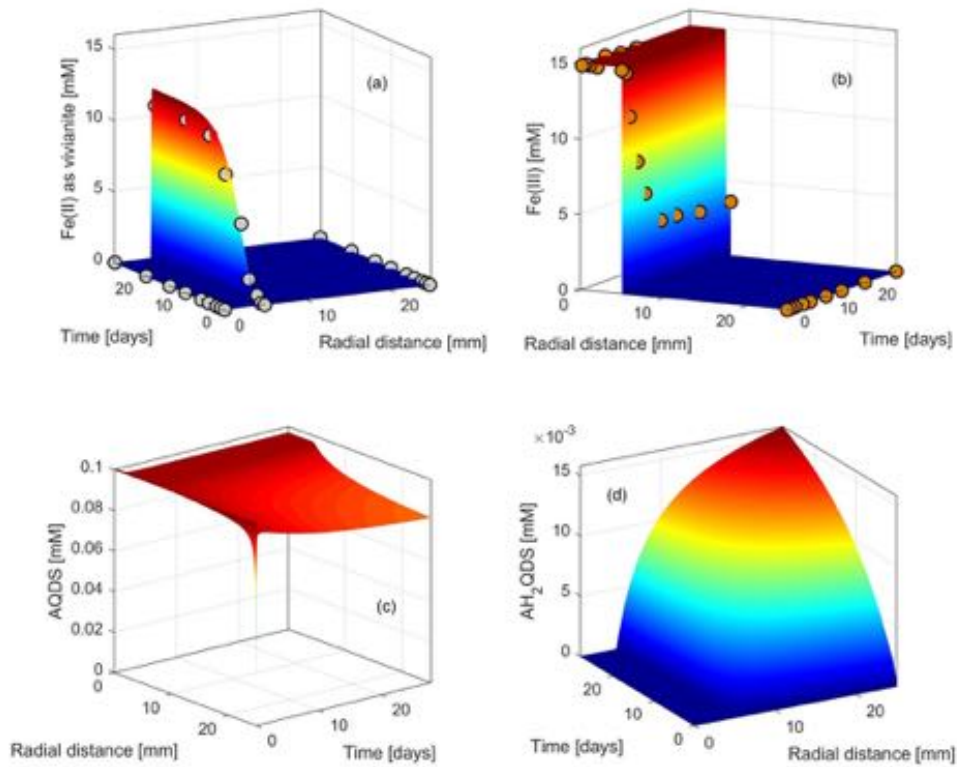
Figure S4.7. Simulation results for the 0.1 mM AQDS concentration treatment. The spatio-temporal output of the model is compared to measured (a) Fe(II) and (b) Fe(III) concentrations at the center of the domain, the ferrihydrite-agar reactive fringe and the outer edge of the domain, where the FeRB are in contact with the agar. Simulated AQDS and AH$_2$QDS concentrations are presented in panels (c) and (d), respectively, these were not measured during the experiment.
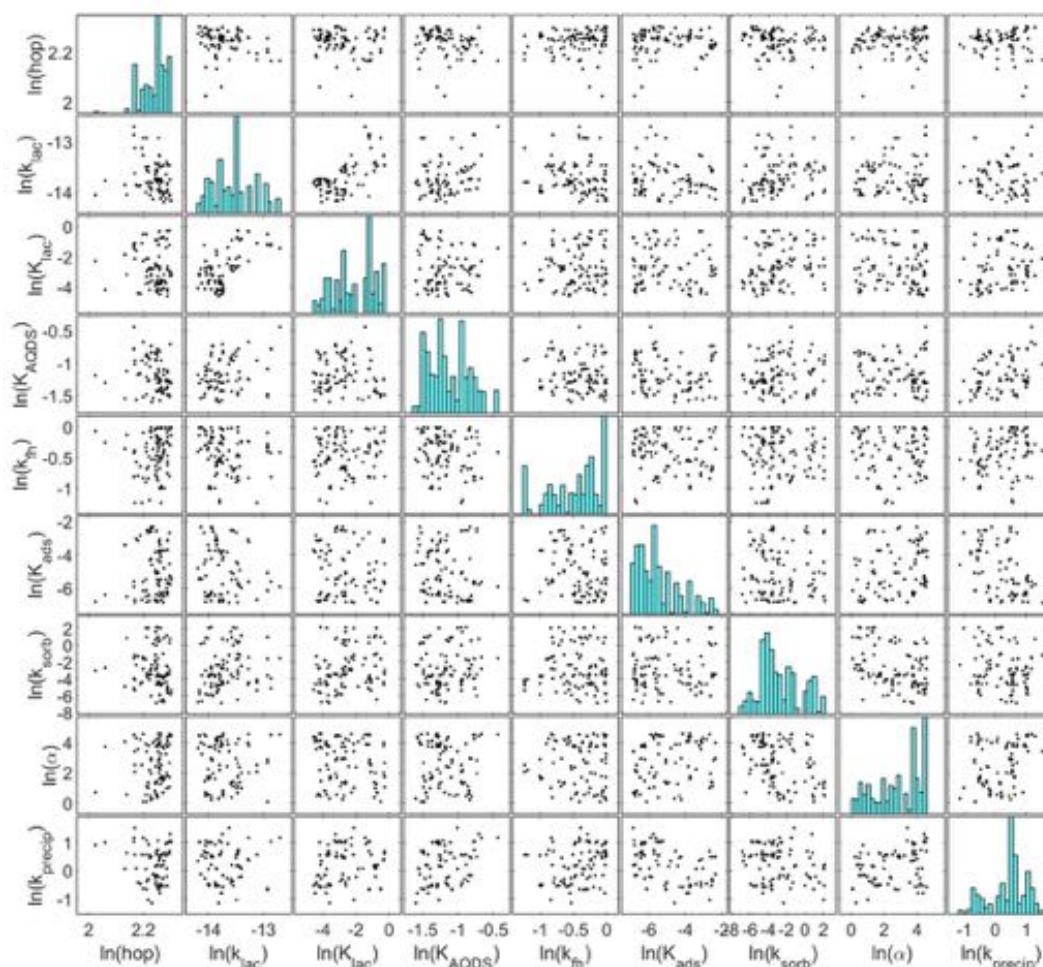
Figure S4.8. Posterior distribution of fitted log-parameters. Bivariate scatter plots and histograms of marginal distributions.
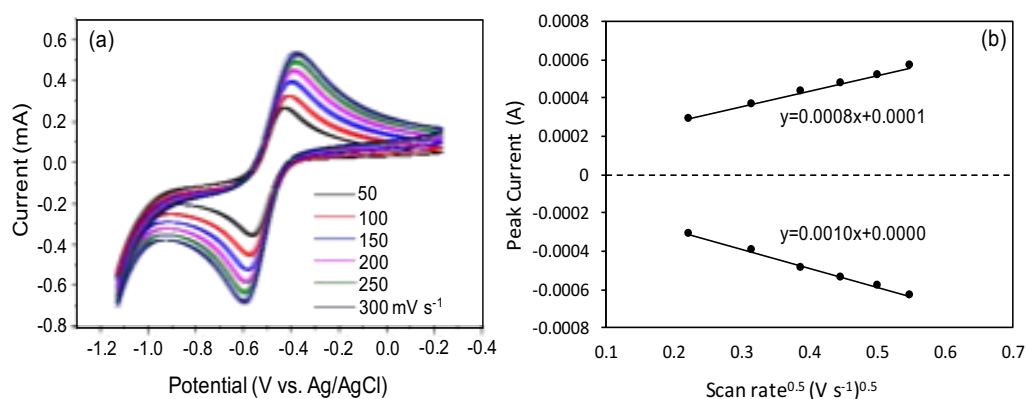
Figure S4.9. Cyclic voltammogram of 5 mM AQDS in 2% agar (a). The correlation of peak current and the scan rate of 5 mM AQDS in 2% agar (b), plotted from the cyclic voltammogram (a).

4.7 References

Aeschbacher, M., Graf, C., Schwarzenbach, R. P. and Sander, M. (2012) Antioxidant properties of humic substances. *Environ. Sci. Technol.* **46** (9), 4916-4925.

Al-Borno, A. and Tomson, M. B. (1994) The temperature dependence of the solubility product constant of vivianite. *Geochim. Cosmochim. Acta* **58** (24), 5373-5378.

Amstaetter, K., Borch, T. and Kappler, A. (2012) Influence of humic acid imposed changes of ferrihydrite aggregation on microbial Fe(III) reduction. *Geochim. Cosmochim. Acta* **85**, 326-341.

Bauer, I. and Kappler, A. (2009) Rates and extent of reduction of Fe(III) compounds and O_2 by humic substances. *Environ. Sci. Technol*. **43** (13), 4902-4908.

Bonneville, S., Van Cappellen, P. and Behrends, T. (2004) Microbial reduction of iron(III) oxyhydroxides: Effects of mineral solubility and availability. *Chem. Geol.* **212** (3-4), 255-268.

Caccavo, F., Lonergan, D. J., Lovley, D. R., Davis, M., Stolz, J. F. and Mcinerney, M. J. (1994) *Geobacter sulfurreducens* sp. nov., a hydrogen- and acetate-oxidizing dissimilatory metal-reducing microorganism. *Appl. Environ. Microb.* **60** (10), 3752-3759.

Cadena, A., Texier, A. C., Gonzalez, I., Cervantes, F. J. and Gomez, J. (2007) Qualitative and quantitative determination of a humic model compound in microbial cultures by cyclic voltammetry. *Environ. Technol.* **28** (9), 1035-1044.

Chen, J., Gu, B. H., Royer, R. A. and Burgos, W. D. (2003) The roles of natural organic matter in chemical and microbial reduction of ferric iron. *Sci. Total Environ.* **307** (1-3), 167-178.

Coker, V. S., Gault, A. G., Pearce, C. I., van der Laan, G., Telling, N. D., Charnock, J. M., Polya, D. A. and Lloyd, J. R. (2006) XAS and XMCD evidence for species-dependent partitioning of arsenic during microbial reduction of ferrihydrite to magnetite. *Environ. Sci. Technol.* **40** (24), 7745-7750.

Cornell, R. M. and Schwertmann, U. (2006) The iron oxides: Structure, properties, reactions, occurrences and uses. Wiley-VCH, Weinheim.

Fredrickson, J. K., Zachara, J. M., Kennedy, D. W., Dong, H. L., Onstott, T. C., Hinman, N. W. and Li, S. M. (1998) Biogenic iron mineralization accompanying the dissimilatory reduction of hydrous ferric oxide by a groundwater bacterium. *Geochim. Cosmochim. Acta* **62** (19-20), 3239-3257.

Gadd, G. M. (2004) Microbial influence on metal mobility and application for bioremediation. *Geoderma* **122** (2-4), 109-119.

Glasser, N. R., Saunders, S. H. and Newman, D. K. (2017) The colorful world of extracellular electron shuttles. *Annu. Rev. Microbiol.* **71**, 731-751.

Gorby, Y. A., Yanina, S., McLean, J. S., Rosso, K. M., Moyles, D., Dohnalkova, A., Beveridge, T. J., Chang, I. S., Kim, B. H., Kim, K. S., Culley, D. E., Reed, S. B., Romine, M. F., Saffarini, D. A., Hill, E. A., Shi, L., Elias, D. A., Kennedy, D. W., Pinchuk, G., Watanabe, K., Ishii, S., Logan, B., Nealson, K. H. and Fredrickson, J. K. (2016) Electrically conductive bacterial nanowires produced by *Shewanella oneidensis* strain MR-1 and other microorganisms. *P. Natl. Acad. Sci. USA* **103** (30), 11358-11363.

Gorski, C. A., Edwards, R., Sander, M., Hofstetter, T. B. and Stewart, S. M. (2016) Thermodynamic characterization of iron oxide-aqueous Fe^{2+} redox couples. *Environ. Sci. Technol.* **50** (16), 8538-8547.

Groh, J. L., Luo, Q. W., Ballard, J. D. and Krumholz, L. R. (2005) A method adapting microarray technology for signature-tagged mutagenesis of *Desulfovibrio desulfuricans* G20 and *Shewanella oneidensis* MR-1 in anaerobic sediment survival experiments. *Appl. Environ. Microb.* **71** (11), 7064-7074.

Hallberg, K. B. and Johnson, D. B. (2001) Biodiversity of acidophilic prokaryotes. *Adv. Appl. Microbiol.* **49**, 37-84.

Hansel, C. M., Benner, S. G., Neiss, J., Dohnalkova, A., Kukkadapu, R. K. and Fendorf, S. (2003) Secondary mineralization pathways induced by dissimilatory iron reduction of ferrihydrite under advective flow. *Geochim. Cosmochim. Acta.* **67** (16), 2977-2992.

Hau, H. H. and Gralnick, J. A. (2007) Ecology and biotechnology of the genus *Shewanella*. *Annu. Rev. Microbiol.* **61**, 237-258.

Hegler, F., Posth, N. R., Jiang, J. and Kappler, A. (2008) Physiology of phototrophic iron(II)-oxidizing bacteria: implications for modern and ancient environments. *Fems. Microbiol. Ecol.* **66**, 250-260.

Huskinson, B., Marshak, M. P., Suh, C., Er, S., Gerhardt, M. R., Galvin, C. J., Chen, X. D., Aspuru-Guzik, A., Gordon, R. G. and Aziz, M. J. (2014) A metal-free organic-inorganic aqueous flow battery. *Nature* **505** (7482), 195-198.

Jiang, J. and Kappler, A. (2008) Kinetics of microbial and chemical reduction of humic substances: Implications for electron shuttling. *Environ. Sci. Technol.* **42** (10), 3563-3569.

Jones, A. M., Collins, R. N., Rose, J. and Waite, T. D. The effect of silica and natural organic matter on the Fe(II)-catalysed transformation and reactivity of Fe(III) minerals. *Geochim. Cosmochim. Acta* **73** (15), 4409-4422.

Kaiser, K. and Guggenberger, G. (2003) Mineral surfaces and soil organic matter. *Eur. J. Soil Sci.* **54** (2), 219-236.

Kappler, A., Benz, M., Schink, B. and Brune, A. (2004) Electron shuttling via humic acids in microbial iron(III) reduction in a freshwater sediment. *Fems. Microbiol. Ecol.* **47** (1), 85-92.

Kappler, A., Wuestner, M. L., Ruecker, A., Harter, J., Halama, M. and Behrens, S. (2014) Biochar as an electron shuttle between bacteria and Fe(III) minerals. *Environ. Sci. Tech. Let.* **1** (8), 339-344.

Klupfel, L., Piepenbrock, A., Kappler, A. and Sander, M. (2014) Humic substances as fully regenerable electron acceptors in recurrently anoxic environments. *Nat. Geosci.* **7** (3), 195-200.

Laloy, E., and Vrugt, J. A. (2012) High-dimensional posterior exploration of hydrologic models using mmultiple-try DREAM(ZS) and high-performance computing. *Water Resour. Res.* **48** (1), 1526-1544.

Liao, S. C., Zong, X., Seger, B., Pedersen, T., Yao, T. T., Ding, C. M., Shi, J. Y., Chen, J. and Li, C. (2016) Integrating a dual-silicon photoelectrochemical cell into a redox flow battery for unassisted photocharging. *Nat. Commun.* **7**, 11474-11482.

Lies, D. P., Hernandez, M. E., Kappler, A., Mielke, R. E., Gralnick, J. A. and Newman, D. K. (2005) *Shewanella oneidensis* MR-1 uses overlapping pathways for iron reduction at a distance and by direct contact under conditions relevant for biofilms. *Appl. Environ. Microb.* **71** (8), 4414-4426.

Lloyd, J. R., Sole, V. A., Van Praagh, C. V. G. and Lovley, D. R. (2000) Direct and Fe(II)-mediated reduction of technetium by Fe(III)-reducing bacteria. *Appl. Environ. Microb.* **66** (9), 3743-3749.

Lovley, D. R., Coates, J. D., BluntHarris, E. L., Phillips, E. J. P. and Woodward, J. C. (1996) Humic substances as electron acceptors for microbial respiration. *Nature* **382** (6590), 445-448.

Lovley, D. R. and Malvankar, N. S. (2015) Seeing is believing: Novel imaging techniques help clarify microbial nanowire structure and function. *Environ. Microbiol.* **17** (7), 2209-2215.

Marin-Spiotta, E., Gruley, K. E., Crawford, J., Atkinson, E. E., Miesel, J. R., Greene, S., Cardona-Correa, C. and Spencer, R. G. M. (2014) Paradigm shifts in soil organic matter research affect interpretations of aquatic carbon cycling: Transcending disciplinary and ecosystem boundaries. *Biogeochemistry* **117** (2-3), 279-297.

Marsili, E., Baron, D. B., Shikhare, I. D., Coursolle, D., Gralnick, J. A. and Bond, D. R. (2008) *Shewanella* secretes flavins that mediate extracellular electron transfer. *P. Natl. Acad. Sci. USA* **105** (10), 3968-3973.

Mellage, A., Smeaton, C. M., Furman, A., Atekwana, E. A., Rezanezhad, F. and Van Cappellen, P. (2018) Linking spectral induced polarization (SIP) and subsurface microbial processes: Results from sand column incubation experiments. *Environ. Sci. Technol.* **52** (4), 2081-2090.

Michelson, K., Sanford, R. A., Valocchi, A. J. and Werth, C. J. (2017) Nanowires of *Geobacter sulfurreducens* require redox cofactors to reduce metals in pore spaces too small for cell passage. *Environ. Sci. Technol.* **51** (20), 11660-11668.

Michelson, K., Alcalde, R. E., Sanford, R. A., Valocchi, A. J. and Werth, C. J. (2019) Diffusion-based recycling of flavins allows *Shewanella oneidensis* MR-1 to yield energy from metal reduction across physical separations. *Environ. Sci. Technol.* **53** (7), 3480-3487.

Mikutta, C., Wiederhold, J. G., Cirpka, O. A., Hofstetter, T. B., Bourdon, B. and Von Gunten, U. (2009) Iron isotope fractionation and atom exchange during sorption of ferrous iron to mineral surfaces. *Geochim. Cosmochim. Acta* **73** (7), 1795-1812.

Myers, C. R. and Myers, J. M. (1997) Replication of plasmids with the p15A origin in *Shewanella putrefaciens* MR-1. *Lett. Appl. Microbiol.* **24** (3), 221-225.

Narayanan, J., Xiong, J. Y. and Liu, X. Y. (2006) Determination of agarose gel pore size: Absorbance measurements vis other techniques. *J. Phys. Conf. Ser.* **28**, 83-86.

Nealson, K. H. and Saffarini, D. (1994) Iron and manganese in anaerobic respiration-environmental significance, physiology, and regulation. *Annu. Rev. Microbiol.* **48**, 311-343.

Nevin, K. P. and Lovley, D. R. (2002) Mechanisms for accessing insoluble Fe(III) oxide during dissimilatory Fe(III) reduction by *Geothrix fermentans*. *Appl. Environ. Microb.* **68** (5), 2294-2299.

Nevin, K. P. and Lovley, D. R. (2002) Mechanisms for Fe(III) oxide reduction in sedimentary environments. *Geomicrobiol. J.* **19** (2), 141-159.

Newsome, L., Morris, K. and Lloyd, J. R. (2014) The biogeochemistry and bioremediation of uranium and other priority radionuclides. *Chem. Geol.* **363**, 164-184.

Orsetti, S., Laskov, C. and Haderlein, S. B. (2013) Electron transfer between iron minerals and quinones: estimating the reduction potential of the Fe(II)-goethite surface from AQDS speciation. *Environ. Sci. Technol.* **47** (24), 14161-14168.

Piepenbrock, A., Dippon, U., Porsch, K., Appel, E. and Kappler, A. (2011) Dependence of microbial magnetite formation on humic substance and ferrihydrite concentrations. *Geochim. Cosmochim. Acta* **75** (22), 6844-6858.

Pipenbrock, A., Schroder, C. and Kappler, A. (2014) Electron transfer from humic substances to biogenic and abiogenic Fe(III) oxyhydroxide minerals. *Environ. Sci. Technol.* **48** (3), 1656-1664.

Pirbadian, S. and El-Naggar, M. Y. (2012) Multistep hopping and extracellular charge transfer in microbial redox chains. *Phys. Chem. Chem. Phys.* **14** (40), 13802-13808.

Poggenburg, C., Mikutta, R., Schippers, A., Dohrmann, R. and Guggenberger, G. (2018) Impact of natural organic matter coatings on the microbial reduction of iron oxides. *Geochim. Cosmochim. Acta* **224**, 223-248.

Priambodo, R., Shih, Y. J. and Huang, Y. H. (2017) Phosphorus recovery as ferrous phosphate (vivianite) from wastewater produced in manufacture of thin film transistor-liquid crystal displays (TFT-LCD) by a fluidized bed crystallizer (FBC). *Rsc. Advances* **7** (65), 40819-40828.

Roden, E. E. and Urrutia, M. M. (1999) Ferrous iron removal promotes microbial reduction of crystalline iron(III) oxides. *Environ. Sci. Technol.* **33** (14), 2492-2492.

Roden, E. E. (2003) Fe(III) oxide reactivity toward biological versus chemical reduction. *Environ. Sci. Technol.* **37** (7), 1319-1324.

Roden, E. E. (2008) Microbiological controls on geochemical kinetics 1: fundamentals and case study on microbial Fe (III) oxide reduction. In Brantley, S. L., Kubicki, J. D., White, A. F. (Ed.), *Kinetics of Water-Rock Interaction*, pp. 335-415.

Roden, E. E., Kappler, A., Bauer, I., Jiang, J., Paul, A., Stoesser, R., Konishi, H. and Xu, H. F. (2010) Extracellular electron transfer through microbial reduction of solid-phase humic substances. *Nat. Geosci.* **3** (6), 417-421.

Rosso, K. M., Smith, D. M. A., Wang, Z. M., Ainsworth, C. C. and Fredrickson, J. K. (2004) Self-exchange electron transfer kinetics and reduction potentials for anthraquinone disulfonate. *J. Phys. Chem. A.* **108** (16), 3292-3303.

Scott, D. T., McKnight, D. M., Blunt-Harris, E. L., Kolesar, S. E. and Lovley, D. R. (1998) Quinone moieties act as electron acceptors in the reduction of humic substances by humics-reducing microorganisms. *Environ. Sci. Technol.* **32** (19), 2984-2989.

Shi, Z., Zachara, J. M., Shi, L., Wang, Z. M., Moore, D. A., Kennedy, D. W. and Fredrickson, J. K. (2012) Redox reactions of reduced flavin mononucleotide (FMN), riboflavin (RBF), and anthraquinone-2,6-disulfonate (AQDS) with ferrihydrite and lepidocrocite. *Environ. Sci. Technol.* **46** (21), 11644-11652.

Shimizu, M., Zhou, J., Schröder, C., Obst, M., Kappler, A. and Borch, T. (2013) Dissimilatory reduction and transformation of ferrihydrite-humic acid coprecipitates. *Environ. Sci. Technol.* **47** (23), 13375-13384.

Snider, R. M., Strycharz-Glaven, S. M., Tsoi, S. D., Erickson, J. S. and Tender, L. M. (2012) Long-range electron transport in *Geobacter sulfurreducens* biofilms is redox gradient-driven. *P. Natl. Acad. Sci. USA* **109** (38), 15467-15472.

Sparks, D.L. (2003) Environmental soil chemistry. Academic Press, Amsterdam; Boston.

Speers, A. M., Schindler, B. D., Hwang, J., Genc, A. and Reguera, G. (2016) Genetic identification of a PilT motor in *Geobacter sulfurreducens* reveals a role for pilus retraction in extracellular electron transfer. *Front. Microbiol.* **7**.

Stookey, L. L. (1970) Ferrozine- a new spectrophotometric reagent for iron. *Anal. Chem.* **42** (7), 779-781.

Subramanian, P., Pirbadian, S., El-Naggar, M. Y. and Jensen, G. J. (2018) Ultrastructure of *Shewanella oneidensis* MR-1 nanowires revealed by electron cryotomography. *P. Natl. Acad. Sci. USA* **115** (14), 3246-3255.

Sun, T. R., Levin, B. D. A., Guzman, J. J. L., Enders, A., Muller, D. A., Angenent, L. T. and Lehmann, J. (2017) Rapid electron transfer by the carbon matrix in natural pyrogenic carbon. *Nat. Commun.* **8**, 14873-14885.

Sun, T. R., Levin, B. D. A., Schmidt, M. P., Guzman, J. J. L., Enders, A., Martinez, C. E., Muller, D. A., Angenent, L. T. and Lehmann, J. (2018) Simultaneous Quantification of Electron Transfer by Carbon Matrices and Functional Groups in Pyrogenic Carbon. *Environ. Sci. Technol.* **52** (15), 8538-8547.

Teal, T. K., Winfree, E., Newman, D. K. and Wold, B. J. (2007) Studies of the spatial organization of metabolism in *Shewanella oneidensis* and *Pseudomonas aeruginosa* biofilms. Ph. D. Dissertation, California Institute of Technology, Pasadena, CA.

Viollier, E., Inglett, P. W., Hunter, K., Roychoudhury, A. N. and Van Cappellen, P. (2000) The ferrozine method revisited: Fe(II)/Fe(III) determination in natural waters. *Appl. Geochem.* **15** (6), 785-790.

von Canstein, H., Ogawa, J., Shimizu, S. and Lloyd, J. R. (2008) Secretion of flavins by *Shewanella* species and their role in extracellular electron transfer. *Appl. Environ. Microb.* **74** (3), 615-623.

Vrugt, J. A. (2016) Markov chain Monte Carlo simulation using the DREAM software package: Theory, concepts, and MATLAB implementation. *Environ. Modell. Softw.* **75**, 273-316.

Watts, M. P., Coker, V. S., Parry, S. A., Pattrick, R. A. D., Thomas, R. A. P., Kalin, R. and Lloyd, J. R. (2015) Biogenic nano-magnetite and nano-zero valent iron treatment of alkaline Cr(VI) leachate and chromite ore processing residue. *Appl. Geochem.* **54**, 27-42.

Wolf, M., Kappler, A., Jiang, J. and Meckenstock, R. U. (2009) Effects of humic substances and quinones at low concentrations on ferrihydrite reduction by *Geobacter metallireducens*.

Chapter 5-Personal contribution

Experiments in this chapter were conceptually designed by me and Dr. Tianran Sun, with the help of Prof. Andreas Kappler and Prof. Stefan B. Haderlein. The microbial Fe(III) reduction experiments were performed by myself, whereas the electrochemical experiments were conducted by me and Dr. Tianran Sun. Data analyses were done by myself and Dr. Tianran Sun. The manuscript was written by me and Dr. Tianran Sun, Prof. Andreas Kappler, Prof. Largus T. Angenent and Prof. Stefan B. Haderlein revised the manuscript.

5. Electron hopping enables rapid electron transfer between quinone-/hydroquinone-containing organic molecules in microbial iron(III) mineral reduction

Yuge Bai[1*], Tianran Sun[2*], Largus T. Angenent[2], Stefan B. Haderlein[3], Andreas Kappler[1]

[1]Geomicrobiology, Center of Applied Geosciences, University of Tübingen, Germany

[2]Environmental Biotechnology, Center of Applied Geosciences, University of Tübingen, Germany

[3]Environmental Mineralogy and Chemistry, Center of Applied Geosciences, University of Tübingen, Germany

*Both authors contributed equally to this work

5.1 Abstract

The mechanism of electron transfer via redox-active particulate natural organic matter (NOM) is still unclear, especially considering its aggregated nature and the resulting low diffusivity of its quinone-/hydroquinone-containing molecules. Here we conducted microbial iron(III)-mineral reduction experiments in which anthraquinone-2,6-disulfonate (AQDS, a widely used analogue for quinone/hydroquinone moieties in NOM) was immobilized in agar to limit its diffusion, therefore simulating electron transfer via quinone-/hydroquinone-containing molecules in particulate NOM. We found that, although the diffusion coefficient of the immobilized AQDS/AH$_2$QDS was 10 times lower in agar than in water, the iron(III) mineral reduction rate (1.60 ± 0.28 mmol L^{-1} Fe(II) d^{-1}) was still comparable in both media, indicating the existence of another mechanism that accelerated the electron transfer under low diffusive conditions. We found the correlation between the heterogeneous electron transfer rate constant (10^{-3} cm s^{-1}) and the diffusion coefficient (10^{-7} cm^2 s^{-1}) fitted well with the "diffusion-electron hopping" model, suggesting that electron transfer via the immobilized AQDS/AH$_2$QDS couple was accomplished through a combination of diffusion and electron hopping. Electron hopping increased the diffusion concentration gradient up to 10^6-fold, which largely promoted the overall electron transfer rate during microbial iron(III) mineral reduction. Our results are helpful to explain the electron transfer mechanisms in particulate NOM.

5.2 Introduction

Natural organic matter (NOM) is a complex mixture of organic molecules that are primarily derived from the decay of plant and microbial residues and it makes up a major fraction of organic matter in soils and sediments (Stevenson, 1994). Based on the particle size that is operationally defined by filtering through 0.45 μm cut-off filters, NOM is categorized into dissolved NOM and particulate NOM (Sparks, 2003). Due to the presence of redox-active moieties such as quinone and hydroquinone, NOM is known to undergo redox cycles thus acting

as an electron shuttle and transferring electrons between spatially separated Fe(III) minerals and Fe(III)-reducing bacteria (Lan et al., 2019; Lovley et al., 1996; Roden et al., 2010). Such an electron shuttling process by NOM has been shown to help Fe(III)-reducing bacteria to overcome the respiratory challenge and perform extracellular electron transfer in anoxic soils and sediments (Sposito, 2011).

Dissolved NOM is usually homogenously distributed in pore waters and possesses a high diffusivity (Balch and Guéguen, 2015) with a measured diffusion coefficient (D_0) of 10^{-6} cm^2 s^{-1}. This diffusion coefficient is in the same order of magnitude as the D_0 of a variety of biological electron shuttle molecules (i.e., flavin mononucleotide (Orita et al., 2016) and pyocyanin (Phalak et al., 2016)) that are known to diffusively transfer electrons up to 100 micrometers (μm) distance (Glasser et al., 2017). In contrast to dissolved NOM, particulate NOM has a much lower physical mobility and commonly accumulates in the solid phase of soils and sediments due to aggregation and co-precipitation (Six et al., 2000). Similar as for dissolved NOM, a stimulation of microbial Fe(III) reduction through electron transfer facilitated by NOM redox cycling has also been observed for particulate NOM (Lau et al., 2015; Roden et al., 2010; Tan et al., 2019). Given the environmental abundance, particulate NOM was proposed to be able to form a redox-active network for long-distance electron transfer across centimeter (cm) distances (Roden et al., 2010; Tan et al., 2019). Such a long-distance electron transfer can bridge energy and matter exchange across liquid and solid interphases in anoxic soils and sediments. However, the electron transfer mechanisms of particulate NOM over cm distance remains unclear. Whereas some study emphasized the importance of dissolved NOM serving as a mediator that diffusively transfers electrons between particulate NOM molecules (Gao et al., 2019), others proposed the formation of an electron-transfer network by particulate NOM, as could be formed by bacterial nanowires (Nielsen et al., 2010), to transfer electrons over cm distance (Piepenbrock and Kappler, 2013).

To advance our understanding of the electron transfer mechanism of particulate (solid-phase) NOM, we used anthraquinone-2,6-disulfonate (AQDS) as an analogue for quinone-containing particulate NOM molecules, and AH_2QDS that was generated from the microbial reduction of AQDS for the hydroquinone-containing molecules in particulate NOM. By immobilizing $AQDS/AH_2QDS$ couple in agar (2%), we mimicked the diffusion-limitation of quinone-/hydroquinone-containing molecules in particulate NOM. We would like to note that we are aware of the fact that the $AQDS/AH_2QDS$ couple was not fully immobilized but instead, its diffusivity was reduced to simulate the electron transfer conditions in particulate NOM. However, for simplicity we termed this reduced diffusion phenomenon as "immobilize" throughout the manuscript. This $AQDS/AH_2QDS$-agar mixture was placed in an incubation system that physically separated the Fe(III)-reducing bacteria (*Shewanella oneidensis* MR-1) and ferrihydrite by 2 cm to inhibit the direct microbial ferrihydrite reduction. We hypothesized that electron hopping (i.e., electron self-exchange reaction occurring between closely compacted redox centers (Rosso et al., 2004)) plays a critical role in the electron transfer between immobilized AQDS and AH_2QDS molecules and accelerate microbial Fe(III) mineral reduction.

5.3 Materials and methods

Cell suspension experiment

Microbial ferrihydrite reduction was carried out in a cell suspension incubation system for which AQDS was immobilized in agar and *S. oneidensis* MR-1 (10^8 cells mL^{-1}) and ferrihydrite (15 mmol L^{-1}) were separated by a distance of 2 cm (Figure 5.1a). The concentrations of AQDS in agar were 5 mmol L^{-1}, 10 mmol L^{-1}, 25 mmol L^{-1}, or 50 mmol L^{-1}. The pore size of the agar (2%) was 100-200 nm (Narayanan et al., 2006), which is small enough to prevent microbes from penetration, and therefore from direct contact to ferrihydrite (Bai et al., 2020a). Phosphate buffer (5 mmol L^{-1}, pH 7.0-7.2) was used in the incubation. Although

phosphate can lead to the formation of Fe(II)-phosphate minerals such as vivianite, this buffer was chosen to allow comparison of our study to previous studies (Jiang and Kappler, 2008; Klupfel et al., 2014; Piepenbrock et al., 2014). More detailed information about the setup of the cell suspension incubation can be found in our previous study (Bai et al., 2020a). For analysis, agar samples from each treatment were taken in triplicates in an anoxic glovebox (100% N_2). A 10-mL syringe, cut at the top, was used to take a core from the agar for quantifying the Fe concentration. Agar slices (1-mm thickness for each slice) were taken from location 1, 2, 3, and 4 of the core as designed in Figure 5.1b. After dissolving in 1 M HCl for 1 h, the Fe(II) and Fe(III) concentrations in each slice were quantified using the spectrophotometric ferrozine assay (Hegler et al., 2008; Viollier et al., 2000).
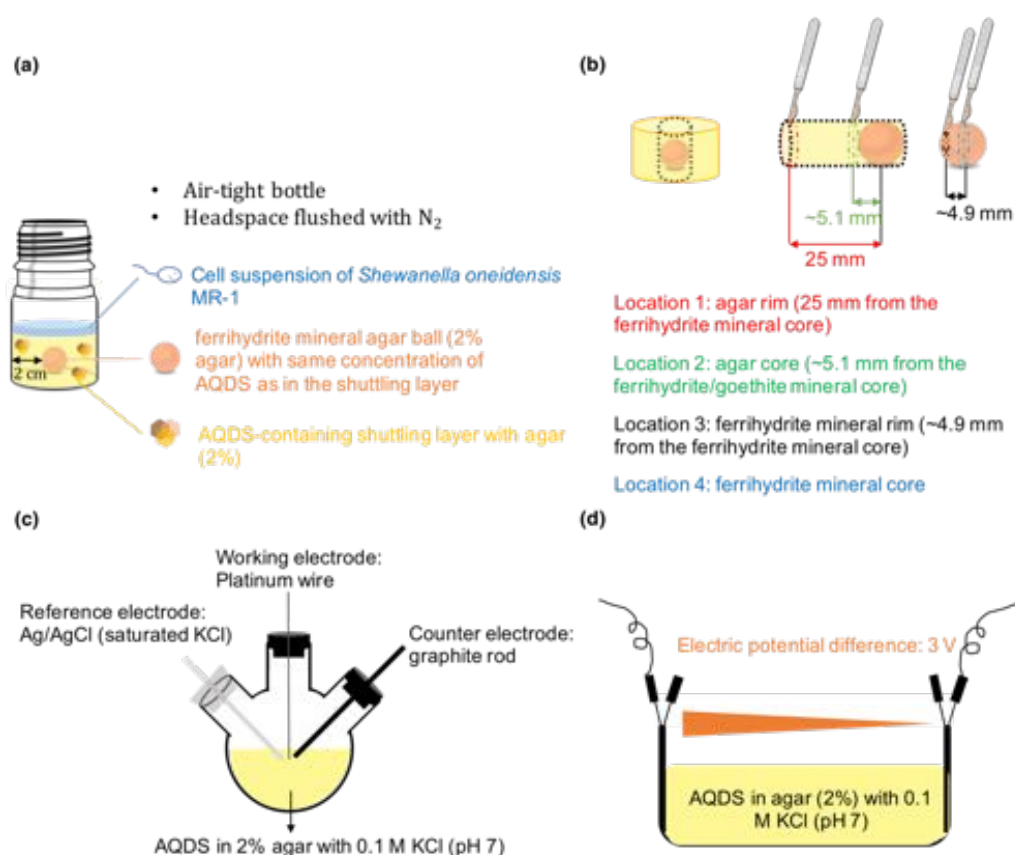
Figure 5.1. Cell suspension incubation system that separates *S. oneidensis* MR-1 and ferrihydrite by 2 cm distance with AQDS as electron shuttle (a). At each sampling point, an agar slice with 1-mm thickness was taken at four locations in an anoxic glovebox (100 % N_2)

(b). The cyclic voltammetry of AQDS was measured in a Bio-logic model VSP potentiostat controlled by the EC-lab platform at room temperature in a three-electrode configured cell at pH 7 (c). The two-electrode configured electrochemical cell (L×W×H = 5×3×2 cm) used to investigate the maximum transfer distance of AH_2QDS after electrode reduction of AQDS (d).

Electrochemical analysis

Cyclic voltammetry was performed to investigate the redox cycling of $AQDS/AH_2QDS$ couple that was immobilized in agar. Potassium chloride (KCl, 0.1 mol L^{-1}) was added as a supporting electrolyte and potassium phosphate (5 mmol L^{-1}) was used to buffer the pH at 7.0-7.2. Cyclic voltammetry was carried out in a three-electrode configured electrochemical cell for which platinum wire, graphite rod, and Ag/AgCl (sat. KCl) were used as working, counter, and reference electrode, respectively (Figure 5.1c). The AQDS concentration was 5 mmol L^{-1}, 10 mmol L^{-1}, 15 mmol L^{-1}, 25 mmol L^{-1}, or 50 mmol L^{-1} to have the same conditions as in the microbial Fe(III) mineral reduction incubations. Potential scan rates ranged from 50 mV s^{-1} to 300 mV s^{-1}.

A two-electrode configured electrochemical cell (L×W×H = 5×3×2 cm, Figure 5.1d) was used to investigate the maximum transfer distance of AH_2QDS after electrode reduction of AQDS. The initial AQDS concentration was 25 mmol L^{-1} or 50 mmol L^{-1}. 0.1 mol L^{-1} KCl and 5 mmol L^{-1} phosphate were added as a supporting electrolyte and pH buffer (7.0-7.2), respectively. Carbon paper was used as both working and counter electrode. A constant voltage (i.e., the potential difference between working and counter electrodes) of 3 V was applied to the electrochemical cell, which was also the tested lowest voltage that was able to initiate the reduction of AQDS in this particular cell configuration. During the experiment, we did not observe any gas bubbles evolving from the electrodes, suggesting that the applied voltage was high enough to drive AQDS reduction but still below the voltage threshold for water splitting.

At the end of experiment, we quantified AQDS and AH$_2$QDS concentrations using a spectrophotometric method. The agar slices (thickness 1 mm) were put into an electroporation cuvette (BTX, 45-0134), and the absorbance of the agar slices at the wavelength from 200 to 550 nm was measured with a fluorescence spectrophotometer (FluoroMax-4, Jobin Yvon-SPEX instruments, New Jersey, USA). Pure agar (2%) with 5 mmol L^{-1} phosphate buffer and 0.1 mol L^{-1} KCl was used as blank. The peak positions of AQDS (320 nm) and AH$_2$QDS (400 nm) are in accordance with previously reported values (Orsetti et al., 2013). We quantified AQDS concentrations based on the concentration-peak height curve of standard samples and estimated the concentrations of AH$_2$QDS through the decrease of AQDS by assuming all decreased AQDS was converted to AH$_2$QDS. For example, in the experiment with an initial AQDS concentration of 25 mmol L^{-1}, we found a 7.2 mmol L^{-1} loss of AQDS, which suggests the formation of 7.2 mmol L^{-1} AH$_2$QDS. The same approach was applied to the experiment with initial AQDS concentrations of 50 mmol L^{-1}, in which a 33.7 mmol L^{-1} AQDS loss, thus, 33.7 mmol L^{-1} AH$_2$QDS formation, was detected.

5.4 Results and discussion

Immobilized AQDS enables microbial ferrihydrite reduction across a 2-cm distance

Our incubations showed that after accepting electrons from microbial metabolism, AQDS was reduced to AH$_2$QDS, which subsequently transferred electrons to ferrihydrite. In the incubation with 5 mmol L^{-1} immobilized AQDS in agar, the Fe(III) concentration at the ferrihydrite-mineral rim (i.e., location 3 in Figure 5.1b) decreased from 14.92 mmol L^{-1} to 3.04 mmol L^{-1} within the first 2 days of incubation (Figure 5.2a). Inversely, the Fe(II) concentration at the same location increased from 0 mmol L^{-1} to 3.34 mmol L^{-1} (Figure 5.2b). However, after 2 days, the Fe(II) concentration at the ferrihydrite-mineral rim started to decrease and its final concentration was stabilized at 0.74 mmol L^{-1} after 10 days of incubation. This concentration decrease was likely caused by a faster Fe(II) diffusion into the agar core (i.e., location 2 in

Figure 5.1b) than Fe(III) reduction at the ferrihydrite-mineral rim. As a result, the Fe(II) concentration at the agar core increased from 0.96 mmol L^{-1} to 10.02 mmol L^{-1} within 10 days of incubation (Figure 5.2c). No Fe(II) was detected at the agar rim (i.e., location 1, Figure 5.1b) during the entire incubation period (Figure S5.1a). This was probably due to the interaction of Fe(II) and phosphate by the formation of Fe(II)-phosphate minerals, such as vivianite (Bai et al., 2020a; Chen et al., 2003; Piepenbrock et al., 2011; Shimizu et al., 2013), that impeded further diffusion of Fe(II) in the agar.
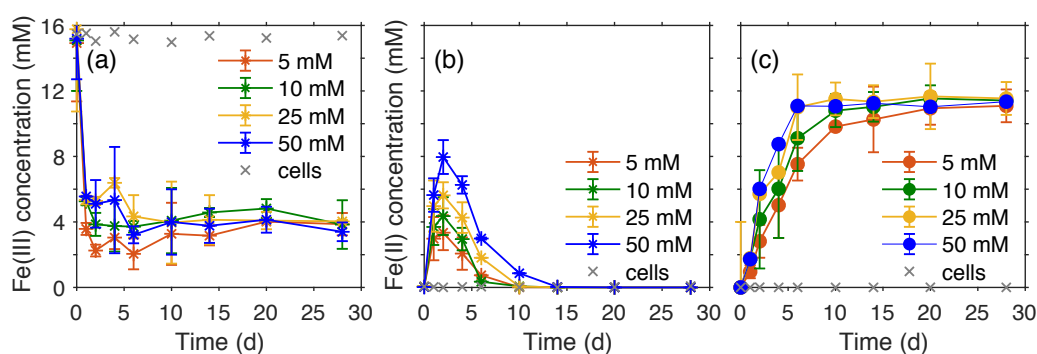
Figure 5.2. Fe(III) (a) and Fe(II) (b) concentrations measured at the ferrihydrite-mineral rim (location 3) and (c) Fe(II) concentration over time at the agar core (location 2) of the 15 mM ferrihydrite reduction by 10^8 mL^{-1} *S. oneidensis* MR-1 in the presence of 15 mM lactate as electron donor amended with either 5 mmol L^{-1} (red), 10 mmol L^{-1} (green), 25 mmol L^{-1} (yellow) or 50 mmol L^{-1} (blue) anthraquinone-2,6-disulfonate (AQDS) as electron shuttle. All experiments were conducted in the cell suspension incubation system at 30 °C in the dark. Data points shown are mean values from triplicate bottles ± 1 standard deviation.

Consistent with the 5 mmol L^{-1} AQDS experiment, ferrihydrite reduction was initiated from the ferrihydrite-mineral rim (location 3) and accumulated Fe(II) in the form of Fe(II)-phosphate minerals (i.e., vivianite) at the agar core (location 2) in the incubations with 10 mmol L^{-1}, 25 mmol L^{-1}, and 50 mmol L^{-1} of immobilized AQDS (Figure 5.2c). However, it should be noticed that a diffusion-reaction model developed in our previous study (Bai et al., 2020a)

showed that the formation of Fe(II)-phosphate mineral should co-occur at the agar core (location 2) and ferrihydrite-mineral rim (location 3). The observation of the accumulation of Fe(II)-phosphate minerals only at the agar core might be caused by the difficulties visually observing the boundary of the ferrihydrite-mineral core to the clean agar during the sampling procedure.

Although higher concentrations of AQDS lead to higher extents of ferrihydrite reduction, and therefore more Fe(II) formation at the ferrihydrite-mineral rim, the ferrihydrite reduction never reached the ferrihydrite-mineral core (i.e., location 4 in Figure 5.1b), which was shown by the stable Fe(III) concentration between 14 mmol L^{-1} to 16 mmol L^{-1} at this location (Figure S5.2c). Similar phenomena of incomplete ferrihydrite reduction were also reported in previous studies (Roden and Urrutia, 2002; Roden and Wetzel, 2002). We attribute the incomplete reduction in our system to the accumulation of Fe(II)-phosphate minerals at the agar core and ferrihydrite-mineral rim, thus reducing the thermodynamic driving force of ferrihydrite reduction (Urrutia et al., 1998) and limiting the acceptance of electrons (Piepenbrock et al., 2011).

With 5 mmol L^{-1}, 10 mmol L^{-1}, 25 mmol L^{-1}, and 50 mmol L^{-1} AQDS immobilized in agar, the average ferrihydrite reduction rates were 1.25 ± 0.05 mmol L^{-1} Fe(II) d^{-1}, 1.52 ± 0.16 mmol L^{-1} Fe(II) d^{-1}, 1.76 ± 0.07 mmol L^{-1} Fe(II) d^{-1}, and 1.88 ± 0.11 mmol L^{-1} Fe(II) d^{-1}, respectively (Figure S5.3). During our previous study, we showed that the diffusion coefficient of AQDS was 10^{-7} cm^2 s^{-1} in agar (Bai et al., 2020a), which is about ten times lower than that in water (10^{-6} cm^2 s^{-1}) (Huskinson et al., 2014; Liao et al., 2016). However, the ferrihydrite reduction rate of the incubations with AQDS immobilized in agar was comparable and in the same order of magnitude than in water (2.36 ± 1.07 mmol L^{-1} Fe(II) d^{-1}) (Bai et al., 2020b). These results indicated that other electron transfer mechanisms existed in addition to diffusion, which enhanced the overall AQDS electron transfer rate in agar.

Electron hopping enhanced AQDS diffusion

Electron hopping between adjacent redox centers has been reported in many materials and dominate the solid-phase electron transfer when molecular diffusivity is low or absent. Several theories and models, notably the Dahms-Ruff model (Dahms, 1968; Ruff and Friedrich, 1971; Ruff et al., 1971), Blauch-Saveant model (Blauch and Saveant, 1992), and Marcus-Hush theory (Bard, 2001; Marcus, 1956), have been established and used to explain the electron hopping in redox-active polymers (Akhoury et al., 2013) and the electron hopping in microbial nanowires that are responsible for extracellular electron transfer (Malvankar and Lovley, 2014; Pirbadian and El-Naggar, 2012). To demonstrate electron hopping in the agar-immobilized AQDS/AH₂QDS couple, we performed cyclic voltammetry and observed two distinct peaks during the reduction (i.e., $AQDS + 2e^- + 2H^+ \rightarrow AH_2QDS$) and oxidation (i.e., $AH_2QDS - 2e^- - 2H^+ \rightarrow AQDS$) scans (Figure S5.4a-e). The fact that the peak current ratio of reduction and oxidation scans was equal to unity and independent of scan rate (Figure 5.3a), indicated that there were no parallel chemical reactions that were coupled to the electron transfer of either AQDS or AH₂QDS. The formal potential (i.e., the average of peak potentials) was determined at -0.3 V (vs. SHE, Figure S5.5) in agar, which is close to the previously reported standard reduction potential (-0.228 V) (Orsetti et al., 2013) and the formal potential (-0.185 V) (Batchelor-McAuley et al., 2010) of AQDS in aqueous solution (at pH 7). The linear dependence of peak current on the square root of the applied potential scan rate (Figure 5.3a) complies with the Randles–Sevcik equation 1,

$$i_p = 269000 \times n^{\frac{3}{2}} \times A \times D_0^{\frac{1}{2}} \times C \times v^{\frac{1}{2}} \qquad (1)$$

$$D_0 = (\frac{Slope}{269000 \times n^{\frac{3}{2}} \times A \times C})^2 \qquad (2)$$

where i_p is the peak current, n (=2) is the number of transferred electrons by the AQDS/AH₂QDS couple, A (0.314 cm²) is the electrode surface area, C is the initial AQDS

concentration in bulk, v indicates the potential scan rate, and D_0 is the diffusion coefficient. Our calculations use the same diffusion coefficient for AQDS and AH$_2$QDS due to their similar molecular structure and because of the symmetric peak current performance between the reduction scan of AQDS and the oxidation scan of AH$_2$QDS (Figure S5.4a-e). A similar D_0 relationship was also observed between the 1,4-benzoquinone and 1,4-hydroquinone redox-couple (Ji et al., 2007). From the slope of the linear plot of i_p as a function of $v^{0.5}$ (equation 2), we determined D_0 at $5.5 \pm 3.2 \times 10^{-7}$ cm^2 s^{-1} (average value of different AQDS concentrations, which is shown in the red dots in Figure 5.3b). We further calculated the heterogeneous electron transfer rate constant (k^0) of AQDS/AH$_2$QDS couple, using equation 3 based on the observed wide separation of reduction and oxidation peak potentials shown in cyclic voltammograms (Bard, 2001),

$$k^0 = \frac{e^{Intercept}}{0.227 \times n \times F \times A \times C} \tag{3}$$

in which the intercept was obtained from a linear fit of the natural logarithm of the absolute value of peak current ($\ln|i_p|$) and overpotential (i.e., difference between peak potential and formal potential, Figure S5.6) at different potential scan rates (Figure 5.3c). F is the Faraday constant, and the rest terms have the same meaning as in eq. 5.1 and 5.2. k^0 was determined at $1.9 \pm 0.2 \times 10^{-3}$ cm s^{-1} (average value for different AQDS concentrations, as shown in blue dots in Figure 5.3b). Both k^0 and D_0 remained relatively constant from low to high AQDS concentrations.
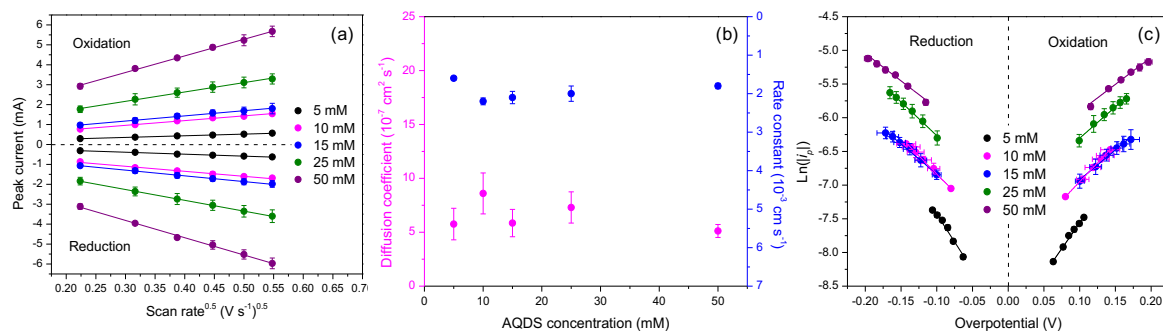
Figure 5.3. Linear dependency of peak current on square root of potential scan rate for different AQDS concentrations in agar (a). The calculated diffusion coefficient D_0 (pink) and heterogeneous electron transfer rate constant k_0 (blue) of AQDS in agar (b). The Tefal plot showing the linear relationship between the natural logarithm of the absolute value of peak current ($\ln|i_p|$) and overpotential (i.e., difference between peak potential and formal potential) at different potential scan rates (c). Original cyclic voltammograms from which Figure 5.3 was derived can be found in Figure S5.4.

The correlation between k^0 and D_0 well fitted with the diffusion-electron hopping model that was recently developed to explain the electron transfer in non-conjugated polymer (Sato et al., 2018). This suggests that the overall electron transfer through immobilized AQDS/AH$_2$QDS was accomplished by a series of diffusion and electron hopping steps, which is shown between interfaces 1 and 2 in equation 4. Interfaces 1 and 2 represent microbe-AQDS and AH$_2$QDS-ferrihydrite interfaces, respectively. Therefore, the overall electron transfer rate constant ($k_{overall}$) can be described by a serial reaction equation based on the classical Noyes expression (equation 5),

$$\text{(4)}$$
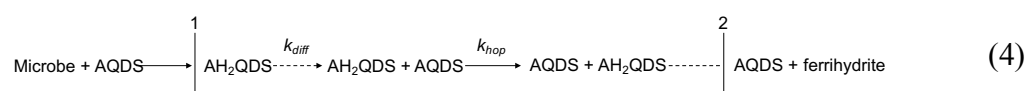
$$\frac{1}{k_{overall}} = \frac{1}{k_{hp}} + \frac{1}{k_{diff}} \tag{5}$$

where, k_{hp} indicates the rate constant of electron hopping between AQDS and AH_2QDS redox centers and k_{diff} is the diffusion constant. It is well known that the reduction of AQDS to AH_2QDS is a two-electron transfer step process, including the formation of a semiquinone radical (i.e., $AQDS + e^- \rightarrow AHQDS^* + e^- \rightarrow AH_2QDS$). However, in our system, these two steps could not be distinguished as only one current peak appeared in either oxidation or reduction cycle in the cyclic voltammograms (Figure S5.4a-e). Therefore, the electron hopping rate constants k_{hp} reflected the overall kinetics of the two steps. We estimated k_{diff} ($\sim 10^6$ L mol^{-1} s^{-1}) by using the Smoluchowski model: $k_{diff} = 16\pi D_0 \alpha N_A$ (α, radius of the redox centers (in the magnitude of nm, Figure S5.7), N_A, Avogadro constant). k_{hp} ($\sim 10^8$ L mol^{-1} s^{-1}) was approximated by the linear fitting of k^0 and D_0 with the published diffusion-electron hopping model (Sato et al., 2018). Since k_{diff} is smaller than k_{hp}, $k_{overall}$ was rate controlled by the diffusion process. This estimation is consistent with the observed linear dependence of the peak current on the square root of the applied potential scan rate (Figure 5.3a) and AQDS concentration (Figure S5.4f), which supported the diffusion-limited electron transfer kinetics and verified the application of diffusion-electron hopping model in our system.

We further performed electrochemical experiments that were combined with spectrophotometric analysis of thin agar slices (1 mm for each slice, Figure 5.1d) to investigate how electron hopping enhanced diffusion, and thus the overall electron transfer rate of diffusion-electron hopping process, in comparison to the case without electron hopping. For an initial AQDS concentration of 25 mmol L^{-1}, a total of 3×10^{-2} mmol AH_2QDS was produced from electrode reduction of AQDS, which reached a maximum transfer distance of 1.6 cm (Figure 5.4a). Dividing the amount of produced AH_2QDS by the surface area of the electrode (6 cm^2) and the reaction time (3 min to reach the maximum transfer distance), we determined the average AH_2QDS production fluxes ($J_{production}$) to be 3.1×10^{-5} mmol cm^{-2} s^{-1}. For the condition without electron hopping, the concentration gradient for AH_2QDS diffusion was

4.3×10^{-3} mmol cm^{-4} by taking the concentration drop of AH$_2$QDS into account of the entire transfer distance (Figure S5.8). Such a concentration gradient, however, would only generate a stationary diffusion flux ($J_{diffusion}$) of 2.2×10^{-9} mmol cm^{-2} s^{-1} (estimated based on Fick's first law $J_{diffusion} = -D_0 \frac{c}{L}$, $D_0 = 5.5 \times 10^{-7}$ cm^2 s^{-1}, as presented in the last section, $-\frac{c}{L} = 4.3 \times 10^{-3}$ mmol cm^{-4}, represents the concentration gradient). This was much smaller than $J_{production}$ (3.1×10^{-5} mmol cm^{-2} s^{-1}), and therefore not sufficient to sustain the AH$_2$QDS transfer to the maximum distance at the given reaction time.
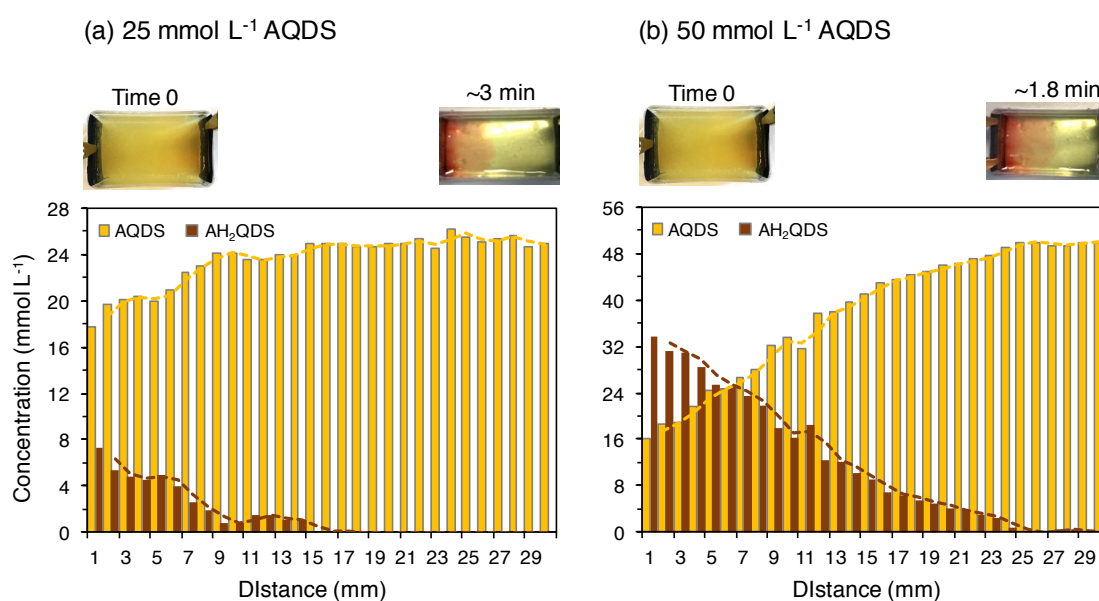
Figure 5.4. AQDS and AH$_2$QDS concentrations measured spectrophotometrically at each 1 mm in agar (2%) in the experiment with a two-electrode configured electrochemical cell (L× W×H = 5×3×2 cm, Figure 5.1d). The initial AQDS concentration was 25 mmol L^{-1} (a) and 50 mmol L^{-1} (b). A voltage (i.e., the potential difference between working and counter electrodes) of 3 V was applied to initiate the reduction of AQDS. The produced AH$_2$QDS showed a bright orange color and it expanded from the working electrode towards the counter electrode over time (as shown in the pictures above the bar plots). Once the expansion of AH$_2$QDS stopped, we recorded the time (3 min and 1.8 min for the experiment with the initial AQDS concentration

of 25 mmol L^{-1} and 50 mmol L^{-1}, respectively), and measured the AQDS and AH$_2$QDS concentrations for each slice of agar (thickness 1mm) from the working electrode to the counter electrode. However, here we only show the concentrations of AQDS and AH$_2$QDS in the first 3 cm of the reacting cell, because no further change of AQDS and AH$_2$QDS concentration was observed in the last 2 cm.

The occurrence of electron hopping, on the other hand, divided the diffusion into several short-distance diffusion segments (i.e., eq. 5.4). In each segment, the diffused AH$_2$QDS was immediately consumed by electron hopping at the encountered surface of the AQDS layer due to the fact that electron hopping is faster than diffusion. Assuming the diffusion flux in each segment ($J_{diffusion, seg}$) was the same and equated to the production flux (i.e., $J_{production} = J_{diffusion,seg} = -D_0 \frac{C_{seg}}{L_{seg}}$) for a stationary AH$_2$QDS transfer till the maximum distance, one could obtain a concentration gradient in each segment ($-\frac{C_{seg}}{L_{seg}}$) of 5.0×10^2 mmol cm^{-4} ($-\frac{C_{seg}}{L_{seg}} = \frac{J_{production}}{D_0}$, $J_{production}$ =3.1×10^{-5} mmol cm^{-2} s^{-1}, D_0 =5.5 × 10^{-7} cm^2 s^{-1}). This calculated concentration gradient was 10^5 times higher than that without electron hopping (Figure S5.8a, 4.3×10^{-3} mmol cm^{-4}). A similar observation was made in the experiment with an initial AQDS concentration of 50 mmol L^{-1} (Figure 5.4b) for which the concentration gradient in each segment ($-\frac{C_{seg}}{L_{seg}} = \frac{J_{production}}{D_0}$ =1.0×10^4 mmol cm^{-4}, $J_{production}$ = 4.6×10^{-3} mmol cm^{-2} s^{-1}) was increased 10^6-fold by electron hopping in comparison to the concentration gradient ($-\frac{C}{L}$ = 1.2×10^{-2} mmol cm^{-4}, Figure S5.8b) for the diffusion without electron hopping. This increasing extent of concentration gradient was 10-fold higher than that in the experiment with the initial AQDS concentration of 25 mmol L^{-1}, which was probably due to the shorter diffusion distance in each diffusion segment as a result of the closer contact of AQDS redox centers and thus higher electron hopping frequency at higher concentrations. The redox-center separation

decreased from 1.29 nm to 0.49 nm as the AQDS concentration increased from 25 mmol L^{-1} to 50 mmol L^{-1} (Figure S5.7). Although simplistic, this calculation highlighted the substantial impact of electron hopping on accelerating diffusion fluxes and enhancing the overall electron transfer kinetics via the AQDS/AH$_2$QDS couple.

5.5 Implications for particulate NOM electron transfer

Here we fit our data to a diffusion-electron hopping model to interpret the electron transfer between immobilized AQDS molecules in agar under diffusion-limited conditions. Such conditions highly resemble the electron transfer process of particulate NOM for which solid-phase quinone and hydroquinone groups are present. However, a certain number of dissolved NOM molecules with redox-active functional groups is also expected to coexist with the particulate NOM matrix, for example, due to the continuous degradation of particulate natural organic matter (Lehmann and Kleber, 2015; Sparks, 2003). After accepting electrons generated from microbial respiration, dissolved quinone groups are transformed to hydroquinone groups, which subsequently diffuse to the particulate NOM due to their high diffusive mobility. Electron hopping between the dissolved hydroquinone and solid-phase quinone groups can largely increase the diffusion concentration gradient and promote the electron transfer of particulate NOM to a rapid and long-distance level. Electron transfer of particulate NOM plays a critical role in element cycling (Lau et al., 2015), contaminant transformation (Zheng et al., 2012), and greenhouse gas emissions (Gao et al., 2019). It is thermodynamically favorable to transfer electrons to different terminal electron acceptors including oxygen, iron(III) and manganese(IV) minerals, as well as to nitrate and oxidized S-compounds from high to low reduction potential (Aeschbacher et al., 2012; Roden et al., 2010). The diffusion-electron hopping model proposed in this study will be relevant for other studies that address the particulate NOM enhanced electron transfer kinetics as well as its impact on environmental electron transfer networks.
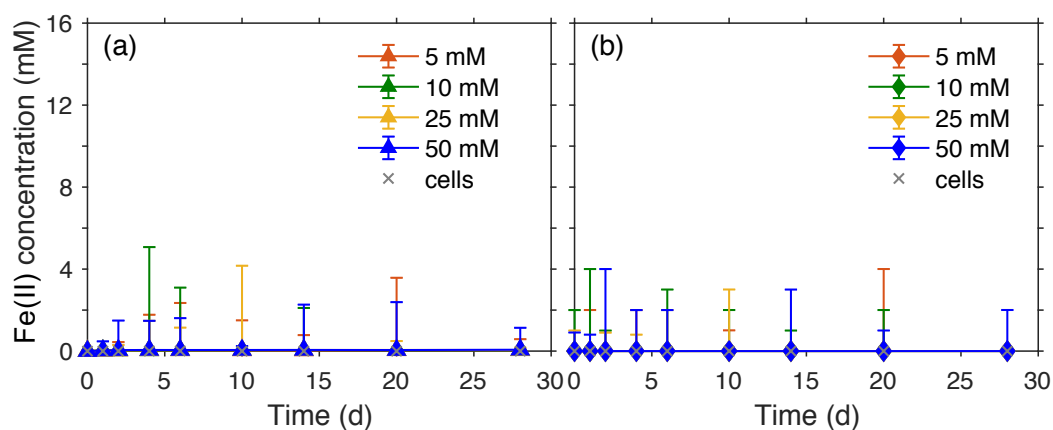
5.6 Supporting information

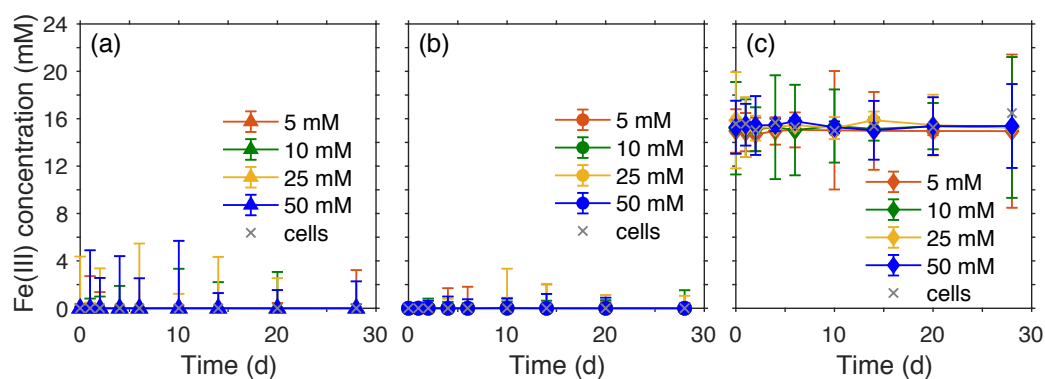**Figure S5.1.** Fe(II) concentrations measured at the agar rim (location 1, a) and at the ferrihydrite-mineral core (location 4, b) of the microbial reduction experiment of 15 mmol L^{-1} ferrihydrite by 10^8 cells mL^{-1} of *S. oneidensis* MR-1 in the presence of 15 mmol L^{-1} lactate as electron donor and amended with either 5 mmol L^{-1} (red), 10 mmol L^{-1} (green), 25 mmol L^{-1} (yellow) or 50 mmol L^{-1} (blue) anthraquinone-2,6-disulfonate (AQDS) as electron shuttle. All experiments were conducted with the agar-solidified incubation setup at 30°C in the dark. Data are means from triplicate bottles ± standard deviations.

Figure S5.2. Fe(III) concentrations measured at the agar rim (location 1, a), agar core (location 2, b) and ferrihydrite-mineral core (location 4, c) of the microbial reduction experiment of 15 mmol L^{-1} ferrihydrite by 10^8 cells mL^{-1} of *S. oneidensis* MR-1 in the presence of 15 mmol L^{-1} lactate as electron donor amended with either 5 mmol L^{-1} (red), 10 mmol L^{-1} (green),

25 mmol L^{-1} (yellow) or 50 mmol L^{-1} (blue) anthraquinone-2,6-disulfonate (AQDS) as electron

shuttle. All experiments were conducted with the agar-solidified incubation setup at 30°C in the

dark. Data are means from triplicate bottles ± standard deviations.
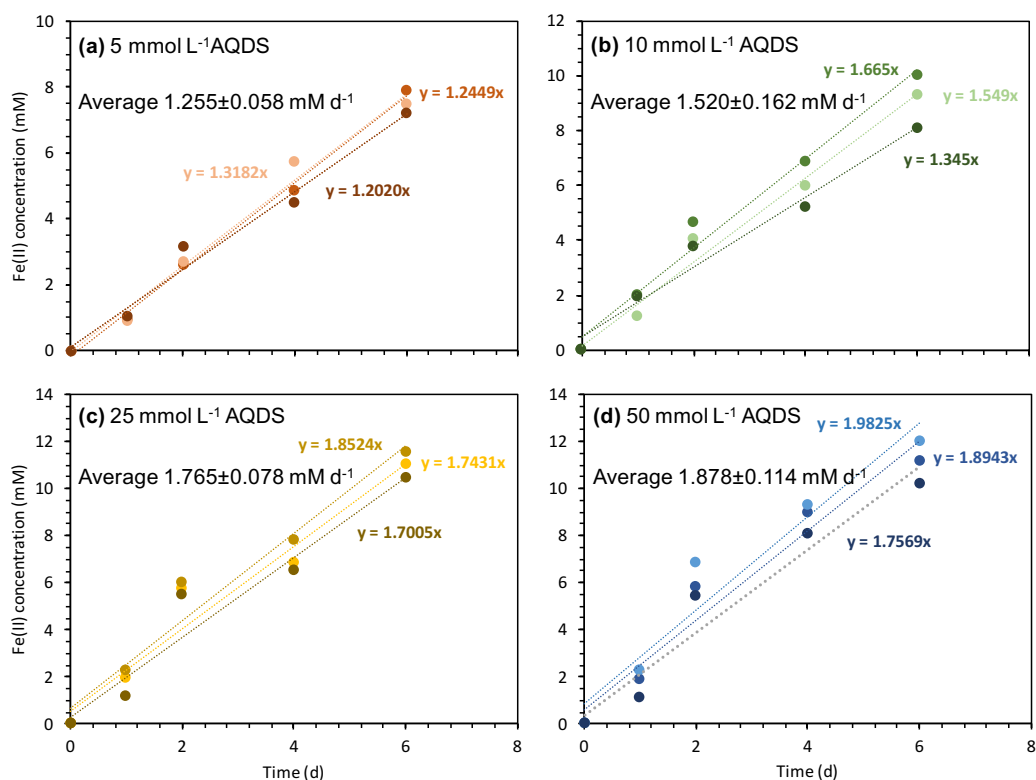
Figure S5.3. Average microbial ferrihydrite reduction rates in experiments amended with either

(a) 5 mmol L^{-1}, (b) 10 mmol L^{-1}, (c) 25 mmol L^{-1} or (d) 50 mmol L^{-1} AQDS calculated from the

Fe(II) concentration measured at the agar core (location 2) in the first 6 days of incubation. The

reduction rates were calculated separately for each of the triplicates; the average values and the

standard deviations of the three rates are shown in each panel.
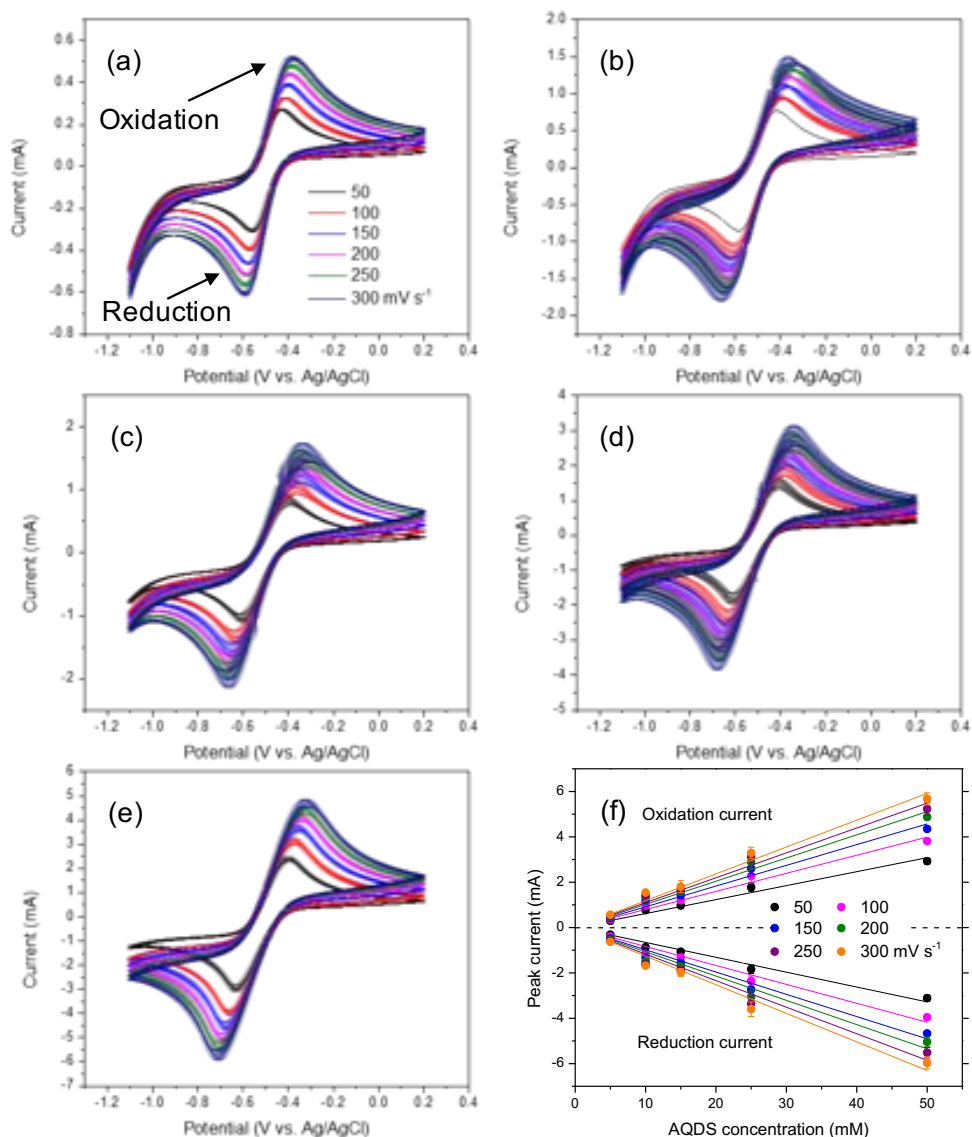
Figure S5.4. Cyclic voltammograms of 5 mmol L^{-1} (a), 10 mmol L^{-1} (b), 15 mmol L^{-1} (c), 25 mmol L^{-1} (d), and 50 mmol L^{-1} (e) AQDS with potential scan rates from 50 mV s^{-1} to 300 mV s^{-1}. Linear relationship of peak current and AQDS concentration at different potential scan rate (f).
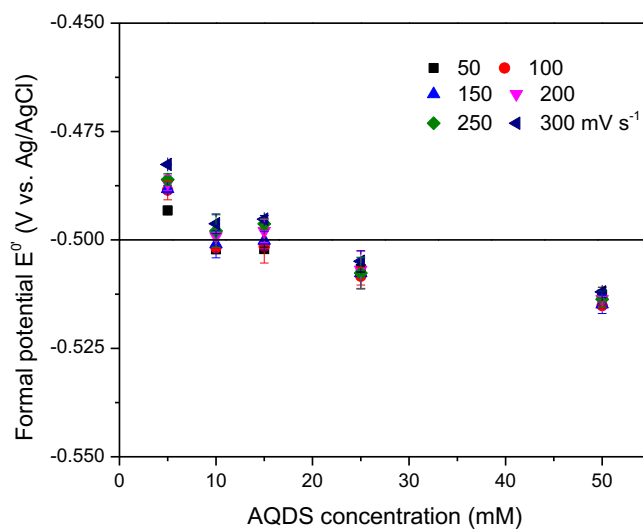
Figure S5.5. The formal potential (i.e., the average of peak potentials showing in Figure S5.4) of different concentrations of AQDS with a potential scan rate from 50 mV s^{-1} to 300 mV s^{-1}.
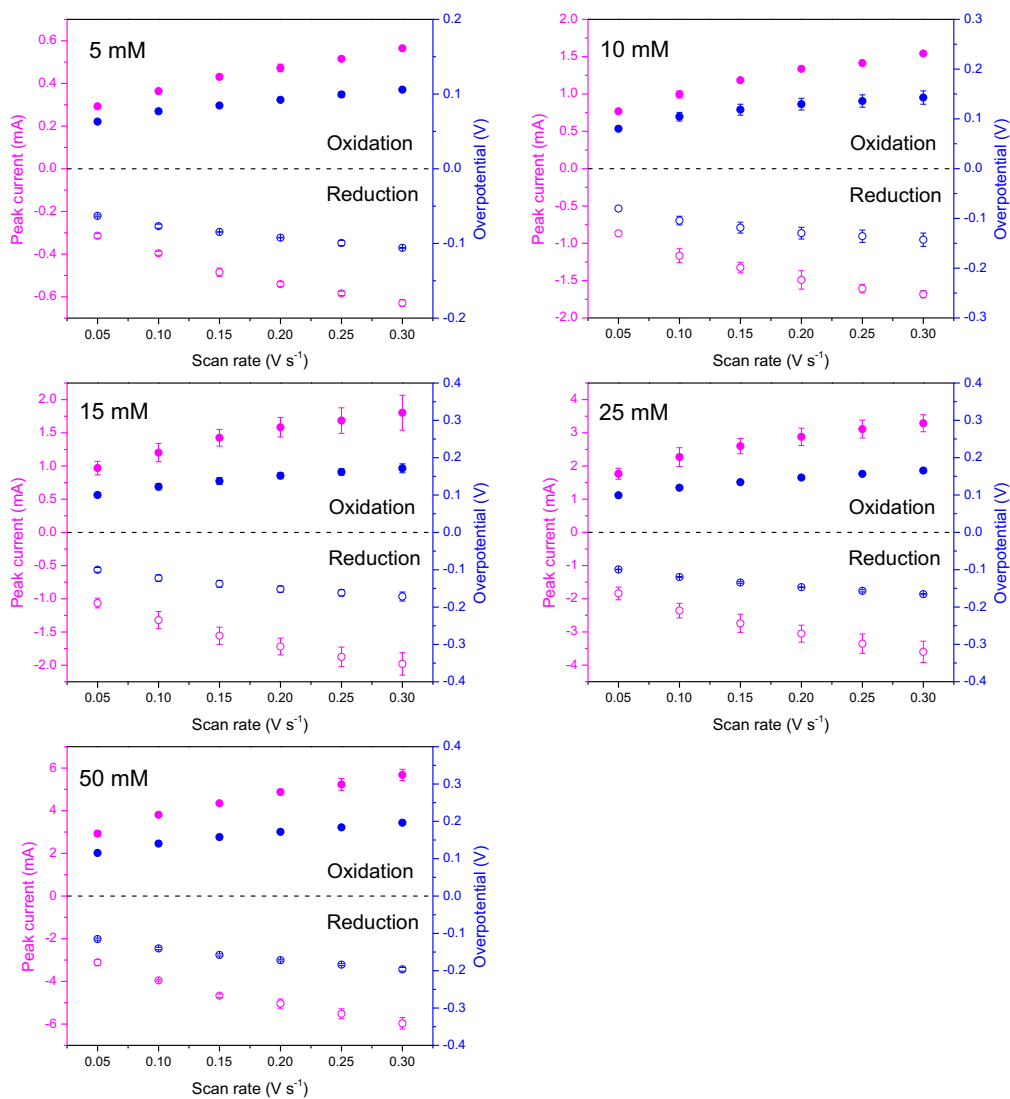
Figure S5.6. Peak current (pink color) and overpotential (i.e., the potential difference between peak potential and formal potential, blue color) as a function of potential scan rate at different concentrations of AQDS.

With the example of 5 mM AQDS:

Volume of the agar: 80 mL=80 cm^3

AQDS molecules: 5 mmol L^{-1} × 80 mL × 6.02*10^{23} = 2.4*10^{20}

Space of each AQDS: 80 cm^3/2.4 × 10^{20} = 330 nm^3

Size of one AQDS molecule : 2.75 nm
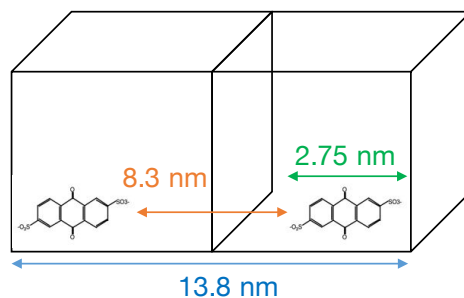
AQDS concentration (mM)	Distance between AQDS molecules (nm)
5	8.30
10	2.74
25	1.29
50	0.49

Figure S5.7. The estimated distance between two AQDS molecules with either 5 mmol L^{-1}, 10 mmol L^{-1}, 25 mmol L^{-1} or 50 mmol L^{-1} AQDS immobilized in agar.
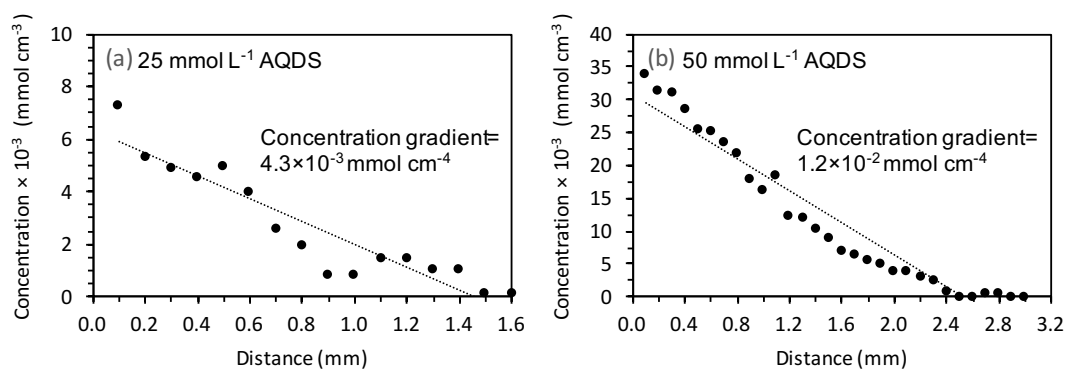
Figure S5.8. Concentration gradient of AH$_2$QDS in the electrolysis experiment with an initial AQDS concentration of 25 mmol L^{-1} (a) and 50 mmol L^{-1}(b). The concentration unit shown on y-axis was converted from mmol L^{-1} to mmol cm^{-3}.

5.7 References

Aeschbacher, M., Graf, C., Schwarzenbach, R. P. and Sander, M. (2012) Antioxidant properties of humic substances. *Environ. Sci. Technol.* **46** (9), 4916-4925.

Akhoury, A., Bromberg, L. and Hatton, T. A. (2013) Interplay of electron hopping and bounded diffusion during charge transport in redox polymer electrodes. *J. Phys. Chem.* **117** (1), 333-342.

Aspuru-Guzik, A., Gordon, R. G. and Aziz, M. J. (2014) A metal-free organic-inorganic aqueous flow battery. *Nature* **505** (7482), 195-198.

Bai, Y., Mellage, A., Cirpka, O. A., Sun, T.; Angenent, L. T., Haderlein, S. B. and Kappler, A. (2020) AQDS and redox-active NOM enables microbial Fe(III)-mineral reduction at cm-scales. *Environ. Sci. Technol.* **54** (7), 4131-4139.

Bai, Y., Subdiaga, E., Haderlein, S. B., Knicker, H. and Kappler, A. (2020) High-pH and anoxic conditions during soil organic matter extraction increases its electron-exchange capacity and ability to stimulate microbial Fe(III) reduction by electron shuttling. *Biogeosciences* **17** (3), 683-698.

Balch, J. and Guéguen, C. (2015) Determination of diffusion coefficients of dissolved organic matter in the Churchill River estuary system, Hudson Bay (Canada). *Environ. Chem.* **12** (2), 253-260.

Bard, A. J. and F., L. R. (2001) Electrochemical Methods: Fundamentals and Applications. Wiley, India.

Batchelor-McAuley, C., Li, Q., Dapin, S. M. and Compton, R. G. (2010) Voltammetric characterization of DNA intercalators across the full pH range: Anthraquinone-2,6-disulfonate and anthraquinone-2-sulfonate. *J. Phys. Chem.* **114** (11), 4094-4100.

Blauch, D. N. and Saveant, J. M. (1992) Dynamics of electron hopping in assemblies of redox centers. Percolation and diffusion. *J. Am. Chem. Soc.* **114** (9), 3323-3332.

Chen, J., Gu, B. H., Royer, R. A. and Burgos, W. D. (2003) The roles of natural organic matter in chemical and microbial reduction of ferric iron. *Sci. Total Environ.* **307** (1-3), 167-178.

Dahms, H. (1968) Electronic conduction in aqueous solution. *J. Phys. Chem.* **72** (1), 362-364.

Gao, C., Sander, M., Agethen, S. and Knorr, K.H. (2019) Electron accepting capacity of dissolved and particulate organic matter control CO_2 and CH_4 formation in peat soils. *Geochimi. Cosmochim. Acta* **245**, 266-277.

Glasser, N. R., Saunders, S. H. and Newman, D. K. (2017) The colorful world of extracellular electron shuttles. *Annu. Rev. Microbiol.* **71**, 731-751.

Hegler, F., Posth, N. R., Jiang, J. and Kappler, A. (2008) Physiology of phototrophic iron(II)-oxidizing bacteria: Implications for modern and ancient environments. *Fems. Microbiol. Ecol.* **66** (2), 250-260.

Huskinson, B., Marshak, M. P., Suh, C., Er, S., Gerhardt, M. R., Galvin, C. J., Chen, X. D., Liao, S. C., Zong, X., Seger, B., Pedersen, T., Yao, T. T., Ding, C. M., Shi, J. Y., Chen, J. and Li, C. (2016) Integrating a dual-silicon photoelectrochemical cell into a redox flow battery for unassisted photocharging. *Nat. Commun.* **7**, 11474.

Ji, X., Banks, C. E., Silvester, D. S., Wain, A. J. and Compton, R. G. (2017) Electrode kinetic studies of the hydroquinone−benzoquinone system and the reaction between hydroquinone and ammonia in propylene carbonate: Application to the indirect electroanalytical sensing of ammonia. *J. Phys. Chem.* **111** (3), 1496-1504.

Jiang, J. and Kappler, A. (2008) Kinetics of microbial and chemical reduction of humic substances: Implications for electron shuttling. *Environ. Sci. Technol.* **42** (10), 3563-3569.

Klupfel, L., Piepenbrock, A., Kappler, A. and Sander, M. (2014) Humic substances as fully re-generable electron acceptors in recurrently anoxic environments. *Nat. Geosci.* **7** (3), 195-200.

Lan, S., Wang, X. M., Yang, P., Qin, Z. J., Zhu, M. Q., Zhang, J., Liu, F., Tan, W. F., Huang, Q. Y. and Feng, X. H. (2019) The catalytic effect of AQDS as an electron shuttle on Mn(II)

oxidation to birnessite on ferrihydrite at circumneutral pH. *Geochim. Cosmochim. Acta* **247**, 175-190.

Lau, M. P., Sander, M., Gelbrecht, J. and Hupfer, M. (2015) Solid phases as important electron acceptors in freshwater organic sediments. *Biogeochemistry* **123** (1-2), 49-61.

Lehmann, J. and Kleber, M. (2015) The contentious nature of soil organic matter. *Nature* **528**, 60.

Lovley, D. R., Coates, J. D., Blunt-Harris, E. L., Phillips, E. J. P. and Woodward, J. C. (1996) Humic substances as electron acceptors for microbial respiration. *Nature* **382** (6590), 445-448.

Malvankar, N. S. and Lovley, D. R. (2014) Microbial nanowires for bioenergy applications. *Curr. Opin. Biotechnol.* **27**, 88-95.

Marcus, R. A. (1956) On the theory of oxidation-reduction reactions involving electron transfer. *J. Chem. Phys.* **24** (5), 966-978.

Narayanan, J., Xiong, J. Y. and Liu, X. Y. (2006) Determination of agarose gel pore size: Absorbance measurements vis other techniques. *J. Phys. Conf. Ser.* **28**, 83-86.

Nielsen, L. P., Risgaard-Petersen, N., Fossing, H., Christensen, P. B. and Sayama, M. (2010) Electric currents couple spatially separated biogeochemical processes in marine sediment. *Nature* **463** (7284), 1071-1074.

Orita, A., Verde, M. G., Sakai, M. and Meng, Y. S. (2016) A biomimetic redox flow battery based on flavin mononucleotide. *Nat. Commun.* **7** (1), 13230.

Orsetti, S., Laskov, C. and Haderlein, S. B. (2013) Electron transfer between iron minerals and quinones: Estimating the reduction potential of the Fe(II)-goethite surface from AQDS speciation. *Environ. Sci. Technol.* **47** (24), 14161-14168.

Phalak, P., Chen, J., Carlson, R. P. and Henson, M. A. (2016) Metabolic modeling of a chronic wound biofilm consortium predicts spatial partitioning of bacterial species. *Syst. Biol.* **10** (1), 90.

Piepenbrock, A., Dippon, U., Porsch, K., Appel, E. and Kappler, A. (2011) Dependence of microbial magnetite formation on humic substance and ferrihydrite concentrations. *Geochim. Cosmochim. Acta* **75** (22), 6844-6858.

Piepenbrock, A. and Kappler, A. (2013) Humic substances and extracellular electron transfer. In: Gescher, J. and Kappler, A., (Ed.), *Microbial metal respiration*, pp. 107-128.

Piepenbrock, A., Schroder, C. and Kappler, A. (2014) Electron transfer from humic substances to biogenic and abiogenic Fe(III) oxyhydroxide minerals. *Environ. Sci. Technol.* **48** (3), 1656-1664.

Pirbadian, S. and El-Naggar, M. Y. (2012) Multistep hopping and extracellular charge transfer in microbial redox chains. *Phys. Chem. Chem. Phys.* **14** (40), 13802-13808.

Roden, E. E. and Urrutia, M. M. (2002) Influence of biogenic Fe(II) on bacterial crystalline Fe(III) oxide reduction. *Geomicrobiol. J.* **19** (2), 209-251.

Roden, E. E. and Wetzel, R. G. (2002) Kinetics of microbial Fe(III) oxide reduction in freshwater wetland sediments. *Limnol. Oceanogr.* **47** (1), 198-211.

Roden, E. E., Kappler, A., Bauer, I., Jiang, J., Paul, A., Stoesser, R., Konishi, H. and Xu, H. F. (2010) Extracellular electron transfer through microbial reduction of solid-phase humic substances. *Nat. Geosci.* **3** (6), 417-421.

Rosso, K. M., Smith, D. M. A., Wang, Z. M., Ainsworth, C. C. and Fredrickson, J. K. (2004) Self-exchange electron transfer kinetics and reduction potentials for anthraquinone disulfonate. *J. Phys. Chem.* **108** (16), 3292-3303.

Ruff, I. and Friedrich, V. J. (1971) Transfer diffusion. I. Theoretical. *J. Phys. Chem.* **75** (21), 3297-3302.

Ruff, I., Friedrich, V. J., Demeter, K. and Csillag, K. (1971) Transfer diffusion. II. Kinetics of electron exchange reaction between ferrocene and ferricinium ion in alcohols. *J. Phys. Chem.* **75** (21), 3303-3309.

Sato, K., Ichinoi, R., Mizukami, R., Serikawa, T., Sasaki, Y., Lutkenhaus, J., Nishide, H. and Oyaizu, K. (2018) Diffusion-cooperative model for charge transport by redox-active nonconjugated polymers. *J. Am. Chem. Soc.* **140** (3), 1049-1056.

Shimizu, M., Zhou, J., Schröder, C., Obst, M., Kappler, A. and Borch, T. (2013) Dissimilatory reduction and transformation of ferrihydrite-humic acid coprecipitates. *Environ. Sci. Technol.* **47** (23), 13375-13384.

Six, J., Paustian, K., Elliott, E. T. and Combrink, C. (2000) Soil structure and organic matter: I. Distribution of aggregate-size classes and aggregate-associated carbon. *Soil Sci. Soc. Am. J.* **64** (2), 681-689.

Sparks, D. L. (2003) Environmental soil chemistry. Academic Press, Amsterdam; Boston.

Sposito, G. (2011) Electron shuttling by natural organic matter: Twenty years after. *Acs. Sym. Ser.* **1071**, 113-127.

Stevenson, F. J. (1994) Humus chemistry: genesis, composition, reaction. Wiley. New York.

Tan, W. B., Yuan, Y., Zhao, X. Y., Dang, Q. L., Yuan, Y., Li, R. F., Cui, D. Y. and Xi, B. D. (2019) Soil solid-phase organic matter-mediated microbial reduction of iron minerals increases with land use change sequence from fallow to paddy fields. *Sci. Total Environ.* **676**, 378-386.

Urrutia, M. M., Roden, E. E., Fredrickson, J. K. and Zachara, J. M. (1998) Microbial and surface chemistry controls on reduction of synthetic Fe(III) oxide minerals by the dissimilatory iron-reducing bacterium *Shewanella alga. Geomicrobiol. J.* **15** (4), 269-291.

Viollier, E., Inglett, P. W., Hunter, K., Roychoudhury, A. N. and Van Cappellen, P. (2000) The ferrozine method revisited: Fe(II)/Fe(III) determination in natural waters. *Appl. Geochem.* **15** (6), 785-790.

Zheng, W., Liang, L. Y. and Gu, B. H. (2012) Mercury reduction and oxidation by reduced natural organic matter in anoxic environments. *Environ. Sci. Technol.* **46** (1), 292-299.

6. General conclusions and outlook

In 1996, Lovley and co-authors reported, for the first time, that the addition of humic substances (HS) (a traditionally used proxy for NOM) significantly enhanced the reduction rate and extent of Fe(III) mineral (ferrihydrite), by *Geobacter metallireducens* (Lovley et al., 1996). After excluding the possibility of HS acting as a chelator thus promoting the dissolution of Fe(III) minerals, these authors proposed that HS stimulated Fe(III) reduction in a two-stage process in which (1) *G. metallireducens* oxidizes the electron donor (acetate), with HS acting as the electron acceptor, and (2) reduced HS donate electrons to Fe(III) minerals. This electron-transfer scheme between the microbes and the Fe(III) minerals by NOM was thereafter referred to as "electron shuttling". Over the past 24 years, many researches have made efforts to promote the development of the concept of NOM electron shuttling. Our study presented in this thesis, further deepened our understanding of this process by providing insights into the possibility of NOM electron shuttling over cm distance to occur in soil systems and the potential underlying mechanism of such a long-distance electron transfer.

6.1 Cm-scale microbial Fe(III)-mineral reduction with NOM as electron shuttles

The experimental proof of NOM (in many studies represented by HS) has been exclusively based on the finding that the rate of microbial Fe(III)-mineral reduction increased in presence of NOM/HS in batch setups (Klupfel et al., 2014; Lovley et al., 1996; Lovley et al., 1998; Stern et al., 2018). However, due to the variety of interactions between NOM/HS and Fe(III) minerals in a batch setup (i.e., sorption, co-precipitation and aggregation), it is very difficult to evaluate the extent to which NOM/HS stimulate microbial Fe(III)-mineral reduction by acting as electron shuttles (Piepenbrock et al., 2011). Moreover, although Fe(III)-mineral reduction facilitated by endogenously produced electron shuttles over micrometers (μm) distance has been shown for different Fe(III)-reducing bacteria (Michelson et al., 2019; Michelson et al., 2017), batch setup does not allow the investigation of whether NOM/HS

electron shuttling can happen over a μm or even longer spatial distance (i.e., centimeter (cm)) between Fe(III) minerals and Fe(III)-reducing bacteria.

In order to circumvent the problem of direct interaction of NOM and Fe(III) minerals and investigate the microbial Fe(III)-mineral reduction over cm distance with NOM as electron shuttles, we developed an agar-solidified setup that separates Fe(III)-reducing bacteria and Fe(III) minerals by 2 cm distance (Chapter 4, 5). This setup consists of a Fe(III)-mineral ball made from agar (2%) that sits in the middle of the setup, an agar (2%) layer surrounding the Fe(III)-mineral ball that contains homogenously distributed electron shuttles (NOM), and a suspension of the Fe(III)-reducing bacteria on top of the agar layer. Agar (2%) has a pore size of 100-200 nm (Narayanan et al., 2006), which is too small for Fe(III)-reducing bacteria to penetrate in, therefore, preventing direct contact between the cells and the Fe(III) minerals (Caccavo et al., 1994; Hau and Gralnick, 2007).

We discovered from experiments conducted in the agar-solidified setup that, with the amendment of 100 mg L^{-1} Pahokee Peat Humic Acid (PPHA) or Suwannee River NOM (SRNOM), around 37% or 48% of ferrihydrite reduction was obtained after 30 days of incubation, regardless of the identity of Fe(III)-reducing bacteria (i.e., *Shewanella oneidensis* MR-1 or *Geobacter sufurreducens*). When replacing ferrihydrite by a more crystalized Fe(III) mineral-goethite, around 3% and 1% of goethite reduction was detected with PPHA and SRNOM as electron shuttles after 50 days of incubation, respectively. These results indicated that these two commonly used electron shuttles (PPHA and SRNOM) can transfer electrons between Fe(III)-reducing bacteria and Fe(III) minerals over 2 cm distance (Chapter 4). Microbial Fe(III)-mineral reduction over 2 cm distance was also observed with anthraquinone-2,6-disulfonate (AQDS, a widely used analogue of the quinone functional groups in NOM) as electron shuttles. With AQDS concentration as low as 0.05 mmol L^{-1}, 60% of ferrihydrite reduction was observed within 28 days of incubation. Based on the experimental results, our diffusion-reaction model (Chapter 4) predicted a complete reduction of Fe(III) minerals such

as ferrihydrite with long-enough time scale even at low concentration of electron shuttles, because of the reversibility of the oxidation/reduction of quinone functional groups.

Quinone functional group has been identified in both solid-phase NOM and dissolved NOM and has been believed to be responsible for the ability of NOM to undergo redox cycles and act as electron shuttles between microbes and Fe(III) minerals (Aeschbacher et al., 2010; Lovley et al., 1996; Roden et al., 2010). The agar-solidified setup we used for the microbial Fe(III) reduction experiment exploited agar (2%) to slow down the diffusion of NOM as electron shuttles by one order of magnitude than in water (Chapter 4, 5). NOM as electron shuttles with such low diffusion in the agar-solidified system is very similar to in soil systems, where most NOM are presented in solid-phase with low diffusivity and a small amount in more-mobile dissolved phase (Sparks, 2003). Therefore, the cm-scale electron transfer between Fe(III)-reducing bacteria and Fe(III) minerals observed in the agar-solidified setup might also occur in soil systems, with both dissolved- and solid-phase NOM as electron shuttles.

6.2 Electron hopping enables cm-scale microbial Fe(III)-mineral reduction

Microbial Fe(III)-mineral reduction over distance with endogenous electron shuttles such as Flavin and *c*-type cytochromes has been intensively studied and the underlying mechanism of this process is believed to be the diffusion of the shuttle molecules (Huang et al., 2018; Marsili et al., 2008; Michelson et al., 2019). In contrast, the mechanism of NOM electron shuttling over distance largely remains unknown. In our studies, we used AQDS to represent the quinone and hydroquinone functional groups in NOM and immobilized AQDS in agar (2%) to imitate the low-diffusion condition of NOM molecules in soil systems. Several observations in our studies indicated the cm-scale electron transfer by the immobilized AQDS in agar (2%) is not likely by diffusion:

(1) Although the diffusion coefficient of AQDS was 10 times lower in agar (2%) than in water (Chapter 4), we found that, the ferrihydrite reduction rate with AQDS as electron shuttles in

agar (1.60 ± 0.28 mmol L^{-}1 Fe(II) d^{-1}, Chapter 5) was comparable to the ferrihydrite reduction rate with AQDS as electron shuttles in water (2.36 ± 1.07 mmol L^{-1} Fe(II) d^{-}1, Chapter 3);

(2) When considering diffusion as the electron-transfer pathway and using the diffusion coefficient of AQDS in agar (5.76×10^{-11} m^2 s^{-1}) in the diffusion-reaction model we developed in Chapter 4, the resulted ferrihydrite reduction rate was too slow to meet the rate we observed in the experiment. Moreover, in order to provide sufficient flux of AQDS to capture the ferrihydrite reduction rate in the experiment, the diffusion coefficient of AQDS used in the model had to be increased by a factor of at least 9.4;

(3) In the electrochemical experiment we performed in Chapter 5, we observed an AH$_2$QDS (i.e., the reduced AQDS) production flux of 3.1×10^{-5} mmol cm^{-2} s^{-1}. However, the calculated diffusion flux of AH$_2$QDS was only 2.2×10^{-9} mmol cm^{-2} s^{-1}, indicating diffusion is not sufficient to sustain the AH$_2$QDS transfer rate as we observed in the experiment.

Overall, these observations indicated that an electron transfer pathway that is faster than diffusion was involved in the electron shuttling process over cm distance with AQDS molecules. Electron hopping is an electron transfer process that was first demonstrated in redox-active polymers (Akhoury et al., 2013) and has been used to explain the electron transfer in bacterial nanowires (Pirbadian and El-Naggar, 2012) and extracellular polymeric substances (EPS) (Xiao et al., 2017). Although electron hopping is known to facilitate fast electron transfer, it requires a distance less than 2 nanometer (nm) between redox centers (Gray and Winkler, 2009). Based on our calculation in Chapter 5, a distance less than 2 nm can only be achieved once the quinone functional group reaches a concentration of 15 mmol L^{-1}, corresponding to 15 mmol L^{-1} AQDS. However, in our experiments with only 0.05 mmol L^{-1} AQDS as electron shuttles, the diffusion of AQDS molecules was still too slow to count for the observed ferrihydrite reduction rate, indicating the involvement of electron hopping. Therefore, we postulate that electron transfer over cm distance by AQDS molecules is achieved by a combination of diffusion and electron

hopping. The higher the AQDS concentration, the more dominant is electron hopping in the electron transfer process. This postulation was confirmed by the linear correlation between the heterogeneous electron transfer constant (k^0) of AQDS ($1.9 \pm 0.2 \times 10^{-3}$ cm s^{-1}) and the diffusion coefficient of AQDS (D_0, 5.76×10^{-11} m^2 s^{-1}) that well fitted to the diffusion-electron hopping model that was developed by Sato and co-authors (Sato et al., 2018) (Chapter 5). Moreover, our study showed that the involvement of electron hopping can increase the electron transfer rate up to 10^6-fold by AQDS molecules over cm distance (Chapter 5).

Because AQDS was used as the analogue for the quinone and hydroquinone functional groups in NOM, the proposed diffusion-electron hopping pathway that facilitates the rapid electron transfer over cm distance in this thesis is of environmental relevance. In 2010, Nielsen et al. (Nielsen et al., 2010) observed an immediate response of the sulfide profile with depth in a marine sediment to the presence and absence of O_2 at the sediment surface over a distance of more than 1 cm. The authors attributed the long-distance electron transfer to a redox-active network formed by bacteria nanowires, with c-type cytochromes as diffusive mediator in the network. Our study presented in this thesis indicated that, such a cm-distance electron transfer can also happen in soil systems with a network built by solid-phase NOM, and with dissolved NOM serve as the diffusive mediators within the network. Dissolved NOM can accept electrons generated form microbial respiration and subsequently diffuse to the solid-phase NOM due to their high diffusive mobility. Electron hopping then occurs between the dissolved NOM and the solid-phase NOM molecules and within the redox-active network of solid-phase NOM. This diffusion-electron hopping pathway promotes the electron transfer by NOM molecules in soil systems to a rapid and long-distance level.

6.3 Alkali-extracted HS is invalid proxy for NOM

The chemical extraction with sodium hydroxide (NaOH) at pH 12 has been widely used to extract HS from soils, sediments and aquifers (Gerke, 2018; Uhle et al., 1999; Wershaw,

1993). The discussion about whether HS is a real fraction of NOM or just a laboratory artefact started since the inventory of the chemical extraction method and has been getting increasingly intensive (Kleber and Lehmann, 2019; Olk et al., 2019). Although receiving a lot of criticism, HS is still used in many studies as the proxy for NOM. In this thesis, we investigated the effects of the chemical extraction on the redox properties of the extracted HS compared to NOM, therefore, contributing to the discussion of whether HS can be treated as a proxy for NOM.

The criticism about the alkaline extraction has been focused on the high pH of 12 of the NaOH solution (Engebretson and Von Wandruszka, 1999; Lehmann and Kleber, 2015; Piccolo, 1988; Sanchez-Monedero et al., 2002). Such high pH is known to hydrolyze esters or cause the degradation of large molecules in the NOM, resulting in higher concentration of carboxyl functional groups and lower molecular weight of the extracted HS compared to the original NOM (Ritchie and Perdue, 2008; Swift and Posner, 1972). Many attempts have been made to reduce the extent of alteration of HS during the alkaline extraction, and one of the most well-recognized measures is to conduct the extraction under anoxic conditions. Anoxic alkaline extraction is also the standard method for the extraction of most HS samples that can be purchased from the International Humic Substances Society (IHSS). Studies showed that, HS extracted by 0.1 M NaOH (pH 12) under anoxic conditions exhibited very similar absorbance values at a wavelength of 254 nm (SUVA$_{254}$), compared to the native dissolved NOM (Sierra et al., 2004; Swift and Posner, 1972). Since SUVA$_{254}$ is an indicator for the molecular weight and the aromaticity of organic matter samples (Korshin et al., 1997), it has been suggested based on these results that the degradation of large molecules is significantly limited under anoxic conditions. Therefore, the extracted HS have a similar chemical structure compared to the original NOM.

However, similar chemical structure does not represent similar redox activity. In our study (Chapter 3), we extracted NOM from a forest soil with water at pH 7 (we name this extracted fraction "water-extractable soil organic matter (SOM)") and anoxically isolated HS

with the chemical extraction method (NaOH, pH 12) from the water-extractable SOM. We found that the HS isolated from the water-extractable SOM by alkali extraction had 3 times higher electron-exchange capacity (EEC) than the water-extractable SOM itself, suggesting the formation of redox-active functional groups during the chemical extraction. When participating in a microbial Fe(III)-mineral reduction experiment as electron shuttles, the HS with higher EEC (i.e. higher redox activity) had a more pronounced impact on the microbial Fe(III) reduction than the water-extractable SOM, i.e., higher Fe(III) reduction rate and greater reduction extent. These results suggest that the reactivity of native NOM can be overestimated in many biogeochemical processes if chemically extracted HS is used to represent native NOM in the laboratory experiments.

Therefore, we suggest that, for future studies, the chemically extracted HS should not be used as a proxy for NOM anymore. Instead, a mild water extraction at pH 7 at room temperature as we performed in Chapter 3 can be used to extract environmental-relevant NOM. Although the extracted material only represented a very small fraction of the total NOM pool (1%-3%), we believe this extracted fraction of NOM is environmentally relevant due to its high mobility and thus, high chance of participating in biogeochemical processes in the environment.

6.4 Environmental implications and outlook

Results in this thesis suggested the potential of microbial Fe(III)-mineral reduction to happen over cm distance with NOM as electron shuttles. The electron transfer over such long distance is likely to be achieved by a redox-active network formed by solid-phase NOM, with dissolved NOM as diffusive mediators in the network (Figure 6.1). Electron hopping is expected to happen within the redox-active network of NOM to facilitate the electron transfer rate up to 10^6-fold. This NOM electron shuttling can not only stimulate the reduction of poorly-crystallized mineral such as ferrihydrite, but also highly-crystallized mineral like goethite.
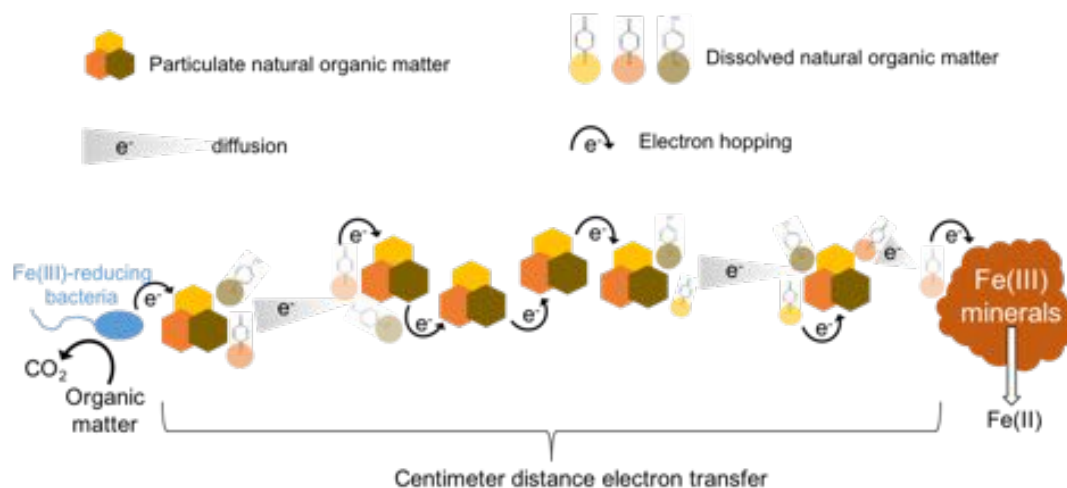
Figure 6.1. The simplified illustration of NOM electron shuttling between Fe(III)-reducing bacteria and Fe(III) minerals over cm distance.

The rate and extent of microbial Fe(III)-mienral reduction is relevant to many biogeochemical processes and contaminants remediation in the environment. For example, microbial Fe(III) reduction affects the migration and the fate of arsenic (As), chromium (Cr) and uranium (U) and other inorganic pollutants (Roberts et al., 2017; Sundman et al., 2020). The Fe(II) produced can be coupled to the degradation of many organic contaminants, including polyhalogenated compounds, nitroaromatis, and azo dyes (Borch et al., 2010; Hofstetter et al., 2006; Pecher et al., 2002). In addition, microbial Fe(III) reduction process with NOM as electron shuttles can effectively compete for the transfer of electrons to methanogens, nitrate-reducing bacteria and sulfate-reducing bacteria under anoxic conditions, thereby inhibiting greenhouse gas emission (Roden and Wetzel, 1996; Valenzuela et al., 2020; Weber et al., 2006). Studies of these processes usually only consider microbial Fe(III) reduction with dissolved NOM as electron shuttles over a distance of no more than μm, therefore, the influence of NOM on microbial Fe(III)-mineral reduction, thus on these processes tend to be underestimated. For future studies, the potential of rapid microbial Fe(III)-mineral reduction at cm-scales with both dissolved and solid-phase NOM as electron shuttles should be considered.

There are also other open questions for future researches, and most of them are related to the importance and relevance of electron shuttling in the environment. First of all, most studies on microbial Fe(III)-mineral reduction with NOM as electron shuttles were conducted in batch setups with single microbial strains and synthetic Fe(III) minerals, while in environmental systems, different microbial strains are present, Fe(III) minerals are also often of biogenic origin (Cornell and Schwertmann, 2006). Furthermore, microbial Fe(III) reduction over distance with endogenous electron shuttles (i.e., Flavin, c-type cytochromes) has always been studied separately from exogenous electron shuttles such as NOM. Therefore, it remains unknown whether the endogenous and exogenous electron shuttles contribute to the long-distance electron transfer concurrently in the environment. Although we suggested solid-phase NOM can form a redox-active network and transfer electrons over cm distance, electron shuttles with high diffusivity such as dissolved NOM is required to transfer electrons initially from microbes to the solid-phase NOM and in the network between solid-phase NOM molecules. Therefore, we postulate that, in the environments, in addition to dissolved NOM, endogenous electron shuttles such as Flavin and c-type cytochromes can also diffusively transfer the microbial respiratory electrons to the solid-phase NOM and participate in the redox-active network as diffusive mediators. Future studies should also consider the participation of other conductive compounds such as magnetite nanoparticles and bacterial nanowires in the formation of the redox-active network. This redox-active network, with heterogeneous electron shuttles and conductive compounds, can help the microbes to transfer electrons to the otherwise unreachable terminal electron acceptors such as Fe(III) minerals over long distance, and increase the overall electron-transfer rate in the environment.

6.5 References

Aeschbacher, M., Sander, M. and Schwarzenbach, R. P. (2010) Novel electrochemical approach to assess the redox properties of humic substances. *Environ. Sci. Technol.* **44** (9), 87-93.

Akhoury, A., Bromberg, L. and Hatton, T. A. (2013) Interplay of electron hopping and bounded diffusion during charge transport in redox polymer electrodes. *J. Phys. Chem. B* **117** (1), 333-342.

Borch, T., Kretzschmar, R., Kappler, A., Van Cappellen, P., Ginder-Vogel, M., Voegelin, A. and Campbell, K. (2010) Biogeochemical redox processes and their impact on contaminant dynamics. *Environ. Sci. Technol.* **44** (1), 15-23.

Caccavo, F., Lonergan, D. J., Lovley, D. R., Davis, M., Stolz, J. F. and Mcinerney, M. J. (1994) *Geobacter sulfurreducens* Sp-Nov, a hydrogen-oxidizing and acetate-oxidizing dissimilatory metal-reducing microorganism. *Appl. Environ. Microb.* **60** (10), 3752-3759.

Cornell, R. M. and Schwertmann, U. (2006) The iron oxides: structure, properties, reactions, occurrences and uses. Wiley-VCH. Weinheim.

Engebretson, R. R. and von Wandruszka, R. (1999) Effects of humic acid purification on interactions with hydrophobic organic matter: Evidence from fluorescence behavior. *Environ. Sci. Technol.* **33** (23), 4299-4303.

Gerke, J. (2018) Concepts and misconceptions of humic substances as the stable part of soil organic matter: A review. *Agronomy* **8** (5), 76-91.

Gray, H. B. and Winkler, J. R. (2009) Electron flow through proteins. *Chem. Phys. Lett.* **483** (1), 1-9.

Hau, H. H. and Gralnick, J. A. (2007) Ecology and biotechnology of the genus *Shewanella*. *Annu. Rev. Microbiol.* **61**, 237-258.

Hofstetter, T. B., Neumann, A. and Schwarzenbach, R. P. (2006) Reduction of nitroaromatic compounds by Fe(II) species associated with iron-rich smectites. *Environ. Sci. Technol.* **40** (1), 235-242.

Huang, L. Y., Tang, J. H., Chen, M., Liu, X. and Zhou, S. G. (2018) Two modes of riboflavin-mediated extracellular electron transfer in *Geobacter uraniireducens*. *Front. Microbiol.* **9** (2886).

Kleber, M. and Lehmann, J. (2019) Humic substances extracted by alkali are invalid proxies for the dynamics and functions of organic matter in terrestrial and aquatic ecosystems. *J. Environ. Qual.* 48 (2), 207-216.

Klupfel, L., Piepenbrock, A., Kappler, A. and Sander, M. (2014) Humic substances as fully regenerable electron acceptors in recurrently anoxic environments. *Nat. Geosci.* **7** (3), 195-200.

Korshin, G. V., Li, C. W. and Benjamin, M. M. (1997) Monitoring the properties of natural organic matter through UV spectroscopy: A consistent theory. *Water Res.* **31** (7), 1787-1795.

Lehmann, J. and Kleber, M. (2015) The contentious nature of soil organic matter. *Nature* **528** (7580), 60-68.

Lovley, D. R., Coates, J. D., BluntHarris, E. L., Phillips, E. J. P. and Woodward, J. C. (1996) Humic substances as electron acceptors for microbial respiration. *Nature* **382** (6590), 445-448.

Lovley, D. R., Fraga, J. L., Blunt-Harris, E. L., Hayes, L. A., Phillips, E. J. P. and Coates, J. D. (1998) Humic substances as a mediator for microbially catalyzed metal reduction. *Acta. Hydroch. Hydrob.* **26** (3), 152-157.

Marsili, E., Baron, D. B., Shikhare, I. D., Coursolle, D., Gralnick, J. A. and Bond, D. R. (2008) *Shewanella* Secretes flavins that mediate extracellular electron transfer. *P. Natl. Acad. Sci.* **105** (10), 3968-3973.

Michelson, K., Alcalde, R. E., Sanford, R. A., Valocchi, A. J. and Werth, C. J. (2019) Diffusion-based recycling of flavins allows *Shewanella oneidensis* MR-1 to yield energy from metal reduction across physical separations. *Environ. Sci. Technol.* **53** (7), 3480-3487.

Michelson, K., Sanford, R. A., Valocchi, A. J. and Werth, C. J. (2017) Nanowires of *Geobacter sulfurreducens* require redox cofactors to reduce metals in pore spaces too small for cell passage. *Environ. Sci. Technol.* **51**(20), 11660-11668.

Narayanan, J., Xiong, J. Y. and Liu, X. Y. (2006) Determination of agarose gel pore size: Absorbance measurements vis a vis other techniques. *J. Phys. Conf. Ser.* **28**, 83-86.

Nielsen, L. P., Risgaard-Petersen, N., Fossing, H., Christensen, P. B. and Sayama, M. (2010) Electric currents couple spatially separated biogeochemical processes in marine sediment. *Nature* **463** (7284), 1071-1074.

Olk, D. C., Bloom, P. R., Perdue, E. M., McKnight, D. M., Chen, Y., Farenhorst, A., Senesi, N., Chin, Y. P., Schmitt-Kopplin, P., Hertkorn, N. and Harir, M. (2019) Environmental and agricultural relevance of humic fractions extracted by alkali from soils and natural waters. *J. Environ. Qual.* **48** (2), 217-232.

Pecher, K., Haderlein, S. B. and Schwarzenbach, R. P. (2002) Reduction of polyhalogenated methanes by surface-bound Fe(II) in aqueous suspensions of iron oxides. *Environ. Sci. Technol.* **36** (8), 1734-1741.

Piccolo, A. (1988) Characteristics of soil humic extracts obtained by some organic and inorganic solvents and purified by HCl-HF treatment. *Soil Sci.* **146** (6), 418-426.

Piepenbrock, A., Dippon, U., Porsch, K., Appel, E. and Kappler, A. (2011) Dependence of microbial magnetite formation on humic substance and ferrihydrite concentrations. *Geochim. Cosmochim. Acta* **75** (22), 6844-6858.

Pirbadian, S. and El-Naggar, M. Y. (2012) Multistep hopping and extracellular charge transfer in microbial redox chains. *Phys. Chem. Chem. Phys.* **14** (40), 13802-13808.

Ritchie, J. D. and Perdue, E. M. (2008) Analytical constraints on acidic functional groups in humic substances. *Org. Geochem.* **39** (6), 783-799.

Roberts, H. E., Morris, K., Law, G. T. W., Mosselmans, J. F. W., Bots, P., Kvashnina, K. and Shaw, S. (2017) Uranium(V) incorporation mechanisms and stability in Fe(II)/Fe(III) (oxyhydr)oxides. *Environ. Sci. Tech. Let.* **4** (10), 421-426.

Roden, E. E., Kappler, A., Bauer, I., Jiang, J., Paul, A., Stoesser, R., Konishi, H. and Xu, H. F. (2010) Extracellular electron transfer through microbial reduction of solid-phase humic substances. *Nat. Geosci.* **3** (6), 417-421.

Roden, E. E. and Wetzel, R. G. (1996) Organic carbon oxidation and suppression of methane production by microbial Fe(III) oxide reduction in vegetated and unvegetated freshwater wetland sediments. *Limnol. Oceanogr.* **41** (8), 1733-1748.

Sanchez-Monedero, M. A., Roig, A., Cegarra, J., Bernal, M. P. and Paredes, C. (2002) Effects of HCl-HF purification treatment on chemical composition and structure of humic acids. *Eur. J. Soil Sci.* **53** (3), 375-381.

Sato, K., Ichinoi, R., Mizukami, R., Serikawa, T., Sasaki, Y., Lutkenhaus, J., Nishide, H. and Oyaizu, K. (2018) Diffusion-cooperative model for charge transport by redox-active nonconjugated polymers. *J. Am. Chem. Soc.* **140** (3), 1049-1056.

Sierra, M. M. D., Fernandes, A. N. and Szpoganicz, B. (2004) Influence of amide linkages on acidity determinations of humic substances-Testing with model-mixtures. *Talanta*. **62** (4), 687-693.

Sparks, D. L. (2003) Environmental soil chemistry. Academic Press, Amsterdam; Boston.

Stern, N., Mejia, J., He, S. M., Yang, Y., Ginder-Vogel, M. and Roden, E. E. (2018) Dual role of humic substances as electron donor and shuttle for dissimilatory iron reduction. *Environ. Sci. Technol.* **52** (10), 5691-5699.

Sundman, A., Vitzthum, A. L., Adaktylos-Surber, K., Figueroa, A. I., van der Laan, G., Daus, B., Kappler, A. and Byrne, J. M. (2020) Effect of Fe-metabolizing bacteria and humic substances on magnetite nanoparticle reactivity towards arsenic and chromium. *J. Hazard. Mater.* **384**, 121450.

Swift, R. S. and Posner, A. M. (1972) Autoxidation of humic acid under alkaline conditions. *J. Soil Sci.* **23** (4), 381-393.

Uhle, M. E., Chin, Y. P., Aiken, G. R. and McKnight, D. M. (1999) Binding of polychlorinated biphenyls to aquatic humic substances: The role of substrate and sorbate properties on partitioning. *Environ. Sci. Technol.* **33** (16), 2715-2718.

Valenzuela, E. I., Padilla-Loma, C., Gomez-Hernandez, N., Lopez-Lozano, N. E. and Casas-Flores, S. (2020) Humic substances mediate anaerobic methane oxidation linked to nitrous oxide reduction in wetland sediments. *Front. Microbiol.* **11** (587).

Weber, K. A., Urrutia, M. M., Churchill, P. F., Kukkadapu, R. K. and Roden, E. E. (2006) Anaerobic redox cycling of iron by freshwater sediment microorganisms. *Environ. Microbiol.* **8** (1), 100-113.

Wershaw, R. L. (1993) Model for humus in soils and sediments. *Environ. Sci. Technol.* **27** (5), 814-816.

Xiao, Y., Zhang, E. H., Zhang, J. D., Dai, Y. F., Yang, Z. H., Christensen, H. E. M., Ulstrup, J. and Zhao, F. (2017) Extracellular polymeric substances are transient media for microbial extracellular electron transfer. *Sci. Adv.* **3** (7), e1700623.

Curriculum Vitae

Personal information

Name: Yuge Bai
Current address: Salzwasenweg 12
                   72074 Tübingen
Germany
Email: yuge.bai@uni-tuebingen.de
Date of birth: January 29th, 1993
Place of birth: Bayannaoer, Inner Mongolia, China
Citizenship: Chinese

Academic Education

Ph.D.   Since November 2016

University and institute: Applied Geoscience, Universität Tübingen, Germany
Ph.D. thesis title: Natural organic matter (NOM) electron shuttling stimulates
                            microbial Fe(III)-mineral reduction at centimeter-scales
Supervisors: Prof. Andreas Kappler and Prof. Stefan B. Haderlein

M.Sc.   2014-2016
University and institute: Plant and Soil Science, University of Delaware, U.S.A.
Master thesis title: Synthesis and degradation of polyphosphate: Scaling-up of
                            molecular reactions to understand phosphorus removal in
                            wastewater treatment plants
Supervisors: Prof. Deb P. Jaisi

B.Sc.   2010-2014
University and institute: Environmental and Natural Resources Science, Huazhong
                            Agricultural University, China
Master thesis title: Effects of orthophosphate and polyphosphate on the dissolution
                            and transportation of ZnO nanoparticles
Supervisors: Prof. Xionghan Feng

Training Experience

Assistance in lab course "Geomicrobiology and Environmental Microbiology" (October 2017 and October 2018), Tübingen, Germany.

Statement of personal contribution

The work described in this PhD thesis was funded by grants from the Deutsche Forschungsgemeinschaft (DFG) to Prof. Andreas Kappler (KA 1736-37/1). The conceptual background to this project was designed by Prof. Andreas Kappler. Prof. Andreas Kappler was the main supervisor throughout the project and Prof. Stefan B. Haderlein was the second supervisor.

Unless otherwise stated, the experiments were conceptualized by myself, together with Prof. Andreas Kappler and Prof. Stefan B. Haderlein. The discussion and analysis of the obtained results as well as writing of all manuscripts were completed in corporation with Prof. Andreas Kappler and Prof. Stefan B. Haderlein; for chapter 4 additionally in cooperation with Dr. Adrian Mellage and Prof. Olaf A. Cirpka; for chapter 5 in addition with Dr. Tianran Sun. In detail, the contributions of the named people including myself, as well as other people are as stated below:

Field work: Soil samples used in this study was taken from the Schönbuch forest by me with great help of Prof. Thomas Scholten.

Chapter 3: Prof. Heike Knicker performed the nuclear magnetic resonance (NMR) analyses on the soil organic matter (SOM) samples and analyzed the NMR data. Dr. Edisson Subdiaga performed the electrochemical measurement and determined the electron exchange capacity of the SOM samples. Dr. Silvia Orsetti helped with the electrochemical-experimental design and data analysis. Dr. Allison Enright and Dr. Zhe Zhou helped to revise the manuscript.

Chapter 4: Ellen Röhm developed the agar-solidified setup and performed preliminary tests. Paula Eisnecker helped with the experimental setup and sampling. Dr. Adrian Mellage developed the diffusion-reaction model, with help of Prof. Olaf A. Cirpka. Dr. Tianran Sun helped with the electrochemical analyses to determine the diffusion coefficient of anthraquinone-2,6-disulfonate (AQDS) in agar. The manuscript was prepared by me, together

with Dr. Adiran Mellage. Prof. Andreas Kappler, Prof. Olaf A. Cirpka, Prof. Stefan B. Haderlein and Prof. Largus T. Angenent revised the manuscript.

Chapter 5: Ellen Röhm developed the agar-solidified setup and performed preliminary tests. Paula Eisnecker helped with the experimental setup and sampling. Dr. Tianran Sun helped with the electrochemical analyses. The manuscript was prepared by me and Dr. Tianran Sun. Prof. Andreas Kappler, Prof. Stefan B. Haderlein and Prof. Largus T. Angenent revised the manuscript.

Acknowledgement

to every team member in the geomicrobiology group, especially my office mates Markus Maisch, Natalia Jakus, Zhen Yang and Jianrong Huang for their help and company. I would like to thank Dr. Muammar Mansor, Timm Bayer, Ankita Chauhan and Yu-ming Huang for proofreading this thesis. I am thankful to Dr. Elisabetha Kraft, Marion Schäffling, Dr. Wolfgang Bott and Paula Silvetti for their administrative help that enabled me to focus on my study.

There are so many others that I should thank, without them, I might never be able to pursue a PhD degree. First is my bachelor supervisors, Prof. Xionghan Feng and Dr. Biao Wan, who offered me the opportunity to work in the lab and patiently taught me all of the basic laboratory skills. Prof. Xionghan Feng also helped me significantly in the application of my master program. I would also like to thank Prof. Deb Jaisi for his generous fellowship offer for my master study that allowed me to start my journey of abroad study.

My time in Tübingen was very enjoyable in large part due to many friends that became part of my life. I am grateful to Dr. Jing He and her husband for helping me to settle down in Tübingen when I just arrived. I thank my friends Dandan Chen, Xiaohua Han, Jing He, Yu-ming Huang and Zhen Yang for bringing me so much laughter and joy during their stay in Tübingen. No matter where they are in the future, thinking about the time with them will always bring smiles on my face. I also appreciate my friends in China, Miao Zhang, Rong Kang and Xiaoxuan Liao, although they are far away on the other side of the continent, their encouragement and care have always been here with me.

Moreover, I want to thank my boyfriend Manuel Schad, who understands me and shares my happiness and sorrow, who encourages me to overcome all obstacles and who makes me into a more confident and strong person with all of his love. I also want to thank Manuel's parents and sisters for treating me as a part of the family. Being far away from home, their company and care make my life much easier, enjoyable and meaningful. At last I would like to thank my family, especially my parents, who have always been open-minded, encouraging and

understanding. I am only able to follow my heart and be proud of who I am with their unconditional love, care and support.